NACA RM A51D02

NACA

RESEARCH MEMORANDUM

INVESTIGATION IN THE AMES 12-FOOT PRESSURE WIND TUNNEL OF A MODEL HORIZONTAL TAIL OF ASPECT RATIO 3 AND TAPER RATIO 0.5 HAVING THE QUARTER-CHORD LINE SWEPT BACK 45°

By Carl D. Kolbe and Angelo Bandettini

Ames Aeronautical Laboratory
Moffett Field, Calif.

NATIONAL ADVISORY COMMITTEE
FOR AERONAUTICS
WASHINGTON
June 25, 1951

NATIONAL ADVISORY COMMITTEE FOR AERONAUTICS

RESEARCH MEMORANDUM

INVESTIGATION IN THE AMES 12-FOOT PRESSURE WIND TUNNEL OF A MODEL HORIZONTAL TAIL OF ASPECT RATIO 3 AND TAPER RATIO 0.5 HAVING THE QUARTER-CHORD LINE SWEPT BACK 45°

By Carl D. Kolbe and Angelo Bandettini

SUMMARY

An investigation has been made to evaluate the effect of Reynolds number and Mach number on the aerodynamic characteristics of a horizontal tail of aspect ratio 3 equipped with a plain, sealed, full-span elevator. The line joining the quarter-chord points of the airfoil sections was swept back 45° and the sections perpendicular to this line were the NACA 64A010.

Increasing the Reynolds number from 2,000,000 to 18,000,000 at a Mach number of 0.25 resulted in a sizable reduction in the drag coefficient at moderate to high lift coefficients. Within this range of Reynolds numbers the lift characteristics of the horizontal tail were little affected by dynamic scale, but the hinge-moment and pitching-moment characteristics of the tail were affected by changes in the Reynolds number, especially at the higher angles of attack or elevator deflections.

Increasing the Mach number from 0.25 to 0.94 for constant Reynolds numbers of 2,000,000 and 4,000,000 caused an increase in the lift-curve slope and in the elevator effectiveness. In general, the hinge-moment coefficient resulting from either angle of attack or elevator deflection increased in magnitude with increasing Mach number. The Mach number at which rapid changes in the elevator hinge-moment coefficient occurred was dependent upon the angle of attack and the elevator deflection.

INTRODUCTION

A systematic investigation has been undertaken at the Ames Aeronautical Laboratory to determine the effects of plan form on the

control-effectiveness and the hinge-moment parameters of horizontal tails having full-span trailing-edge flaps. References 1 through 7 present results of wind-tunnel tests of both swept and unswept horizontal tails of several aspect ratios, all having the same taper ratio and airfoil section as the subject model.

As a part of this investigation the tests reported herein were conducted to evaluate the effects of compressibility and of Reynolds number on the control-surface characteristics of a horizontal tail having 45° of sweepback. Since this model also represents a wing with a full-span flap, drag and pitching-moment data are included in addition to the lift and hinge-moment data.

NOTATION

A aspect ratio $\left(\frac{b^2}{S}\right)$

$\frac{b}{2}$ semispan, measured perpendicular to the plane of symmetry, feet

C_D drag coefficient $\left(\frac{\text{drag}}{qS}\right)$

C_h elevator hinge-moment coefficient $\left(\frac{\text{elevator hinge moment}}{2q\ M_A}\right)$

C_L lift coefficient $\left(\frac{\text{lift}}{qS}\right)$

C_m pitching-moment coefficient about the quarter point of the mean aerodynamic chord $\left(\frac{\text{pitching moment}}{qS\bar{c}}\right)$

c chord, measured parallel to the plane of symmetry, feet

$\bar{c}$ mean aerodynamic chord $\left(\frac{\int_0^{b/2} c^2 dy}{\int_0^{b/2} c\ dy}\right)$, feet

c_e' chord of elevator behind the hinge line measured perpendicular to the hinge line, feet

$\frac{L}{D}_{max}$ maximum lift-to-drag ratio

M Mach number

M_A first moment about the hinge line of the elevator area behind the hinge line, feet cubed

$\frac{\Delta p}{q}$ pressure coefficient across the elevator-nose seal (pressure below the seal minus the pressure above the seal divided by the free-stream dynamic pressure)

q free-stream dynamic pressure, pounds per square foot

R Reynolds number, based on the mean aerodynamic chord

S horizontal-tail area, square feet

y lateral distance perpendicular to the plane of symmetry, feet

α corrected angle of attack, degrees

α_u angle of attack, uncorrected for tunnel-wall interference and angle-of-attack counter correction, degrees

βA reduced aspect ratio $\left(\sqrt{1-M^2}\ A\right)$

δ elevator deflection (positive to increase lift) measured in a plane normal to the elevator hinge line, degrees

C_{L_α} $\left(\frac{\partial C_L}{\partial \alpha}\right)_{\delta = o}$

C_{h_α} $\left(\frac{\partial C_h}{\partial \alpha}\right)_{\delta = o}$

(measured at $\alpha = 0$), per degree

C_{L_δ} $\left(\frac{\partial C_L}{\partial \delta}\right)_{\alpha = o}$

C_{h_δ} $\left(\frac{\partial C_h}{\partial \delta}\right)_{\alpha = o}$

C_{m_δ} $\left(\frac{\partial C_m}{\partial \delta}\right)_{\alpha = o}$

(measured at $\delta = 0$,) per degree

$C_{m_{C_L}}$ $\left(\frac{\partial C_m}{\partial C_L}\right)_{\delta = o}$ (measured at $C_L = 0$)

The subscripts after the parentheses represent the factors held constant during the measurement of the parameters.

MODEL

The model used in this investigation represented a horizontal tail of aspect ratio 3 and taper ratio 0.5. The geometric properties of the model are shown in figure 1. The airfoil section was the NACA 64A010 (table I) in planes inclined 45° to the plane of symmetry. The line joining the quarter-chord points of the airfoil sections was swept back 45°. This line was at 29.63 percent of the chord parallel to the plane of symmetry (table II). The tip of the model horizontal tail was formed by a half body having a diameter equal to the corresponding thickness of the tip section.

The stabilizer of the model was constructed of a tin-bismuth compound bonded to a laminated steel spar. The model was equipped with a full-span, radius-nose, sealed elevator machined from solid steel. The chord of the elevator was 30 percent of the NACA 64A010 section chord. The ratio of the elevator area behind the hinge line to the total area of the model was 0.253. The model was mounted vertically with the tunnel floor serving as a reflection plane as shown in figure 2. The gap between the elevator and the tunnel floor was approximately 0.02 inch when the elevator was undeflected. The juncture between the stabilizer and the tunnel floor was sealed with a rubber gasket. The elevator was attached to the stabilizer by three hinges. One hinge was located 6.4 percent of the semispan below the plane of symmetry, while the other two were at 50.2 and 90.6 percent of the semispan above the plane of symmetry. The latter two hinges and a close-fitting block at the plane of symmetry divided the balance chamber into three separate sections. The gap between the elevator nose and the stabilizer was sealed with a rubber diaphram. This balance chamber seal was closely fitted to the ends of each chamber to reduce leakage to a minimum. Details of the balance chamber are shown in figure 1. The turntable, to which the model was attached, was directly connected to the force-measuring apparatus. The elevator hinge moments were measured by means of a resistance-type electric strain gage located immediately under the lower elevator hinge. The elevator was positioned while the tunnel was in operation by a remotely controlled electric drive motor mounted below the tunnel floor.

TESTS

Tests of the model horizontal tail were conducted in two different sequences. In the first series of tests, the elevator deflection was

maintained at constant values and the angle of attack was varied from -10° to 30°. For the second series of tests, the angle of attack was maintained at 0° and the elevator deflection was varied from -16° to 16°. These angle ranges were reduced at the higher Mach numbers and Reynolds numbers where wind-tunnel power limitations prevented testing at the higher angles. The aeroelastic effects on the model due to angle of attack or elevator deflection are believed to be small. The elevator deflections referred to in this report were measured in a plane perpendicular to the elevator-hinge line. The following equation relates these elevator deflections to the deflection in streamwise planes:

$$\tan \delta_{||} = \cos \Lambda_h \tan \delta_{\perp}$$

where

$\delta_{||}$ elevator deflection measured in the streamwise direction

Λ_h sweep angle of the elevator hinge line, 38.66°

Tests to Evaluate the Effects of Reynolds Number

The effects of Reynolds number on the lift, drag, pitching moment, and elevator hinge moment were measured at a Mach number of 0.25 for Reynolds numbers of 2,000,000, 4,000,000, 8,000,000, 12,000,000, and 18,000,000. At higher Mach numbers, data were obtained at Reynolds numbers of 2,000,000 and 4,000,000. The scope of the investigation that was made to study the effects of Reynolds number on the subject model is presented in the following table:

Coefficients	M	R	α_u	δ
C_L, C_h, C_m, C_D	0.25	2,000,000 to 18,000,000	-10° to 30°	0°, $\pm 20^{\circ}$, $\pm 30^{\circ}$
C_L, C_h, C_m	.25	2,000,000 to 18,000,000	0°	-16° to 16°
C_L, C_h, C_m, C_D	0.60, 0.80, 0.90, 0.94	2,000,000 and 4,000,000	-10° to 30°	0°
C_L, C_h, C_m	0.60, 0.80, 0.90, 0.94	2,000,000 and 4,000,000	0°	-16° to 16°

Tests to Evaluate the Effects of Mach Number

The effects of compressibility on the lift, drag, pitching moment, hinge moment, and the pressure difference across the elevator-nose seal were measured at a Reynolds number of 4,000,000 at Mach numbers of 0.25, 0.60, 0.80, 0.85, 0.90, 0.92, and 0.94. The scope of this phase of the investigation is indicated in the following table:

Coefficients	M	α_u	δ
C_L, C_h, C_m, C_D, and $\frac{\Delta p}{q}$	0.25	-10° to 30°	6° to -30°
	.60	-10° to 30°	6° to -30°
	.80	-10° to 18°	6° to -30°
	.85	-10° to 14°	6° to -30°
	.90	-10° to 12°	6° to -30°
	.92	-10° to 12°	6° to -30°
	.94	-8° to 8°	6° to -25°
C_L, C_h, C_m	0.25,0.60, 0.80,0.90, and 0.94	0°	16° to -16°

Tests to Evaluate the Effects of Standard Roughness and of the Elevator-Nose Seal

Tests were also made to evaluate the separate effects of standard leading-edge roughness (reference 8) and of removing the elevator-nose seal on the lift, drag, pitching-moment, and elevator hinge-moment characteristics. Data were obtained at a Reynolds number of 4,000,000 over the angle-of-attack range at Mach numbers up to 0.94 and over the elevator deflection range at 0° angle of attack for Mach numbers of 0.25, 0.60, 0.80, 0.90, and 0.94.

CORRECTIONS TO DATA

The data were corrected for the effects of tunnel-wall interference resulting from lift on the model by the method of reference 9, using the theoretical span loading calculated by the methods of reference 10. The corrections that were added to the angle of attack and the drag coefficient were:

$$\Delta\alpha = 0.769\ C_L, \text{ degrees}$$

$$\Delta C_D = 0.0109\ C_L^{\ 2}$$

No attempt was made to separate the tunnel-wall-interference effects resulting from lift due to elevator deflection from those resulting from lift due to angle of attack. No corrections were applied to the hinge-moment or the pitching-moment data, but the effects of tunnel-wall interference on these data are believed to be small.

Certain data in this report are presented for values of uncorrected angle of attack α_u. The relation between the corrected and uncorrected angle of attack is as follows:

$$\alpha = 0.99\ \alpha_u + \Delta\alpha$$

The constant 0.99 is the ratio between the geometric angle of attack and the uncorrected reading of the angle-of-attack counter, and the factor $\Delta\alpha$ is the correction for the tunnel-wall interference. The uncorrected angle of attack does not differ from the corrected value by more than 0.8° for any of the test data presented.

The constriction effects due to the presence of the tunnel walls were evaluated by the method of reference 11 and were not modified to allow for the effect of sweep. The following table shows the magnitude of these corrections:

Corrected Mach number	Uncorrected Mach number	$\frac{q_{corrected}}{q_{uncorrected}}$
0.250	0.250	1.003
.600	.599	1.004
.800	.795	1.008
.850	.843	1.010
.900	.888	1.014
.920	.905	1.018
.940	.920	1.022

Pressures measured at orifices in the wind-tunnel walls were used to determine the test conditions at which wind-tunnel choking may have influenced the data. The positions of the tunnel-wall pressure orifices relative to the model are shown in figure 3. It was noted that a local Mach number of unity was attained at the wind-tunnel wall at a free-stream Mach number considerably less than the maximum free-stream Mach number that could be obtained. This suggests that partial choking of the tunnel existed at Mach numbers below that for which a normal shock wave extended

across the test section. Some of the data were obtained at test conditions for which the local Mach number at the wind-tunnel wall exceeded unity. These data are included in the figures but are faired with dotted curves to indicate that they may have been influenced by wind-tunnel choking.

Approximate corrections to the drag were made to compensate for the drag force on the exposed turntable. These corrections were determined from tests with the model removed from the turntable. The corrections are presented in the following table:

$R \times 10^{-6}$	M	C_{D_t}
2.0	0.25	0.0028
2.0	.60	.0030
2.0	.80	.0033
2.0	.90	.0036
2.0	.94	.0038
4.0	.25	.0028
4.0	.60	.0030
4.0	.80	.0033
4.0	.85	.0034
4.0	.90	.0036
4.0	.92	.0037
4.0	.94	.0038
8.0	.25	.0024
12.0	.25	.0023
18.0	.25	.0022

No attempt was made to evaluate tares due to possible interference between the model and the turntable.

RESULTS AND DISCUSSION

The effects of Reynolds number on the low-speed aerodynamic characteristics of the model are shown in figures 4 through 8 and are summarized in figures 9 and 10. The effects of increasing the Reynolds number from 2,000,000 to 4,000,000 at Mach numbers up to 0.94 are shown in figures 11 and 12. The results of tests conducted to evaluate the effects of Mach number at a Reynolds number of 4,000,000 are presented in figures 13 through 21 and are summarized in figures 22 and 23.

Data from tests conducted to evaluate the separate effects of leading-edge roughness and of the elevator-nose seal are presented in figures 24 and 25 and are summarized in figure 26.

Effect of Reynolds Number

Mach number 0.25.- The effects of increasing the Reynolds number from 2,000,000 to 18,000,000 at a Mach number of 0.25 on the lift, drag, pitching-moment, and elevator hinge-moment characteristics are presented in figures 4 through 8. In general, the effects of Reynolds number on the aerodynamic characteristics of the model were small. At the higher angles of attack or elevator deflections, increasing the Reynolds number delayed the onset of separation on the wing to higher values of lift coefficient as evidenced by the drag data of figure 7. This same effect of Reynolds number is noted in the hinge-moment data of figure 5.

The effects of Reynolds number on the lift and moment parameters of the horizontal tail are summarized in figure 9. These parameters, which are measured at zero lift, are further evidence of the lack of dynamic-scale effect on the characteristics of this model at low lift coefficients. The effect of Reynolds number on the drag of the model is summarized in figure 10. These data show that, at moderate to high lift coefficients, increasing the Reynolds number resulted in sizable reductions in the drag coefficient.

Mach numbers 0.60, 0.80, 0.90, 0.94.- The effects of an increase in Reynolds number from 2,000,000 to 4,000,000 at Mach numbers up to 0.94 on the aerodynamic characteristics of the model with the elevator undeflected are presented in figure 11. The effects of increasing Reynolds number on lift, hinge-moment, and pitching-moment coefficients as functions of elevator deflection for 0° angle of attack are presented in figure 12. In general, the increase in Reynolds number from 2,000,000 to 4,000,000 caused only small changes in the aerodynamic characteristics of the model.

Effect of Mach Number

The aerodynamic characteristics of the horizontal tail at a Reynolds number of 4,000,000 are presented in figures 13 through 21 for Mach numbers from 0.25 to 0.94. The effects of Mach number on the lift, hinge-moment, pitching-moment, and drag characteristics are summarized in figures 22 and 23.

Lift.- The variation of lift coefficient with angle of attack for various elevator deflections is presented in figure 13. These data show that the elevator was effective in producing changes in lift throughout the elevator-deflection and angle-of-attack range.

The variation of lift coefficient with elevator deflection at an angle of attack of 0° is presented in figure 14. The range of elevator deflection over which the elevator effectiveness remained constant decreased with increasing Mach number.

The variations of the parameters C_{L_α} and C_{L_δ} with Mach number are compared with values predicted from theory in figure 22. The theoretical variation of C_{L_α} with Mach number has been calculated by the method of reference 10 and C_{L_δ} has been calculated by the method described in appendix A. The methods are based on a simplified lifting-surface concept and are modified to account for the effects of compressibility by the Prandtl-Glauert relationship. Being subject to these two limitations, the theoretical values are terminated at a Mach number of 0.85 beyond which Mach number the theory is not believed applicable for an airfoil having as low an aspect ratio as the subject model. The stabilizer effectiveness parameter C_{L_α} increased from 0.049 per degree at a Mach number of 0.25 to a value of 0.067 per degree at a Mach number of 0.94. The theoretical values of C_{L_α} are in good agreement with the experimental values at Mach numbers up to 0.85.

At a Mach number of 0.94, the elevator effectiveness parameter C_{L_δ} had increased approximately 20 percent over the value obtained at a Mach number of 0.25. The variation of C_{L_δ} with Mach number was predicted by means of method 2, reference 12, and was modified to account for the effects of compressibility through the application of the Prandtl-Glauert rule. The agreement between the theoretical curve and the experimental data in figure 22 is considered good. An explanation of the application of the Prandtl-Glauert rule to the prediction of C_{L_δ}, C_{h_α} and C_{h_δ} is given in appendix A.

Hinge moment.- The variation of elevator hinge-moment coefficient with angle of attack for various elevator deflections is presented in figure 15. Figure 16 presents the variation of elevator hinge-moment coefficient with elevator deflection for 0° angle of attack. These two figures show that the variation of elevator hinge-moment coefficient was approximately linear through 0° angle of attack and 0° elevator deflection for all Mach numbers. Increasing the Mach number to 0.94 resulted in an increase in the absolute values of the slopes of the hinge-moment curves and a reduction in the angular range over which the hinge-moment characteristics were linear.

The Mach number at which rapid changes occurred in the elevator hinge-moment coefficients was dependent upon the elevator deflection and angle of attack. This is illustrated in figure 17(a) which presents the

variation of elevator hinge-moment coefficient with Mach number for several uncorrected angles of attack at 0° elevator deflection and in figure 17(b) which presents the variation of elevator hinge-moment coefficient with Mach number for several elevator deflections at an uncorrected angle of attack of 0°.

The hinge-moment parameters C_{h_α} and C_{h_δ} are presented as a function of Mach number in figure 22. The low-speed value of C_{h_α} was approximately -0.0030 and was little affected by compressibility up to a Mach number of 0.90. With further increase in Mach number the value of C_{h_α} changed rapidly, attaining a value of -0.0040 at a Mach number of 0.94. At low Mach numbers, the value of C_{h_δ} was approximately -0.0070. The value of C_{h_δ} became more negative with increasing Mach number, particularly above 0.90, and at a Mach number of 0.94 had attained a value of -0.0095. Method 2 of reference 12, modified to account for the effects of compressibility, was used to predict the variations of C_{h_α} and C_{h_δ} with Mach number. These data are presented as dashed curves in figure 22. The agreement of the theoretical values of C_{h_α} with the experimental data is excellent. The theory predicts a value of C_{h_δ} which is less negative than the experimental value, but the predicted variation of C_{h_δ} with Mach number is in good agreement with the experimental data.

Pressure difference across the elevator-nose seal.- Figure 18 shows the effects of elevator deflection and angle of attack on the pressure difference across the elevator-nose seal at various Mach numbers. The differences in balancing pressure at the various spanwise stations are believed to be the result of the spanwise distribution of loading, leakage around the ends of the seals at the hinges, and imperfections in the alinement of the balance-chamber cover plates.

Inspection of the data in figure 18 shows that the rate of change of the pressure coefficient across the elevator-nose seal with elevator deflection decreased at large angles of attack or elevator deflections. Increasing the Mach number decreased the range of angles at which increases in balancing pressures accompanied increases in deflection. These data indicate that, if the elevator were equipped with a sealed internal nose balance, the resulting hinge-moment characteristics of the balanced elevator would be nonlinear at the higher Mach numbers and that only a small amount of balancing effectiveness would exist at elevator deflections greater than about 6° or 8° at Mach numbers above 0.90.

Pitching moment.- The pitching-moment coefficients about the quarter point of the wing mean aerodynamic chord are presented in figure 19 as functions of lift coefficient. The variation of pitching-moment coefficient with elevator deflection at 0° angle of attack is presented in figure 20.

The data presented in figures 19 and 20 are summarized in figure 22 where $C_{m_{C_L}}$ and C_{m_δ} are presented as functions of Mach number. Since the subject model has neither camber nor twist, the values of $C_{m_{C_L}}$ presented in figure 22 are indicative of the chordwise position of the aerodynamic center. As the Mach number was increased above 0.25, the aerodynamic center moved rearward, the rate of rearward movement increasing rapidly as the Mach number was increased above 0.80. Calculations by the method of reference 10 indicate a value of $C_{m_{C_L}}$ which is zero for a Mach number of zero with a slight increase to a positive value as the Mach number is increased. This theory considers only the effect of compressibility on the spanwise location of the center of pressure. The disparity between the theoretical and experimental values of $C_{m_{C_L}}$ may be due to differences between the theoretical and the experimental spanwise location of the center of pressure or to the fact that the theory does not take into account the effects of compressibility on the chordwise location of the wing center of pressure.

The pitching-moment effectiveness parameter C_{m_δ} changed from -0.0073 at a Mach number of 0.25 to -0.0127 at a Mach number of 0.94. The values of C_{m_δ} predicted by the method described in appendix B are shown in figure 22. The agreement between theory and experiment is good at the lower Mach numbers, but the measured effects of compressibility are greater than those predicted by the theory.

Drag.- The drag data of figure 21 are summarized in figure 23 where the drag coefficient for constant lift coefficients, maximum lift-to-drag ratio, and the lift coefficient at which the maximum lift-drag ratio occurred are presented as functions of Mach number for 0° elevator deflection. The Mach number for drag divergence, defined as the Mach number at which $\partial C_D/\partial M = 0.10$, was 0.93 for a lift coefficient of 0.2. A maximum lift-to-drag ratio of 18.0 was obtained at Mach numbers up to 0.60. The value of the maximum lift-to-drag ratio decreased with further increase in Mach number to a value of approximately 12 at a Mach number of 0.94. The lift coefficient for maximum lift-to-drag ratio was approximately 0.2 throughout the Mach number range.

Effects of Leading-Edge Roughness and Elevator-Nose Seal

The independent effects of leading-edge roughness and removal of the elevator-nose seal are presented in figures 24 and 25. The data presented in these figures are summarized in figure 26. The results of tests without leading-edge roughness and with the elevator nose sealed are presented in all these figures for purposes of comparison.

The addition of leading-edge roughness resulted in a slight reduction in the lift-curve slope near zero lift and in a reduction in maximum lift coefficient (fig. 24(a)). The elevator effectiveness was reduced (fig. 25(a)) when roughness was applied to the leading edge. The largest reduction in the stabilizer and elevator effectiveness occurred at a Mach number of 0.94 where C_{L_α} and C_{L_δ} were reduced by 0.009 per degree and 0.006 per degree, respectively (fig. 26(a)). It can be seen in figure 26(a) that leading-edge roughness caused a reduction in the absolute value of both C_{h_α} and C_{h_δ}. The magnitude of this reduction increased with increasing Mach number.

The effects of leading-edge roughness on the pitching-moment effectiveness of the elevator C_{m_δ} and on the pitching-moment-curve slope $C_{m_{C_L}}$ are presented in figure 26(b). Leading-edge roughness caused a reduction in the effectiveness of the elevator in producing pitching moment; the magnitude of this reduction increased with increasing Mach number. The effect of compressibility on the pitching-moment-curve slope at zero lift was reduced by the addition of leading-edge roughness to the model. As would be expected, application of leading-edge roughness resulted in an increase in drag. Figures 24(d) and 26(b) show that the increase of minimum drag coefficient due to leading-edge roughness at $\delta = 0^\circ$ and $C_L = 0$ was about 0.0040 at low speed and about 0.0030 at a Mach number of 0.94.

It can be seen in figure 26(a) that unsealing the elevator nose caused slight reductions in C_{L_α} and C_{L_δ} but had no important effects on the hinge-moment-curve slopes (fig. 26). Figure 26(b) shows that unsealing the elevator nose had little effect on the pitching-moment characteristics of the horizontal tail or on the minimum drag.

CONCLUDING REMARKS

The results of wind-tunnel tests conducted to evaluate the independent effects of Reynolds number and Mach number on the aerodynamic characteristics of a horizontal tail of aspect ratio 3.0 with the quarter-chord line swept back 45° have been presented.

Increasing the Reynolds number from 2,000,000 to 18,000,000 at a Mach number of 0.25 resulted in a sizable reduction in the drag coefficient at moderate to high lift coefficients. The lift characteristics of the horizontal tail were little affected by this change in Reynolds number, but the hinge-moment and pitching-moment characteristics of the tail were affected by changes in Reynolds number, especially at the higher angles of attack or elevator deflections.

As the Mach number was increased from 0.25 to 0.94 the lift-curve slope increased 36 percent, the lift effectiveness of the elevator increased 20 percent, the pitching-moment effectiveness of the elevator increased 74 percent, and the absolute magnitude of the variation of elevator hinge-moment coefficient with either angle of attack or elevator deflection increased about 35 percent. These increases were measured through 0° angle of attack and 0° elevator deflection. The Mach number at which compressibility effects resulted in large changes in the elevator hinge-moment coefficient was dependent upon the angle of attack and the elevator deflection. Increasing the Mach number from 0.25 to 0.94 also caused a reduction in the maximum lift-to-drag ratio of from 18 to 12 and a small rearward movement of the aerodynamic center.

Measurements of the pressure difference across the elevator-nose seal indicate that, if the elevator were equipped with a sealed internal nose balance, the resulting hinge-moment characteristics of the balanced elevator would be nonlinear at the higher Mach numbers and that only a small amount of balancing effectiveness would exist at elevator deflections greater than about 6° or 8° at Mach numbers above 0.90.

The addition of leading-edge roughness caused reductions in lift-curve slope, elevator effectiveness, stability, and elevator hinge-moment parameters. The magnitude of these reductions increased with increasing Mach number.

Removal of the elevator-nose seal caused slight reductions in the elevator effectiveness but had no important effects on the lift-curve slope, stability, drag, or hinge-moment parameters.

Ames Aeronautical Laboratory
National Advisory Committee for Aeronautics
Moffett Field, Calif.

APPENDIX A

APPLICATION OF THE PRANDTL-GLAUERT FACTOR TO THE EQUATIONS FOR C_{L_δ}, C_{h_α}, AND C_{h_δ} FROM REFERENCE 12

The equations of reference 12, method 2, have been modified through the application of the Prandtl-Glauert rule to account for first-order compressibility effects.

The method consists of determining the incompressible-flow characteristics of an equivalent wing the lateral dimensions of which are reduced in the ratio of $\sqrt{1 - M^2} : 1$. The aspect ratio is thus reduced and the tangent of the sweep angle is increased as the Mach number is increased. The incompressible-flow characteristics of the equivalent wing thus derived are then modified to account for the effects of compressibility through the application of the Prandtl-Glauert rule. The following are the equations of reference 12, method 2, as modified to account for the effects of compressibility.

$$\left(C_{L_\delta}\right)_c = \frac{\left(c_{l_{\delta_o}}\right)_{\Lambda=o}}{\sqrt{1-M^2}} \cos \Lambda_e \cos \Lambda_h \left[1 - \left(\frac{\alpha_i}{\alpha}\right)_e\right] \tag{A1}$$

where the subscripts

i average induced value

e characteristics of the equivalent wing for incompressible flow

h hinge line

c modification to account for the effects of compressibility

Since the term $\cos \Lambda_h$ merely relates the elevator deflection in streamwise planes to the elevator deflection in planes perpendicular to the hinge line, the value of Λ_h used in the equations is that of the actual wing rather than that of the equivalent wing.

$$\left(C_{h_\alpha}\right)_{LS_c} = \frac{\left(c_{h_{\alpha_o}}\right)_{\Lambda=o}}{\sqrt{1-M^2}} \cos \Lambda_e \left[1 - \left(\frac{\alpha_i}{\alpha}\right)_e\right] + \frac{\left(\Delta C_{h_\alpha}\right)_{SC}}{\sqrt{1-M^2}} \tag{A2}$$

where the subscripts

LS lifting surfaces

SC induced camber or streamline curvature

$$\left(C_{h_\delta}\right)_{LS_c} = \frac{(c_{h_\delta})_{\Lambda=0}}{\sqrt{1-M^2}} \cos \Lambda_e \cos \Lambda_h +$$

$$(\alpha_\delta)_{C_{L_c}} \left[\frac{(c_{h_{\alpha_0}})_{\Lambda=0}}{\sqrt{1-M^2}} \cos \Lambda_e - (C_{h_\alpha})_{LS_c} \right] \quad \text{(A3)}$$

where

$$(\alpha_\delta)_{C_{L_c}} = -\frac{(C_{L_\delta})_c}{(C_{L_\alpha})_c}$$

In the three-dimensional linearized-compressible flow theory used herein to account for the effects of compressibility, the actual aspect ratio becomes an effective aspect ratio or reduced aspect ratio βA which approaches zero as M approaches 1.0. Analysis of the simplified lifting-surface theory indicates that when βA becomes less than approximately 2 the predicted theoretical values will diverge rapidly from the experimental values. For the subject airfoil, the reduced aspect ratio becomes 2 at a Mach number of about 0.80. Prediction of the airfoil characteristics is not attempted at Mach number above 0.85. The reduced aspect ratio βA is discussed in detail in reference 13.

APPENDIX B

CALCULATION OF THE FLAP PITCHING-MOMENT EFFECTIVENESS C_{m_δ} FOR A SWEPT-BACK AIRFOIL

In order to determine the pitching moment caused by the deflection of a flap on a swept-back airfoil, the position of the center of pressure must be established. The longitudinal position of the airfoil center of pressure with respect to the quarter point of the mean aerodynamic chord is established through the use of section data, simple sweep theory, and a correction to the location of the section center of pressure for the effects of finite aspect ratio. The spanwise position of the center of pressure with respect to the plane of symmetry can be established from consideration of the spanwise distribution of the lift as affected by the deflection of a control surface.

Reference 13 presents a method whereby the spanwise loading due to flap deflection can be found for wings having a constant sweep of the quarter-chord line. This reference shows that, for a wing having a constant-percent chord, full-span control surface, the spanwise position of the center of pressure of the lift due to flap deflection is coincident with the spanwise center of pressure due to angle of attack. Thus, the spanwise location of the center of pressure, for the subject model, may be calculated by the Weissinger method.

The longitudinal position of the wing center of pressure must be determined by less direct means. The known characteristics of the reference section, the NACA 64A010, measured in planes perpendicular to a line swept back 45° are used. This line is the locus of the quarter-chord points of the reference sections. The center of pressure due to flap deflection for an NACA 64A010 airfoil section having a 0.30-chord, plain flap is located at 0.40 chord (reference 14). When a linear variation of C_m with C_L at $C_L = 0$ and $C_m = 0$ is assumed, the moment equation referred to the quarter-chord point of the airfoil section is

$$\left(C_{m_{0.25\bar{c}}}\right)_o = -C_{L_o}\left(c.p._o - 0.25\right) \tag{B1}$$

where the subscript o indicates the value for two-dimensional flow. For a finite wing, use is made of equation 1 of reference 15

$$c.p._{f_1}' = \frac{a_o'}{a_u} (c.p._{f_o}' - 0.25) + 0.25 \tag{B2}$$

where

$c.p._{f_1}'$ center of pressure location of incremental lift load due to flap deflection, fraction of chord of sections parallel to the plane of symmetry

$c.p._{f_o}'$ center of pressure location, fraction of chord of section parallel to the plane of symmetry

a_o' lift-curve slope of sections parallel to the plane of symmetry

a_u theoretical lift-curve slope of the finite wing, computed by the method of reference 10 for incompressible flow

The section lift-curve slope of a swept wing of infinite span may be estimated, from simple sweep theory, by the following expression

$$a_o' = a_o \cos \Lambda \tag{B3}$$

The geometric relationship between the chordwise center-of-pressure position on a tapered swept-back wing expressed as a fraction of a chord parallel to the plane of symmetry in terms of a fraction of a chord inclined at the angle of sweepback Λ is

$$c.p._{f_o}' = \frac{c.p._o\left(1 + \frac{\tan^2 \Lambda - \tan \Lambda \tan T}{1 + \tan \Lambda \tan T}\right)}{\left(1 - \frac{\tan \Lambda \tan \theta - \tan^2 \Lambda}{1 + \tan \theta \tan \Lambda}\right) + c.p._o \tan \Lambda\left(\frac{\tan \Lambda - \tan T}{1 + \tan \Lambda \tan T} + \frac{\tan \theta - \tan \Lambda}{1 + \tan \theta \tan \Lambda}\right)} \tag{B4}$$

where

θ sweep of the leading edge of the finite-span wing with respect to a perpendicular to the plane of symmetry, degrees

Λ sweep of the locus of the quarter-chord points of the 64A010 sections, with respect to a perpendicular to the plane of symmetry, degrees

T sweep of the trailing edge of the finite-span wing with respect to a perpendicular to the plane of symmetry, degrees

By substitution of the values obtained for a_o' and $c.p._{f_o}'$ from equations (B3) and (B4), respectively, in equation (B2), this equation can then be rewritten as:

$$c.p._{f_1}' = \frac{a_o \cos \Lambda}{a_u}\left[\frac{c.p._o\left(1 + \frac{\tan^2 \Lambda - \tan \Lambda \tan T}{1 + \tan \Lambda \tan T}\right)}{\left(1 + \frac{\tan \Lambda \tan \theta - \tan^2 \Lambda}{1 - \tan \theta \tan \Lambda}\right) + c.p._o \tan \Lambda\left(\frac{\tan \Lambda - \tan T}{1 + \tan \Lambda \tan T} + \frac{\tan \theta - \tan \Lambda}{1 + \tan \theta \tan \Lambda}\right)} - 0.25\right] + 0.25 \tag{B5}$$

Through solution of equation (B5) a constant-percent chord line approximating the locus of the centers of pressure of sections parallel to the plane of symmetry was established. The effect of finite aspect ratio on the slope of this line near the root and tip sections is neglected. The wing center of pressure is defined as the point of intersection of the locus of the section centers of pressure with a chord line (taken parallel to the plane of symmetry) that passes through the spanwise center of pressure (fig. 27).

Pitching moments for a wing of finite aspect ratio are referred to an axis that passes through the quarter point of the mean aerodynamic chord and is perpendicular to the plane of symmetry. Therefore, in order to present the pitching moment in terms of a percent of the mean aerodynamic chord, it is necessary to consider the change in percent local chord that is introduced when the airfoil center of pressure is projected to the mean aerodynamic chord (fig. 27). This change in chordwise position is calculated from the relation

$$x = \frac{(y_{c.p.} - y_{\bar{c}})}{\bar{c}} \tan \psi \tag{B6}$$

where

$y_{c.p.}$ lateral distance to the wing center of pressure measured perpendicularly from the plane of symmetry, feet

$y_{\bar{c}}$ lateral distance to the mean aerodynamic chord measured perpendicularly from the plane of symmetry, feet

ψ sweep of the locus of the section centers of pressure due to flap deflection with respect to a perpendicular to the plane of symmetry, degrees

x fraction of the mean aerodynamic chord

The longitudinal distance to the wing center of pressure on the mean aerodynamic chord X measured from the leading edge of the mean aerodynamic chord and expressed as a fraction of the mean aerodynamic chord can be written as:

$$X = c.p._{f_1}' + x \tag{B7}$$

where $c.p._{f_1}'$ and x, defined by equations (B5) and (B6), respectively, are both fractions of the mean aerodynamic chord.

If moments are taken about the quarter point of the mean aerodynamic chord of the finite wing, the equation can be written as

$$C_{m_{0.25\bar{c}}} = - C_L (X - 0.25) \tag{B8}$$

If a linear variation of C_m with C_L at $C_L = 0$ and $C_m = 0$ is assumed, then from a differentiation of equation (B8) with respect to δ,

$$C_{m_\delta} = - C_{L_\delta} (X - 0.25) \tag{B9}$$

Substituting for X, defined by equation (B7) in equation (B9)

$$C_{m_\delta} = - C_{L_\delta} \left\{ \frac{a_o \cos \Lambda}{a_u} \left[\frac{c.p._o \left(1 + \frac{\tan^2 \Lambda - \tan \Lambda \tan T}{1 + \tan \theta \tan \Lambda}\right)}{\left(1 - \frac{\tan \Lambda \tan \theta - \tan^2 \Lambda}{1 + \tan \theta \tan \Lambda}\right) + c.p._o \tan \Lambda \left(\frac{\tan \Lambda - \tan T}{1 + \tan \theta \tan T}\right) + \left(\frac{\tan \theta - \tan \Lambda}{1 + \tan \theta \tan \Lambda}\right)} - 0.25 \right] + \left(\frac{y_{c.p.} - y_{\bar{c}}}{\bar{c}}\right) \tan \psi \right\} \tag{B10}$$

In modifying equation (B10) to account for the effects of compressibility, the assumption is made that the position of the center of pressure for a given flap deflection is independent of the Mach number. The modified equation (B10) then becomes

$$\left(C_{m_\delta}\right)_c = -\left(C_{L_\delta}\right)_c \left\{ \frac{a_o \cos \Lambda}{a_u} \right.$$

$$\left[\frac{c.p._o\left(1 + \frac{\tan^2 \Lambda - \tan \Lambda \tan T}{1 + \tan \Lambda \tan T}\right)}{\left(1 - \frac{\tan \Lambda \tan \theta - \tan^2 \Lambda}{1 + \tan \theta \tan \Lambda}\right) + c.p._o \tan \Lambda \left(\frac{\tan \Lambda - \tan T}{1 + \tan \theta \tan T}\right) + \left(\frac{\tan \theta - \tan \Lambda}{1 + \tan \theta \tan \Lambda}\right)} - 0.25 \right] +$$

$$\left. \left(\frac{y_{c.p.} - y_{\bar{c}}}{\bar{c}}\right) \right\} \tan \psi \qquad \text{(B11)}$$

where $\left(C_{L_\delta}\right)_c$ may be computed by means of equation (A1) in appendix A and a_u can be computed directly by the method of reference 10.

REFERENCES

1. Dods, Jules B., Jr.: Wind-Tunnel Investigation of Horizontal Tails. I – Unswept and 35° Swept-Back Plan Forms of Aspect Ratio 3. NACA RM A7K24, 1948.

2. Dods, Jules B., Jr.: Wind-Tunnel Investigation of Horizontal Tails. II – Unswept and 35° Swept-Back Plan Forms of Aspect Ratio 4.5. NACA RM A8B11, 1948.

3. Dods, Jules B., Jr.: Wind-Tunnel Investigation of Horizontal Tails. III – Unswept and 35° Swept-Back Plan Forms of Aspect Ratio 6. NACA RM A8H30, 1948.

4. Dods, Jules B., Jr.: Wind-Tunnel Investigation of Horizontal Tails. IV – Unswept Plan Form of Aspect Ratio 2 and a Two-Dimensional Model. NACA RM A8J21, 1948.

5. Dods, Jules B., Jr.: Wind-Tunnel Investigation of Horizontal Tails. V – 45° Swept-Back Plan Form of Aspect Ratio 2. NACA RM A9D05, 1949.

6. Tinling, Bruce E., and Dickson, Jerald K.: Tests of a Model Horizontal Tail of Aspect Ratio 4.5 in the Ames 12-Foot Pressure Wind Tunnel. I – Quarter-Chord Line Swept Back 35°. NACA RM A9G13, 1949.

7. Tinling, Bruce E., and Dickson, Jerald K.: Tests of a Model Horizontal Tail of Aspect Ratio 4.5 in the Ames 12-Foot Pressure Wind Tunnel. II – Elevator Hinge-Line Normal to the Plane of Symmetry. NACA RM A9H11a, 1949.

8. Abbott, Ira H., von Doenhoff, Albert E., and Stivers, Louis S., Jr.: Summary of Airfoil Data. NACA Rep. 824, 1945. (Formerly ACR L5C05)

9. Sivells, James C., and Deters, Owen J.: Jet-Boundary and Plan-Form Corrections for Partial-Span Models With Reflection Plane, End Plate, or no End Plate in a Closed Circular Wind Tunnel. NACA Rep. 843, 1946. (Formerly NACA TN 1077)

10. DeYoung, John, and Harper, Charles W.: Theoretical Symmetric Span Loading at Subsonic Speeds for Wings Having Arbitrary Plan Form. NACA Rep. 921, 1948. (Formerly NACA TN's 1476, 1491, and 1772)

11. Herriot, John G.: Blockage Corrections for Three-Dimensional-Flow Closed-Throat Wind Tunnels, With Consideration of the Effect of Compressibility. NACA Rep. 995, 1950. (Formerly NACA RM A7B28).

12. Dods, Jules B., Jr.: Estimation of Low-Speed Lift and Hinge-Moment Parameters for Full-Span Trailing-Edge Flaps on Lifting Surfaces With and Without Sweepback. NACA TN 2288, 1951.

13. DeYoung, John: Theoretical Symmetric Span Loading Due to Flap Deflection for Wings of Arbitrary Plan Form at Subsonic Speeds. NACA TN 2278, 1951.

14. Peterson, Robert F.: The Boundary-Layer and Stalling Characteristics of the NACA 64A010 Airfoil Section. NACA TN 2235, 1950.

15. Pitkin, Marvin, and Maggin, Bernard: Analysis of Factors Affecting Net Lift Increment Attainable With Trailing-Edge Split Flaps on Tailless Airplanes. NACA ARR L4I18, 1944.

TABLE I.- COORDINATES FOR THE NACA 64A010 AIRFOIL SECTION

[All dimensions in percent chord]

Upper and Lower Surfaces	
Station	Ordinate
0	0
.50	.804
.75	.969
1.25	1.225
2.50	1.688
5.00	2.327
7.50	2.805
10.00	3.199
15.00	3.813
20.00	4.272
25.00	4.606
30.00	4.837
35.00	4.968
40.00	4.995
45.00	4.894
50.00	4.684
55.00	4.388
60.00	4.021
65.00	3.597
70.00	3.127
75.00	2.623
80.00	2.103
85.00	1.582
90.00	1.062
95.00	.541
100.00	.021
L. E. radius:	0.687
T. E. radius:	0.023

TABLE II.- COORDINATES FOR THE AIRFOIL SECTIONS PARALLEL TO PLANE OF SYMMETRY OF MODEL

[All dimensions in percent chord]

Upper and Lower Surfaces	
Station	Ordinate
0	0
.63	.673
.95	.811
1.57	1.023
3.14	1.406
6.23	1.925
9.29	2.306
12.31	2.612
18.23	3.074
24.00	3.401
29.63	3.622
35.13	3.757
40.49	3.813
45.72	3.788
50.83	3.667
55.82	3.469
60.69	3.212
65.46	2.910
70.12	2.574
74.67	2.213
79.12	1.836
83.48	1.456
87.74	1.083
91.92	.720
96.00	.363
100.00	.014
L. E. radius:	0.485
T. E. radius:	0.016

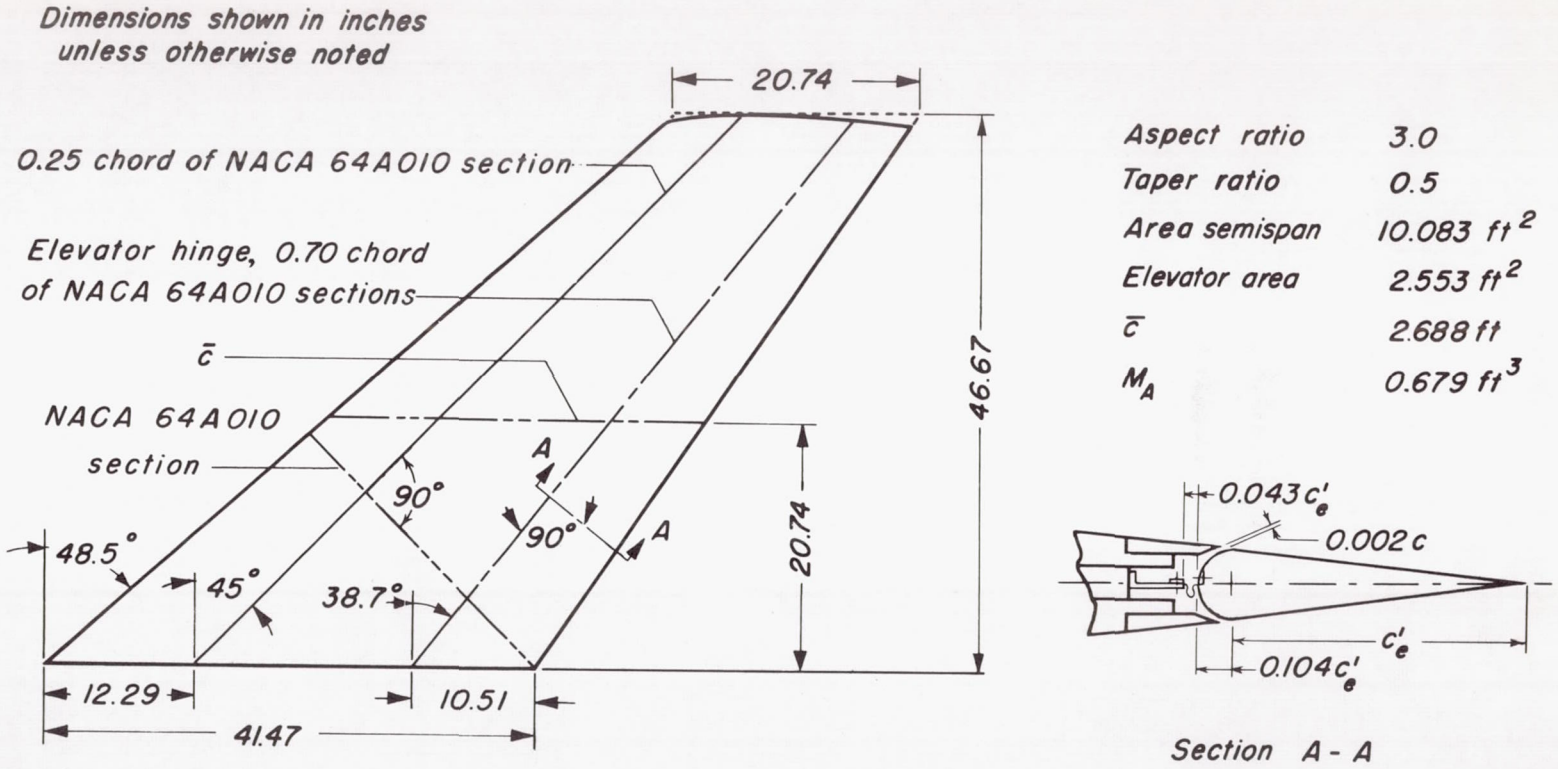

Figure 1.- The horizontal-tail model.

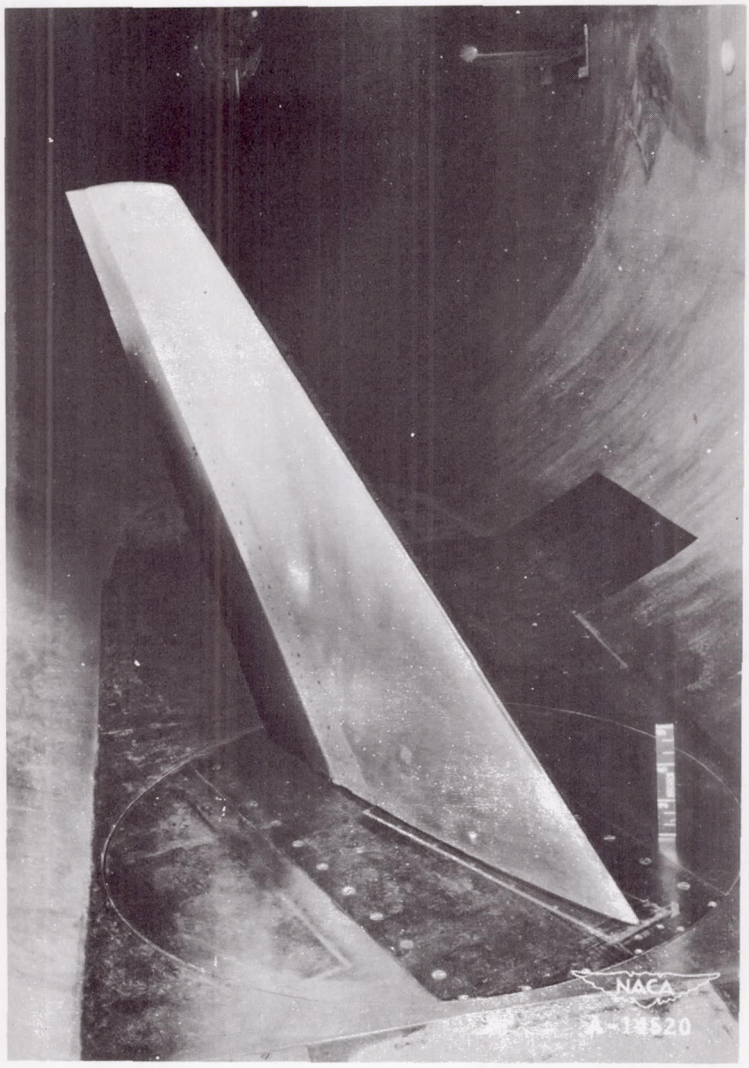

Figure 2.- The horizontal tail model mounted in the Ames 12-foot pressure wind tunnel.

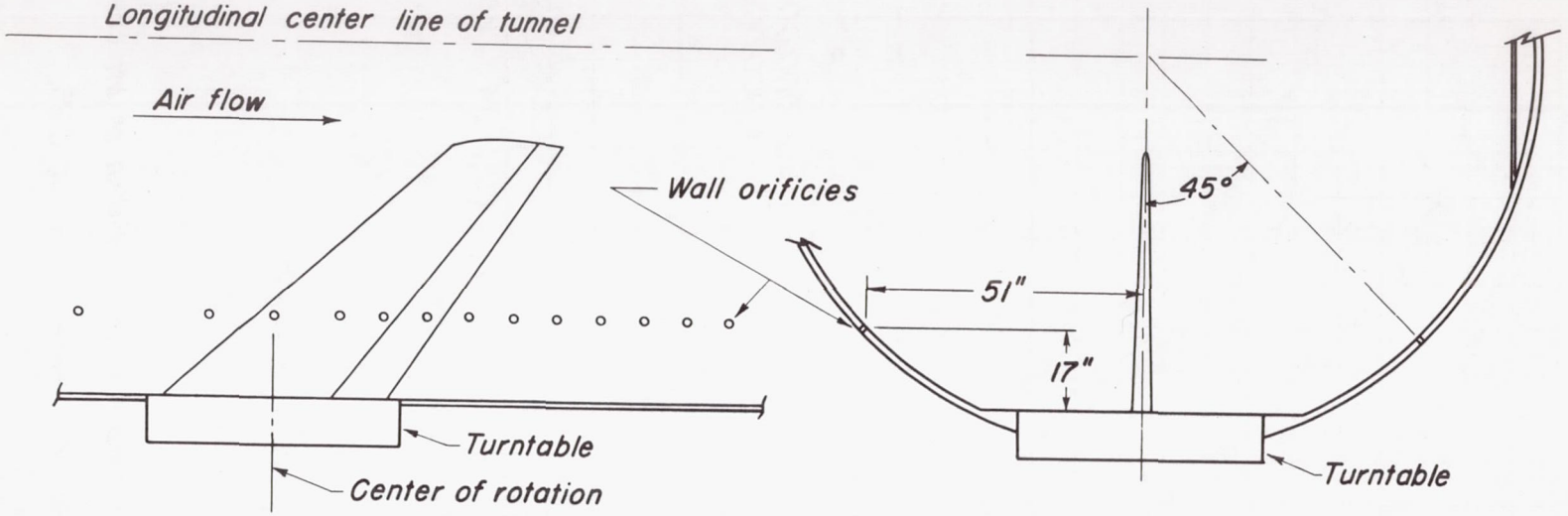

Figure 3.- The location of the wall orifices relative to the model in the Ames 12-foot pressure wind tunnel.

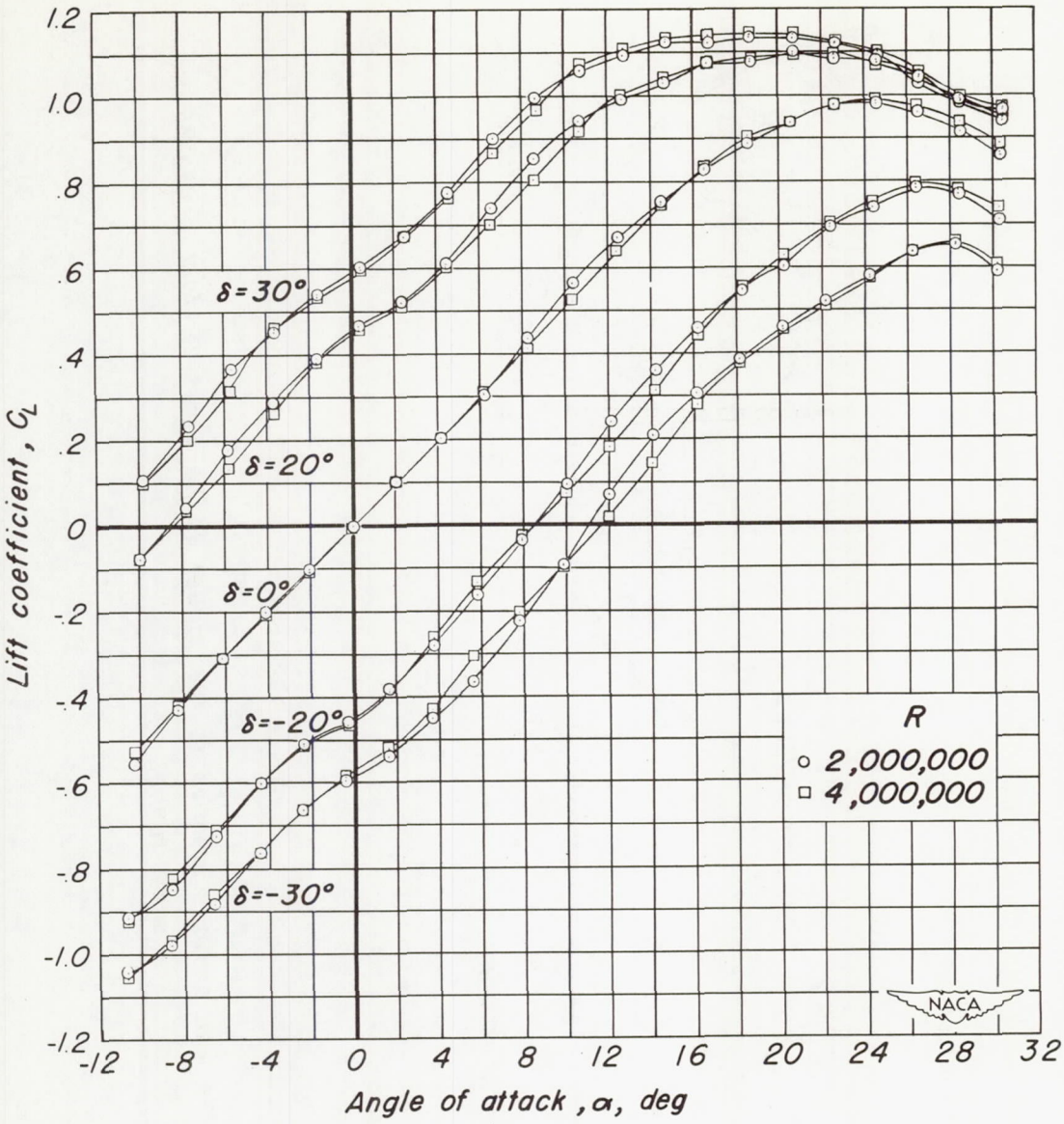

(a) R, 2,000,000 ; R, 4,000,000

Figure 4.—The effect of Reynolds number on the variation of lift coefficient with angle of attack at a Mach number of 0.25.

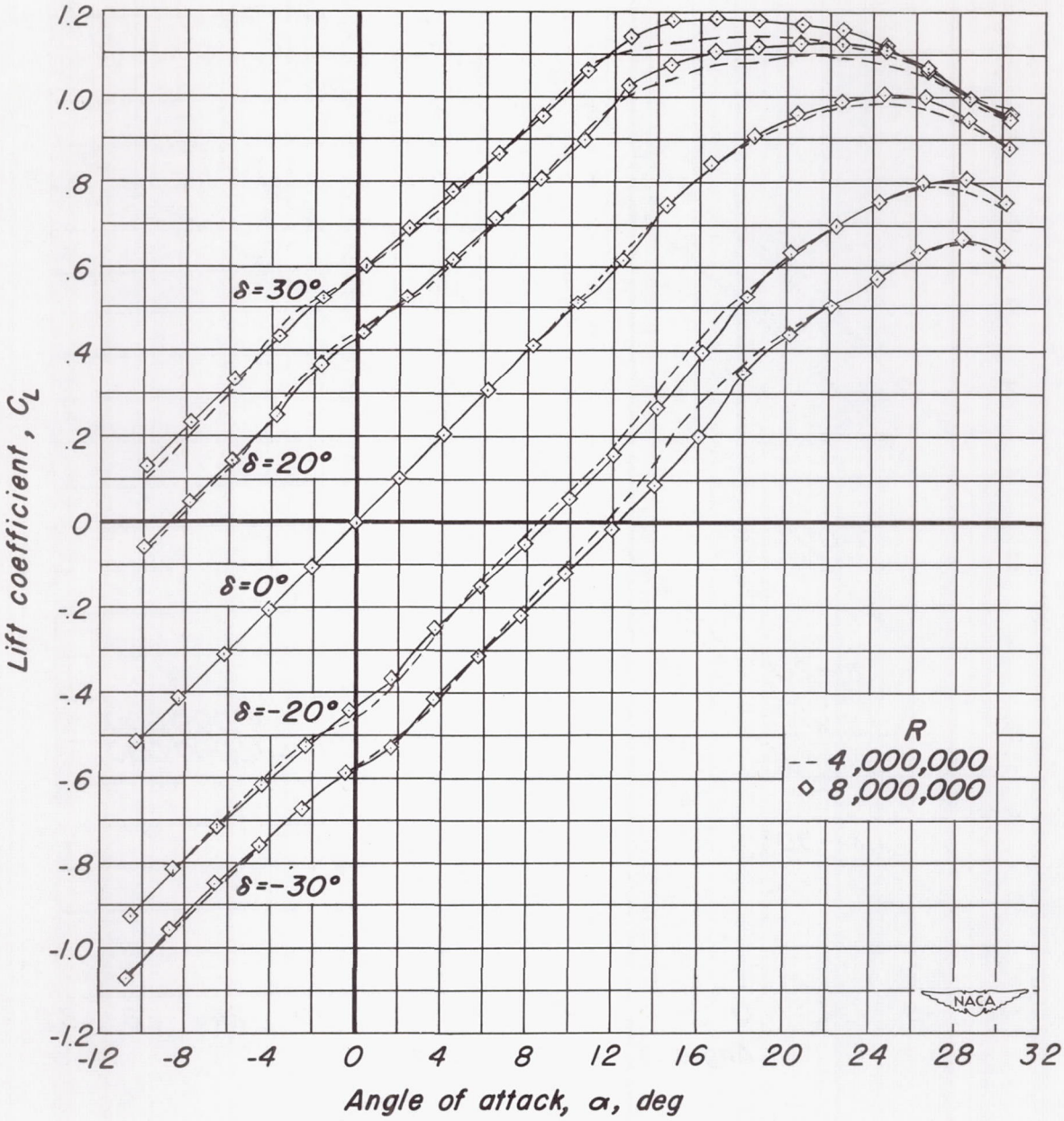

(b) R, 4,000,000 ; R, 8,000,000

Figure 4.—Continued.

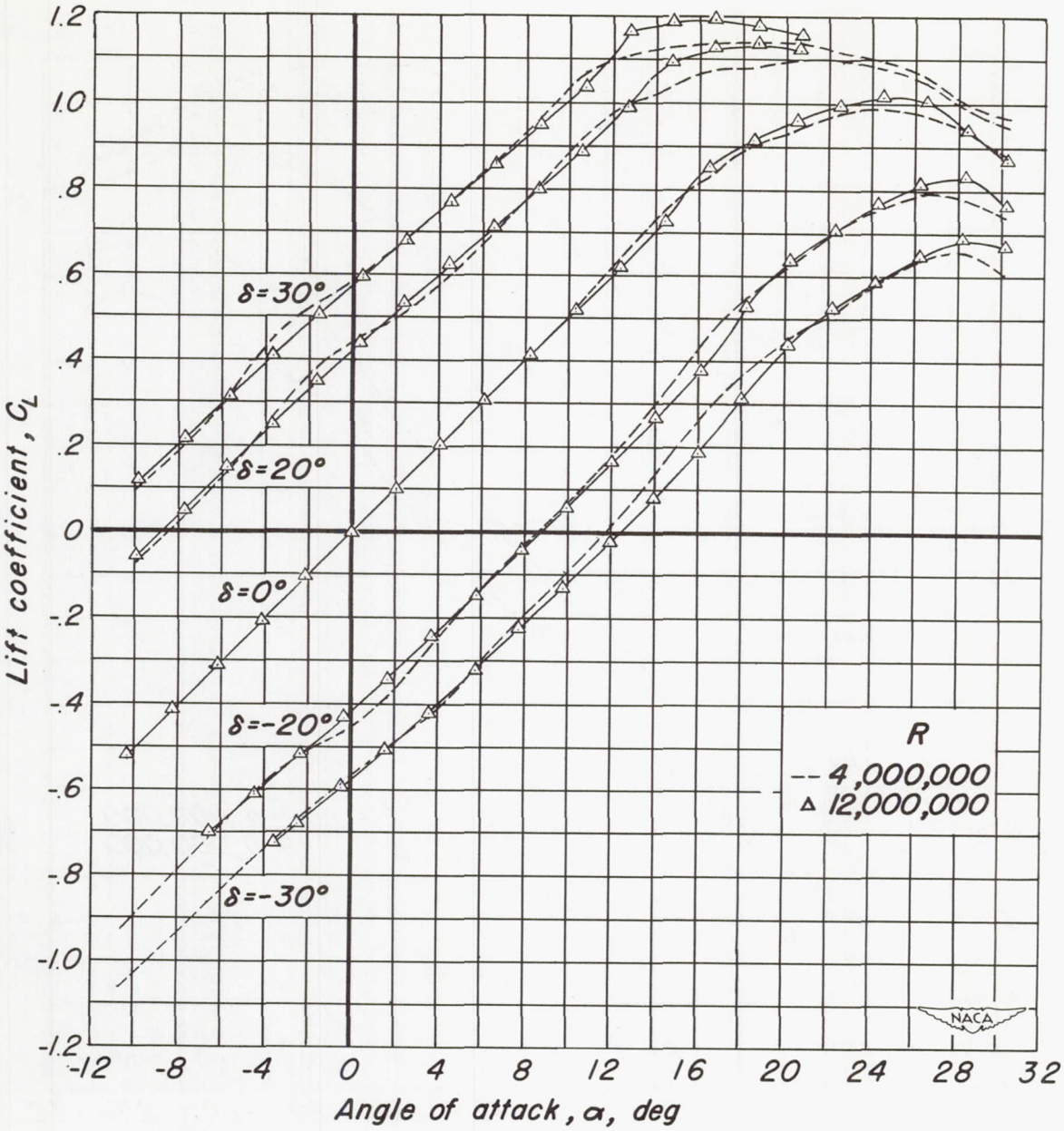

(c) R, 4,000,000; R, 12,000,000

Figure 4.—Continued.

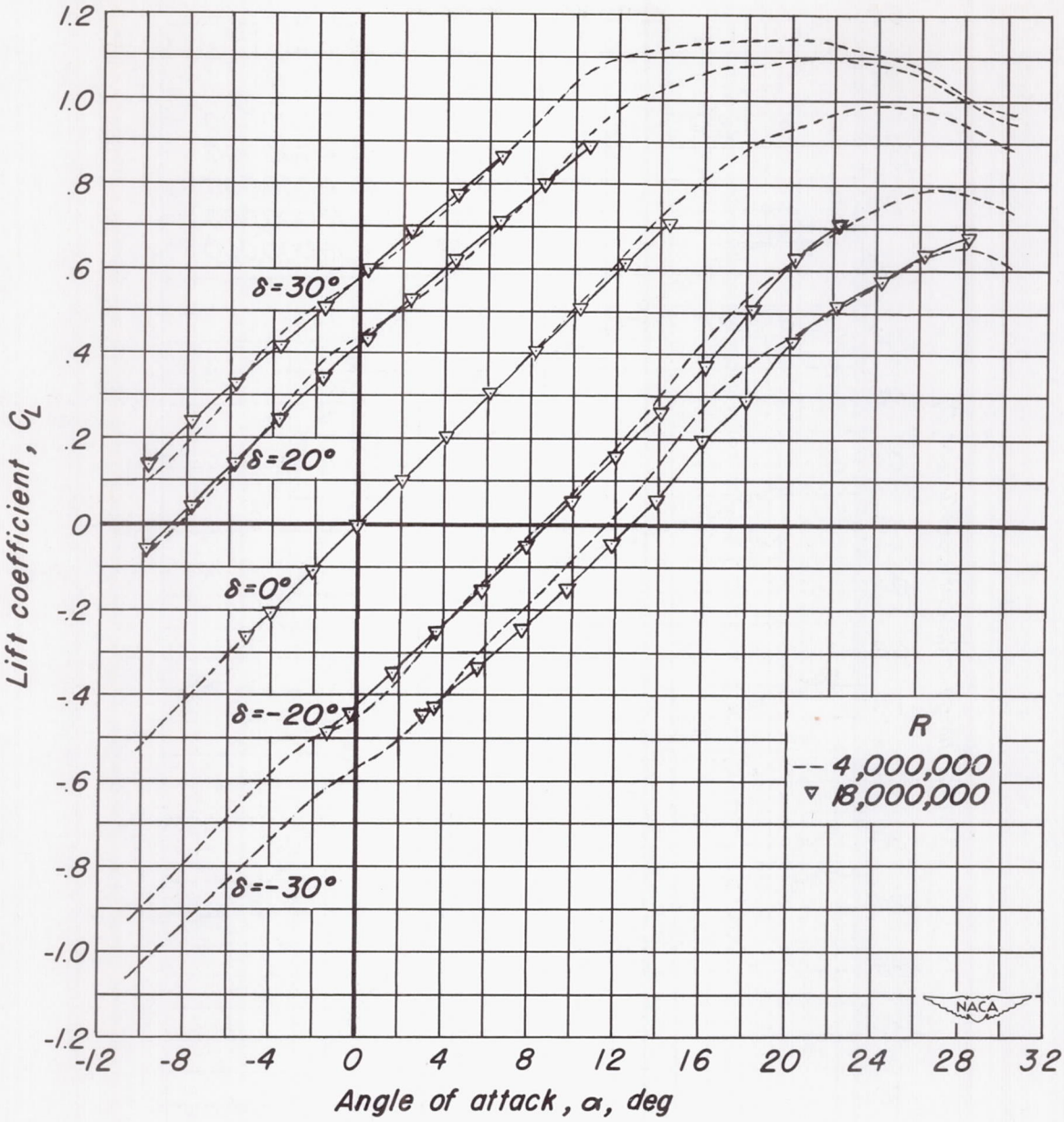

(d) R, 4,000,000 ; R, 18,000,000

Figure 4.—Concluded.

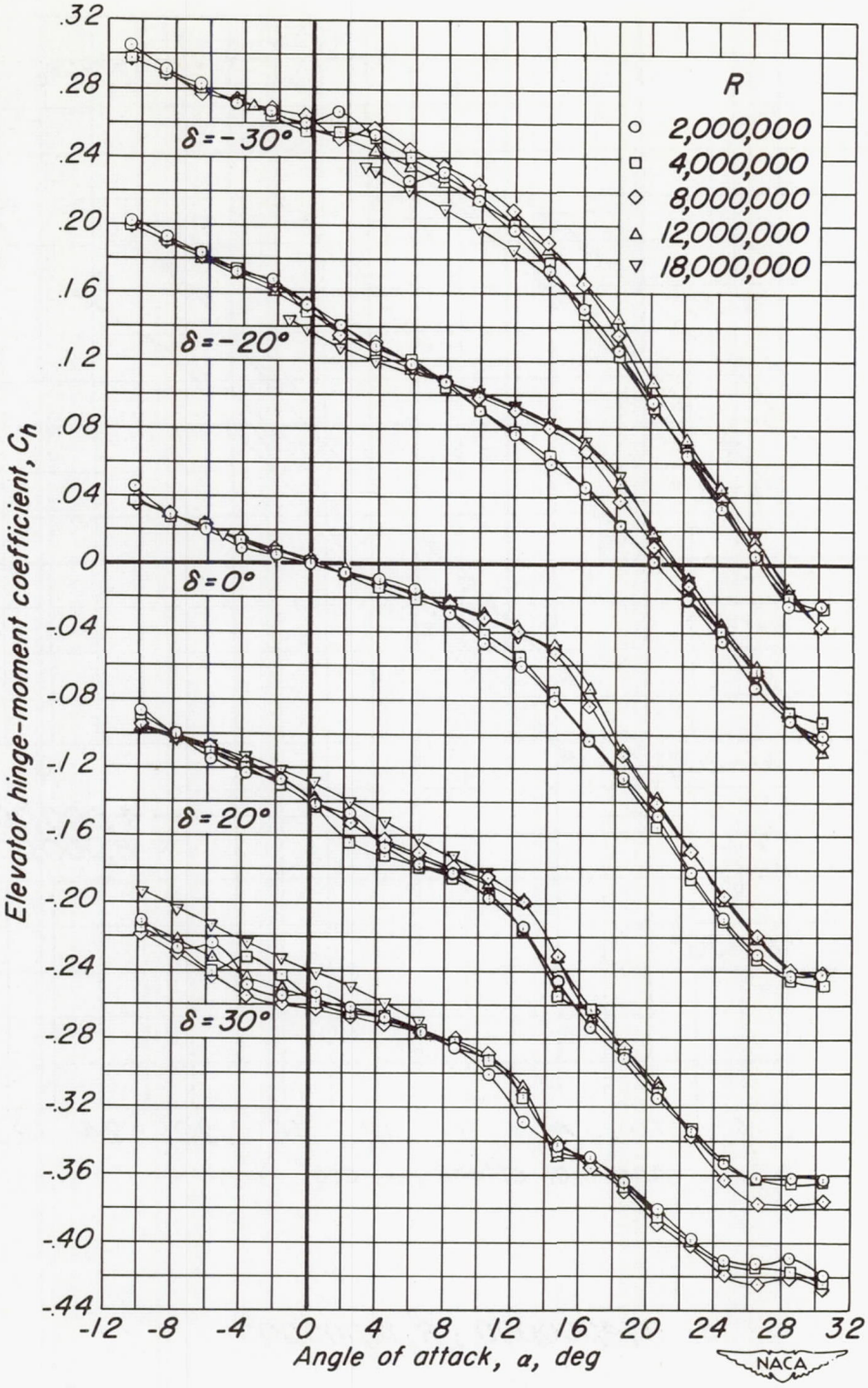

Figure 5.—The effect of Reynolds number on the variation of elevator hinge-moment coefficient with angle of attack at a Mach number of 0.25.

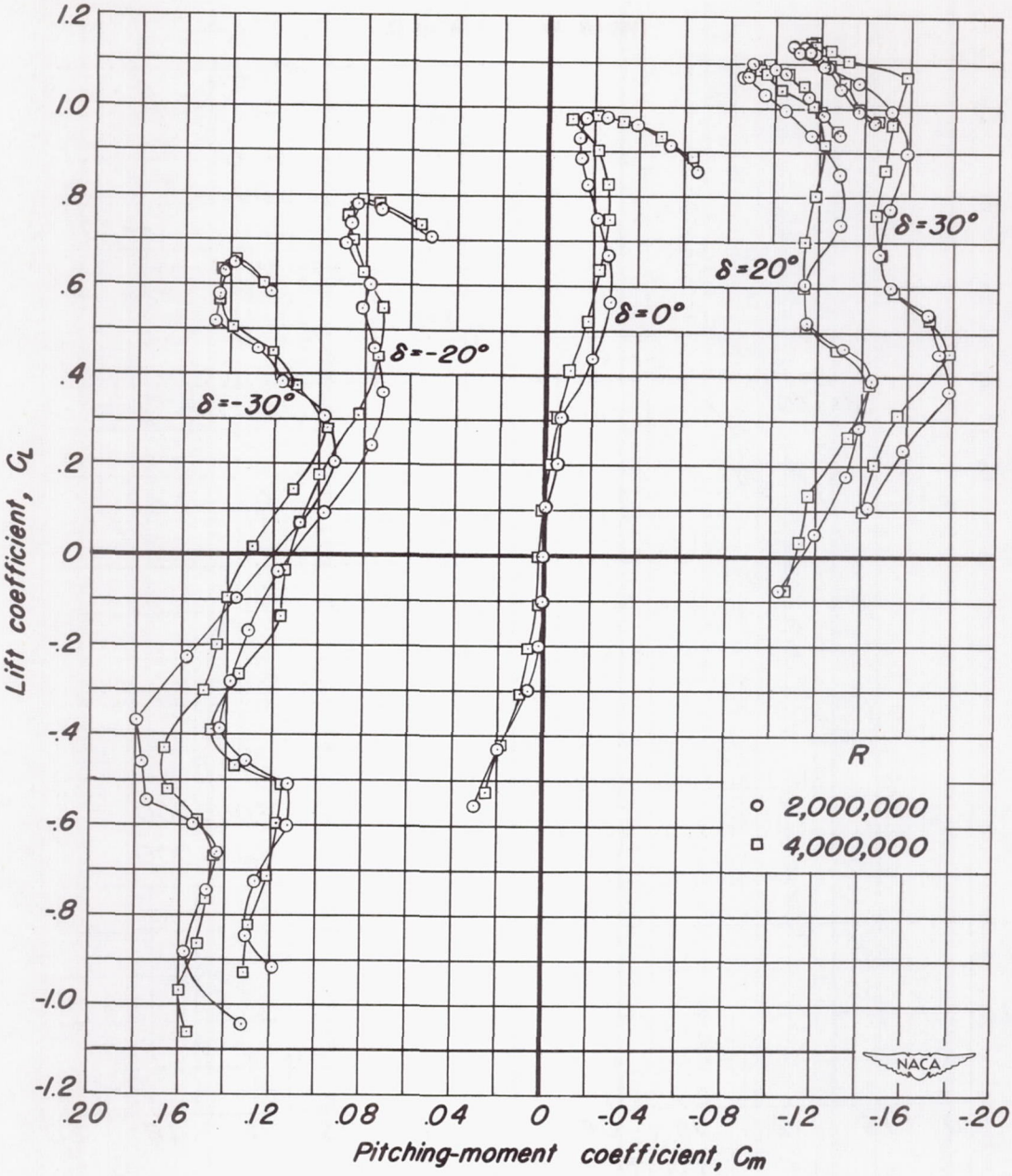

(a) R, 2,000,000 ; R, 4,000,000

Figure 6.— The effect of Reynolds number on the variation of lift coefficient with pitching-moment coefficient at a Mach number of 0.25.

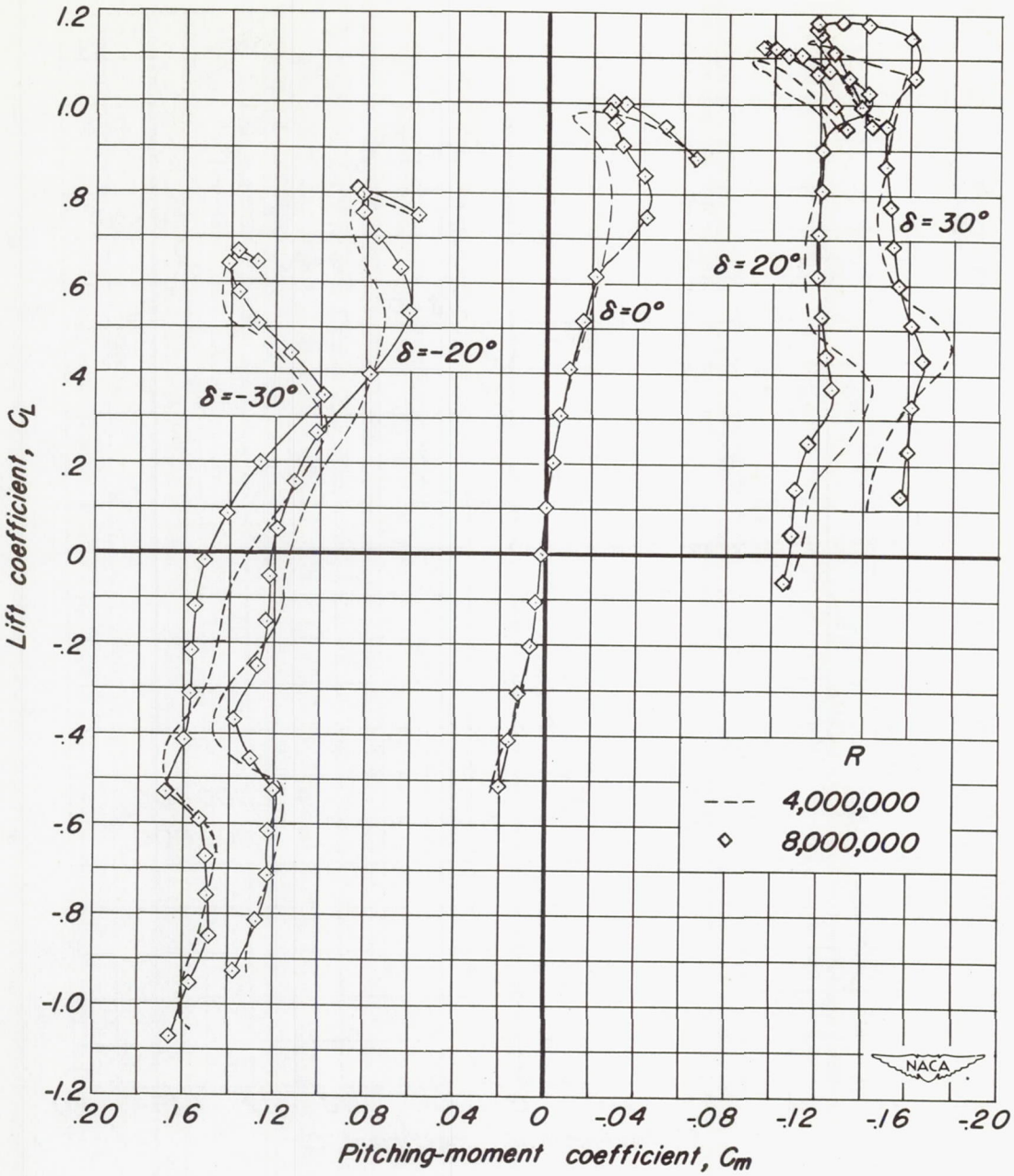

(b) R, 4,000,000 ; R, 8,000,000

Figure 6.— Continued.

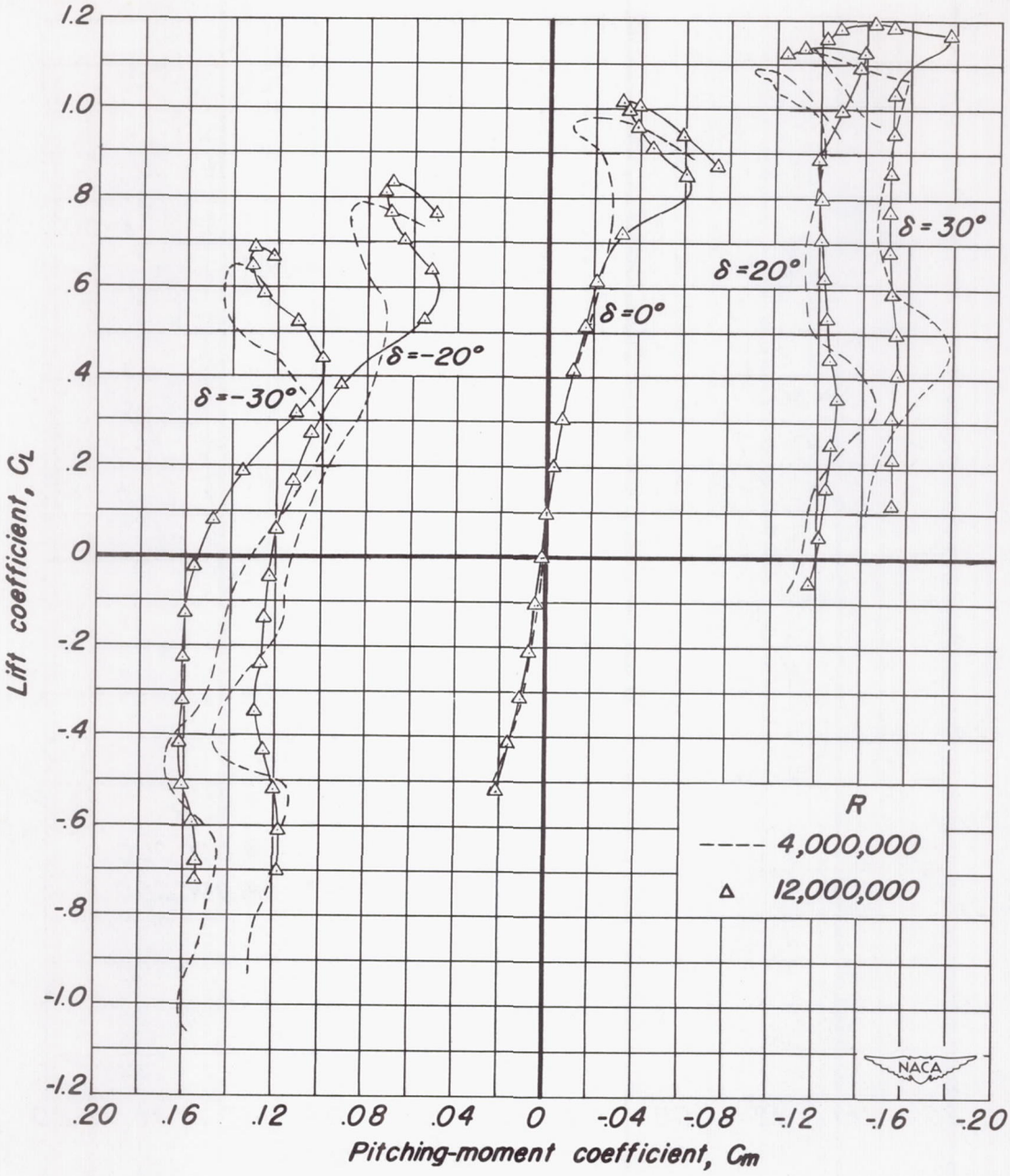

(c) R, 4,000,000; R, 12,000,000

Figure 6. — Continued.

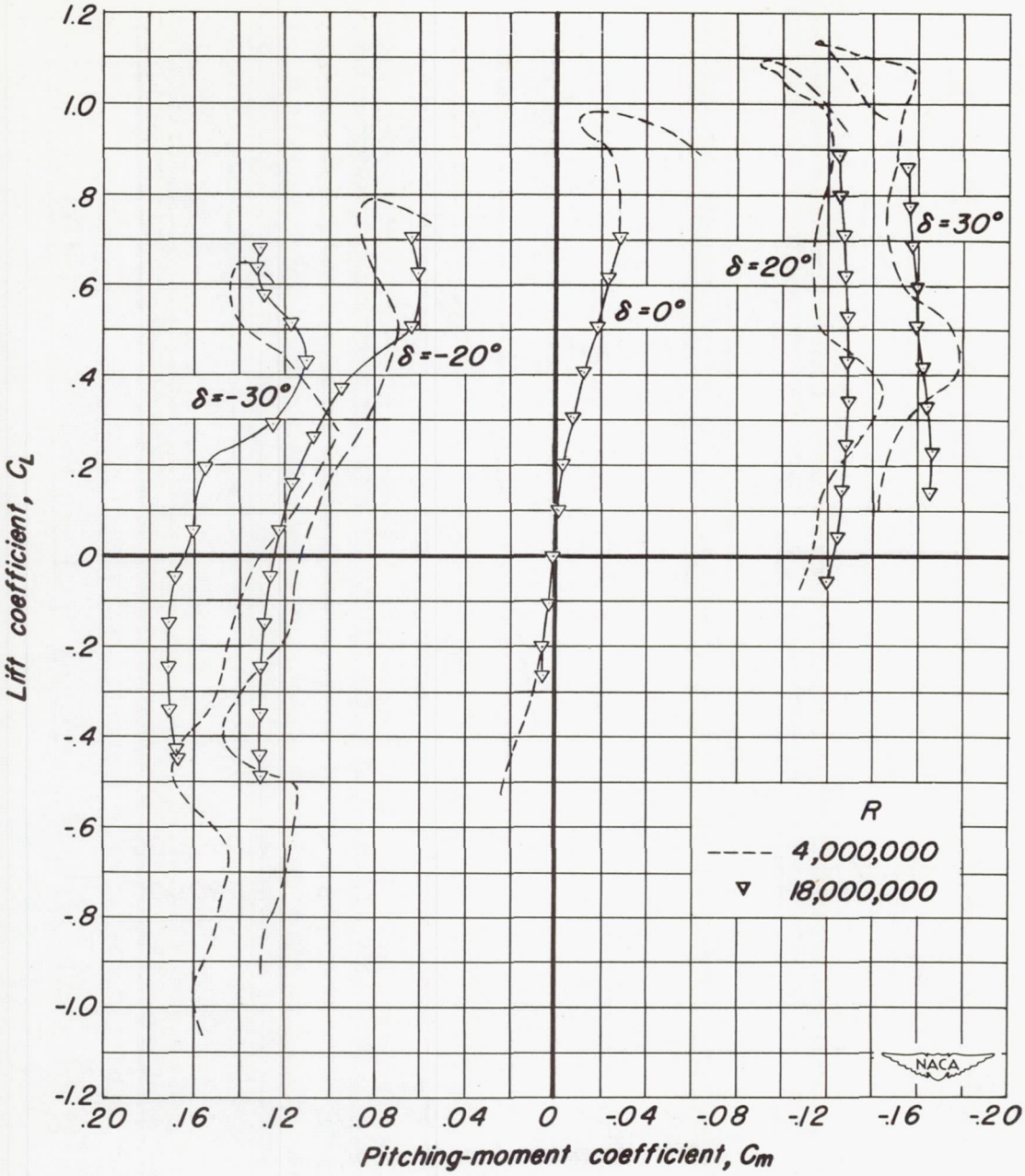

(d) R, 4,000,000 ; R, 18,000,000

Figure 6. — Concluded.

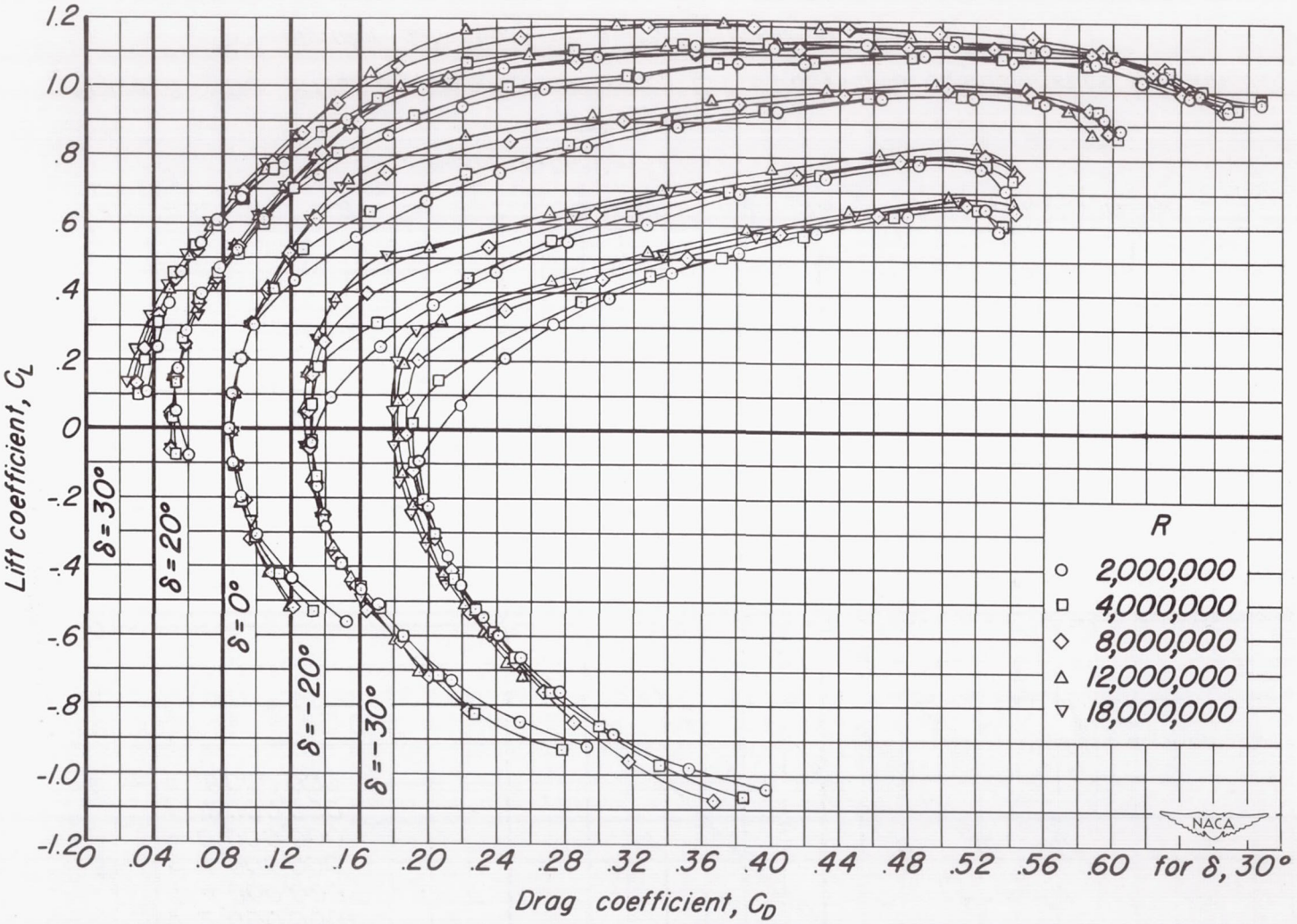

Figure 7.—The effect of Reynolds number on the variation of lift coefficient with drag coefficient at a Mach number of 0.25.

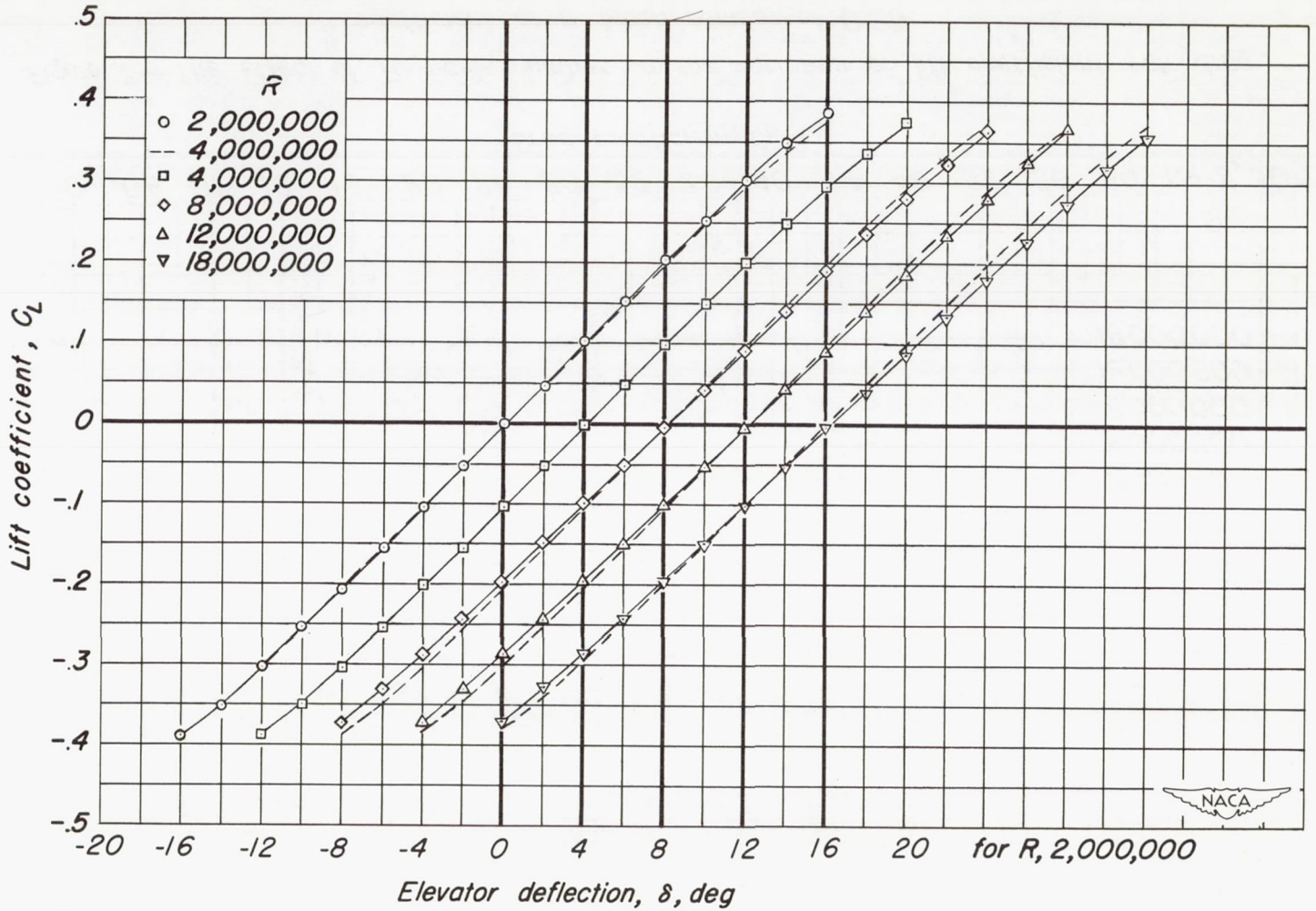

(a) C_L vs δ

Figure 8.— The effect of Reynolds number on the aerodynamic characteristics for various elevator deflections at a Mach number of 0.25. α_u, 0°.

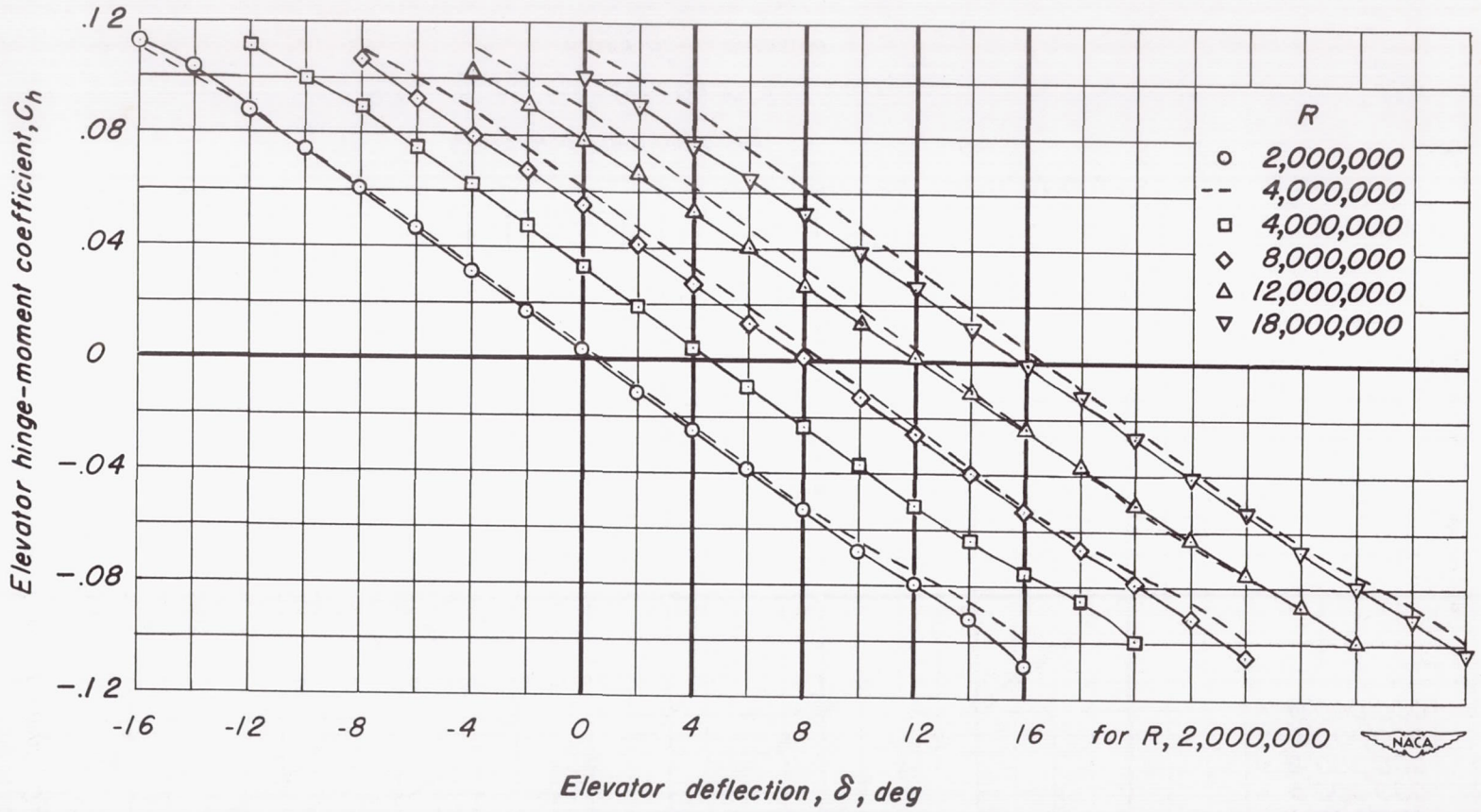

(b) C_h vs δ

Figure 8.—Continued.

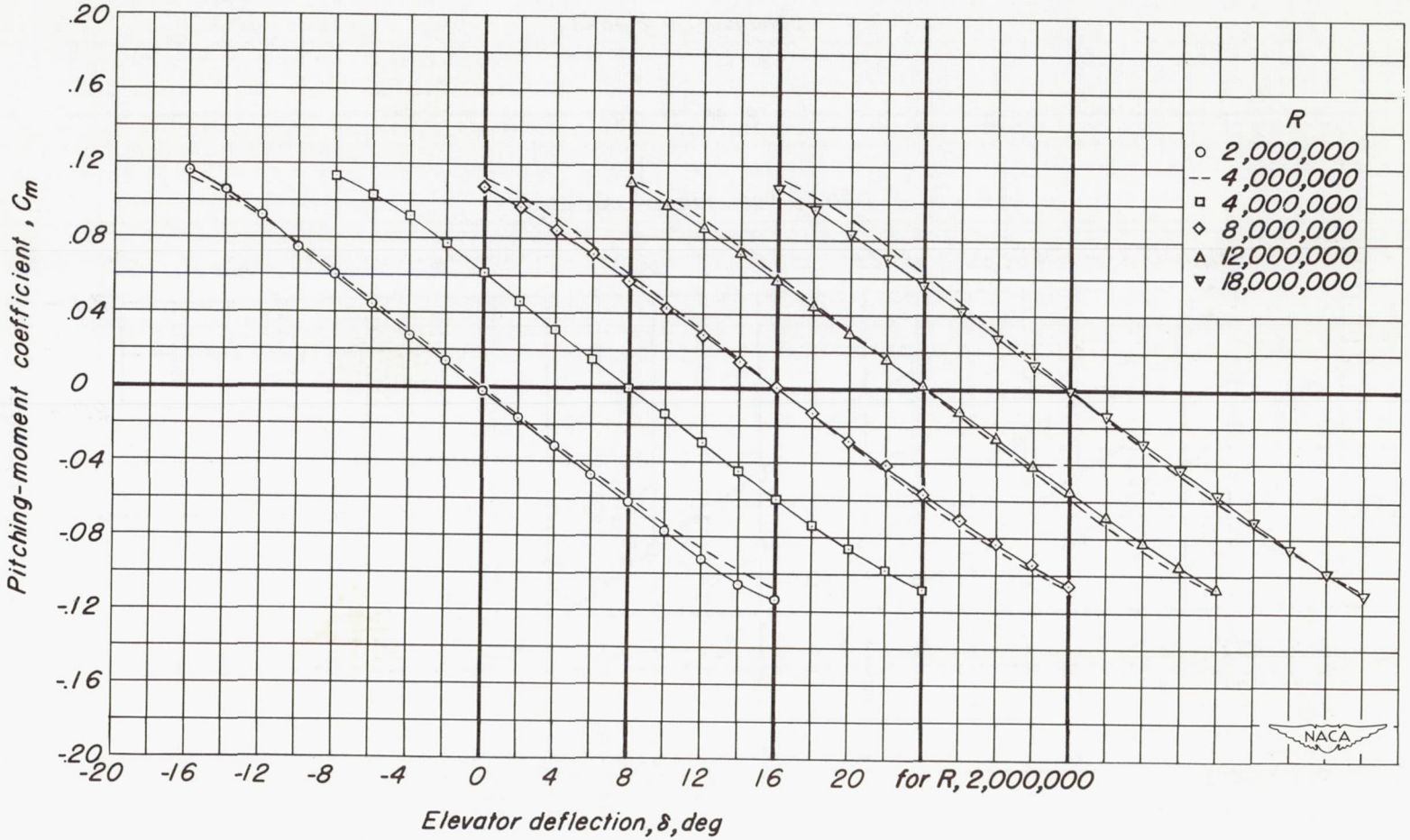

(c) C_M vs δ

Figure 8.— Concluded.

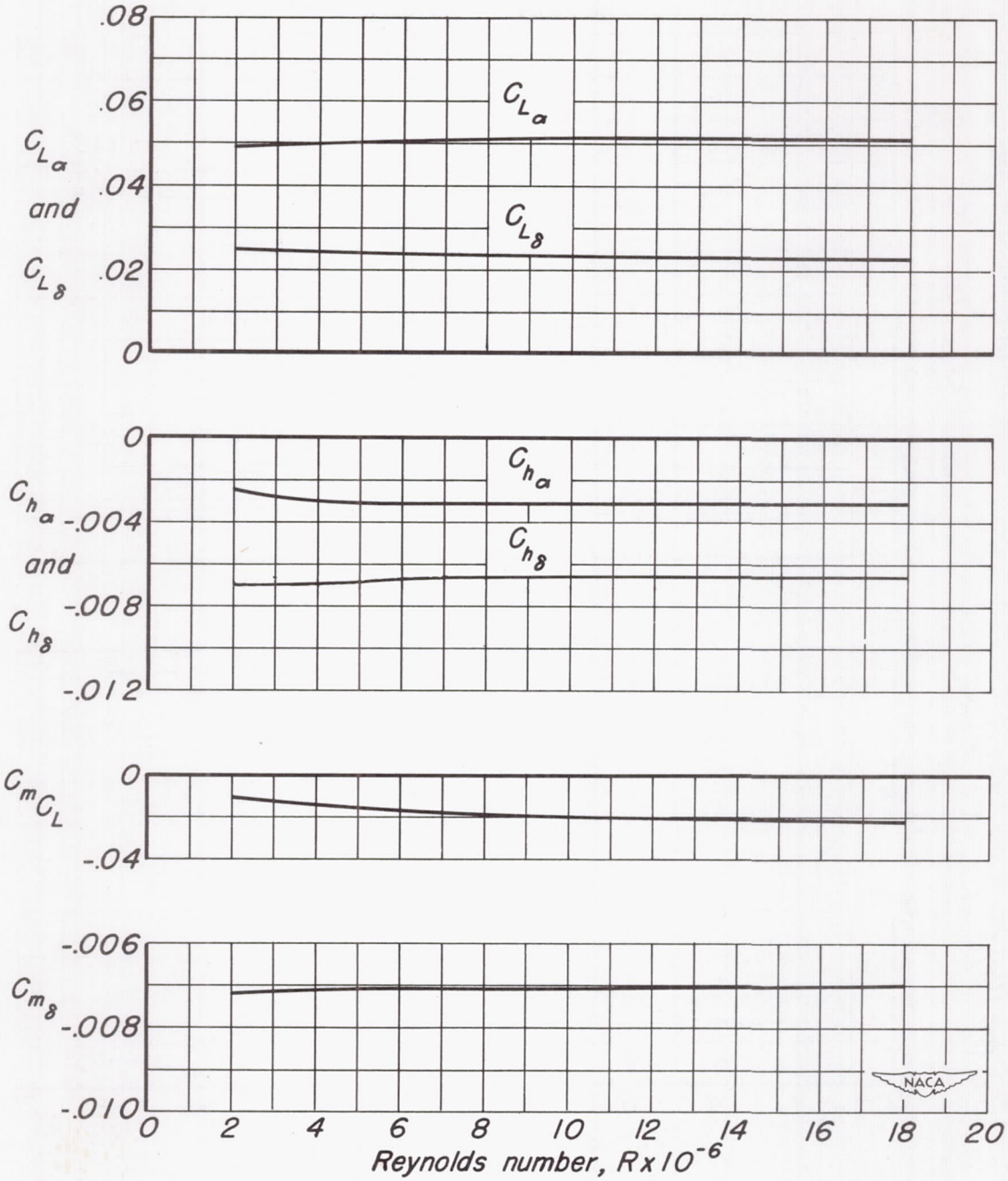

Figure 9.- The variation of C_{L_α}, C_{L_δ}, C_{h_α}, C_{h_δ}, $C_{m_{C_L}}$, and C_{m_δ} with Reynolds number at a Mach number of 0.25.

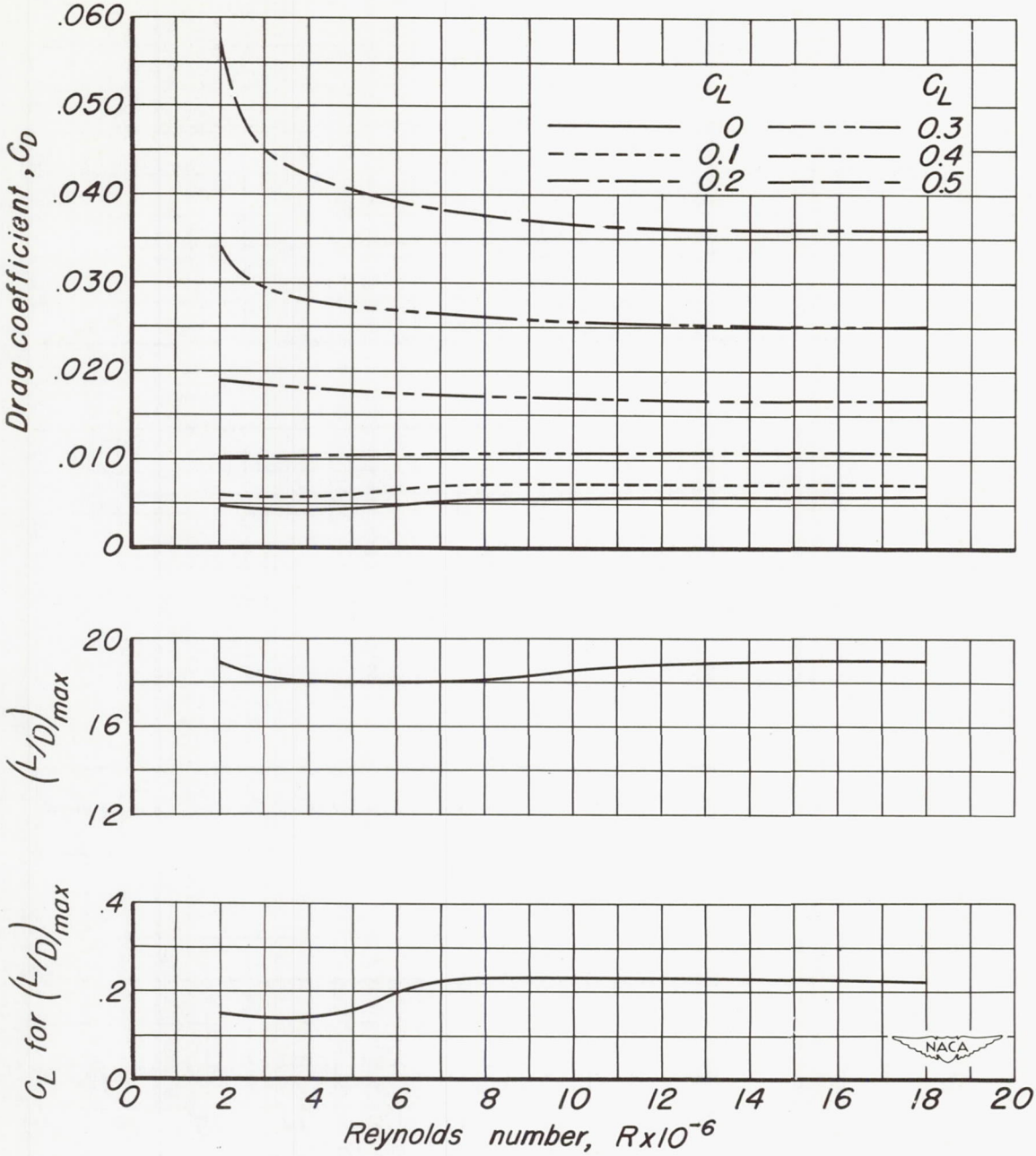

Figure 10.- The variations of drag, maximum lift-to-drag ratio, and lift coefficient for maximum lift-to-drag ratio with Reynolds number at a Mach number of 0.25; δ, 0°.

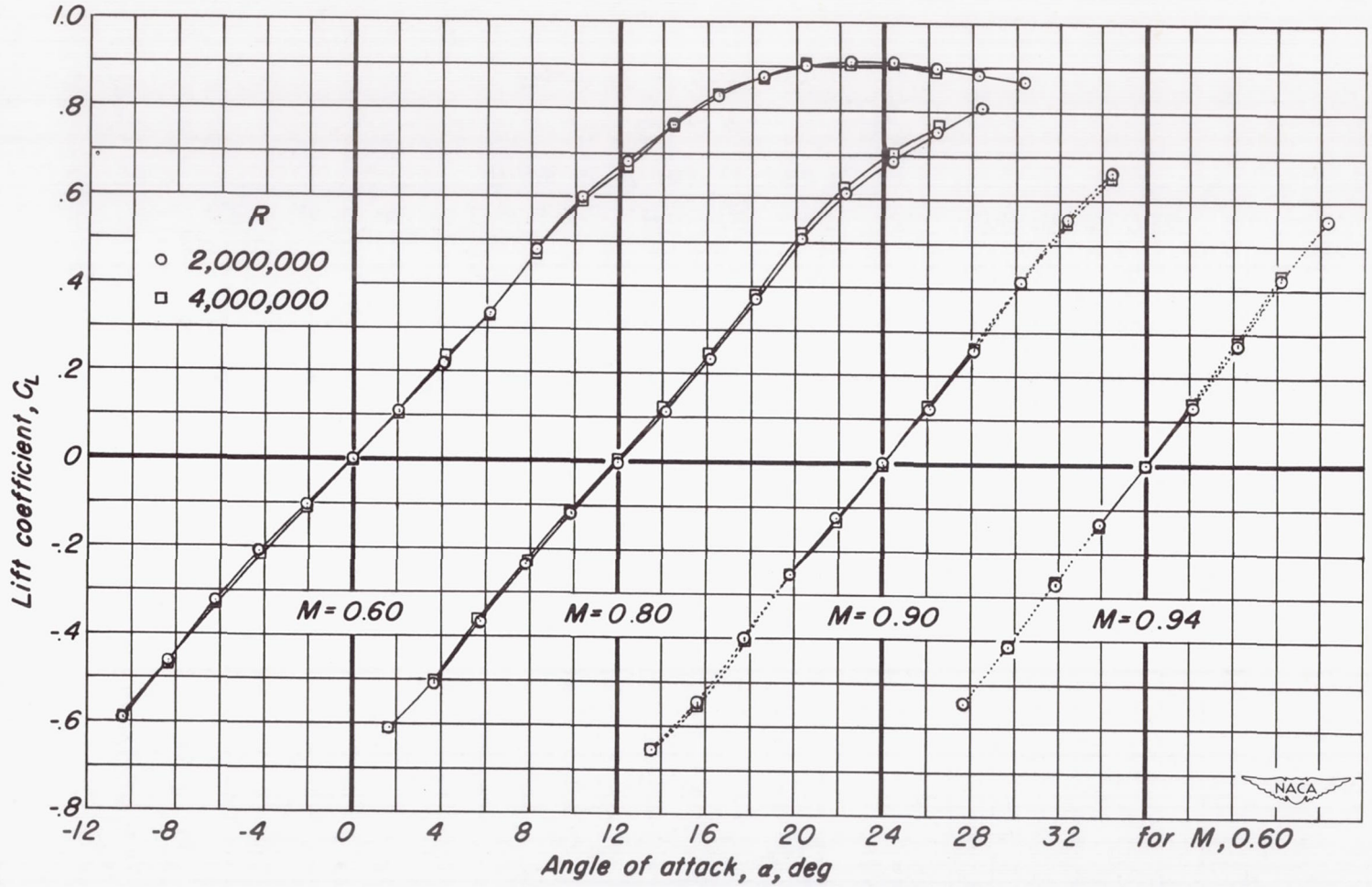

(a) C_L vs α

Figure 11.— The effect of Reynolds number on the aerodynamic characteristics at Mach numbers of 0.60, 0.80, 0.90 and 0.94. δ, 0°.

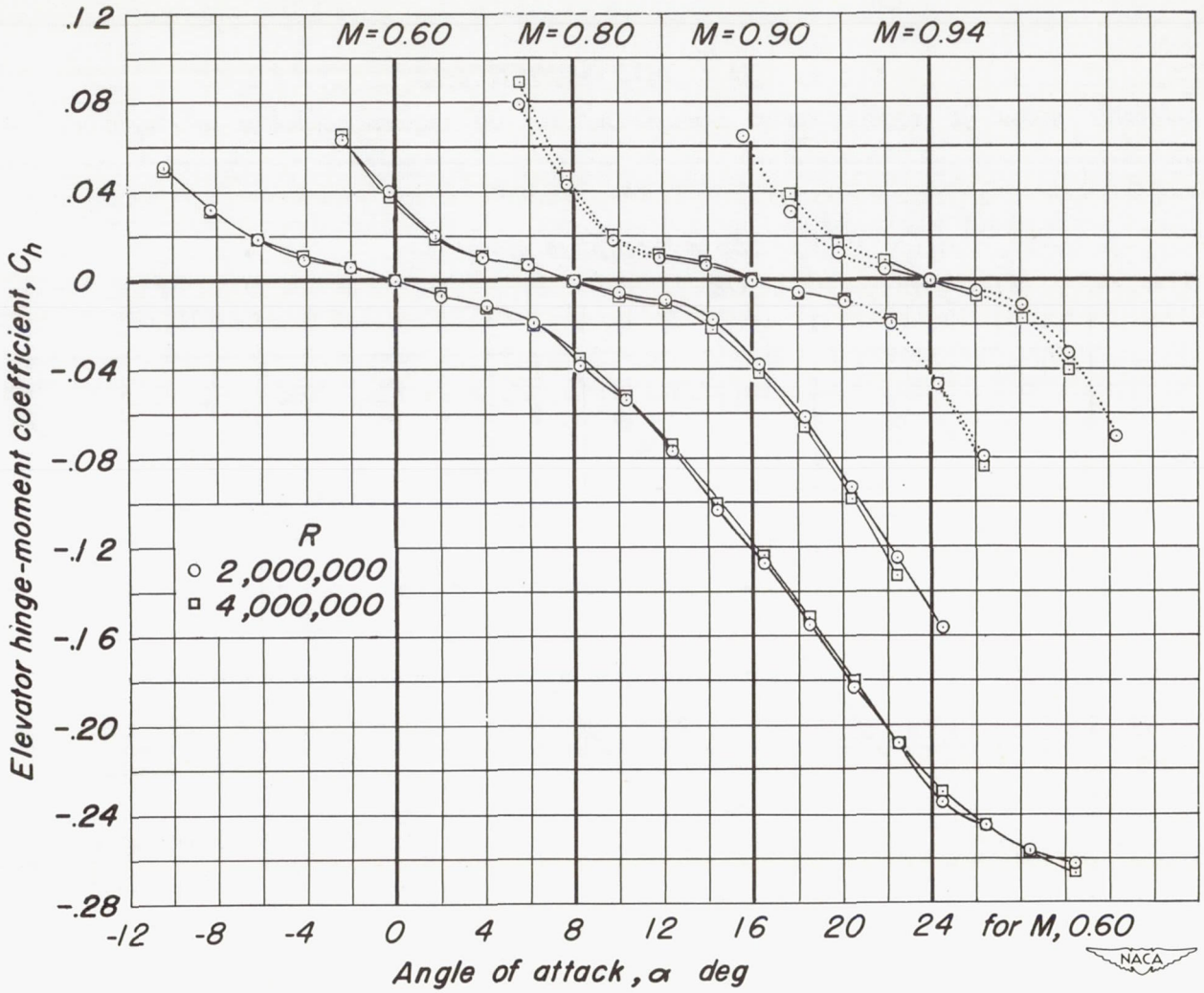

(b) C_h vs α

Figure 11. — Continued.

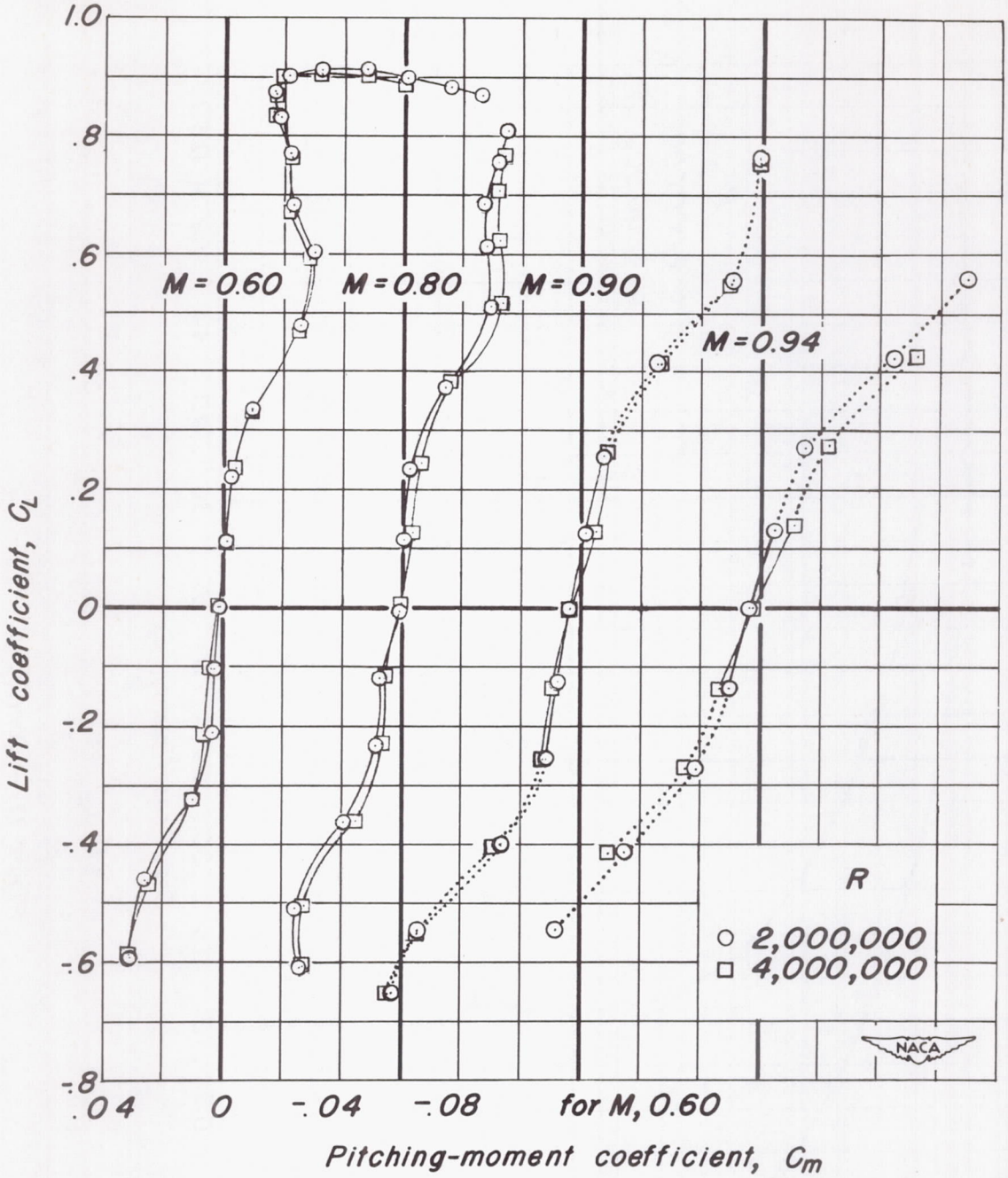

(c) C_L vs C_M

Figure 11.—Continued.

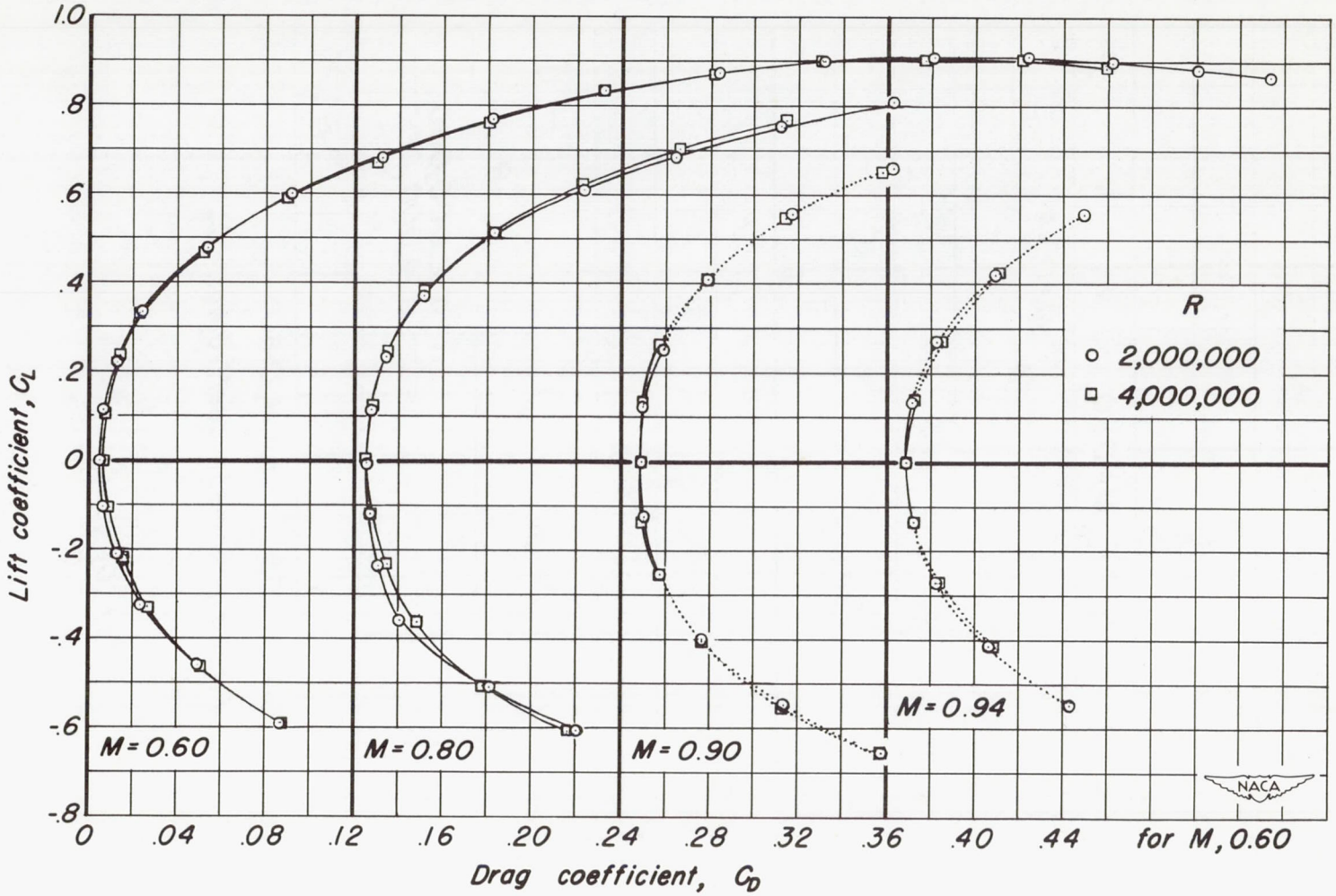

(d) C_L vs C_D

Figure 11. — Concluded.

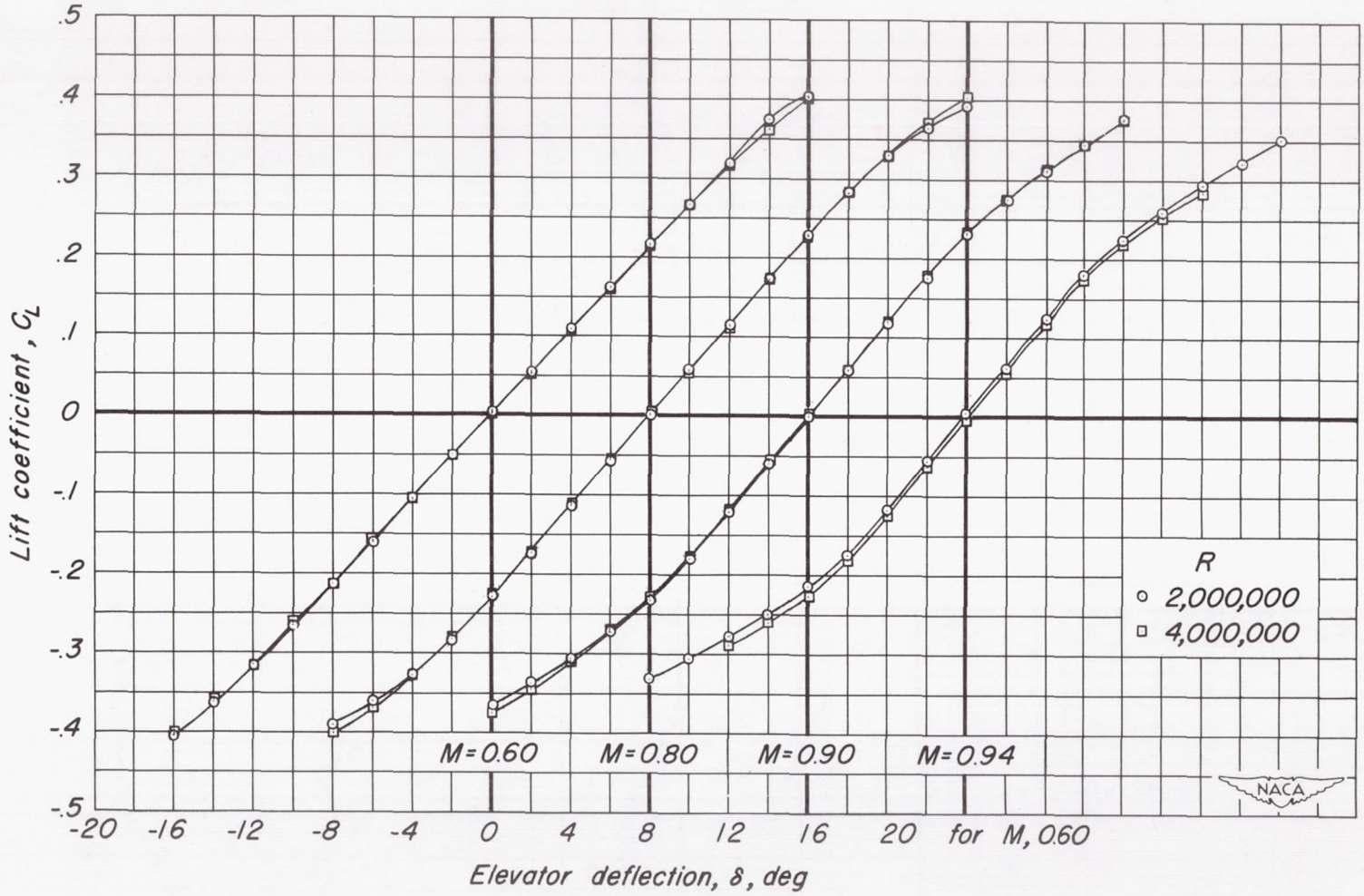

(a) C_L vs δ

Figure 12.—The effect of Reynolds number on the aerodynamic characteristics for various elevator deflections at Mach numbers of 0.60, 0.80, 0.90, and 0.94. α_u, 0°.

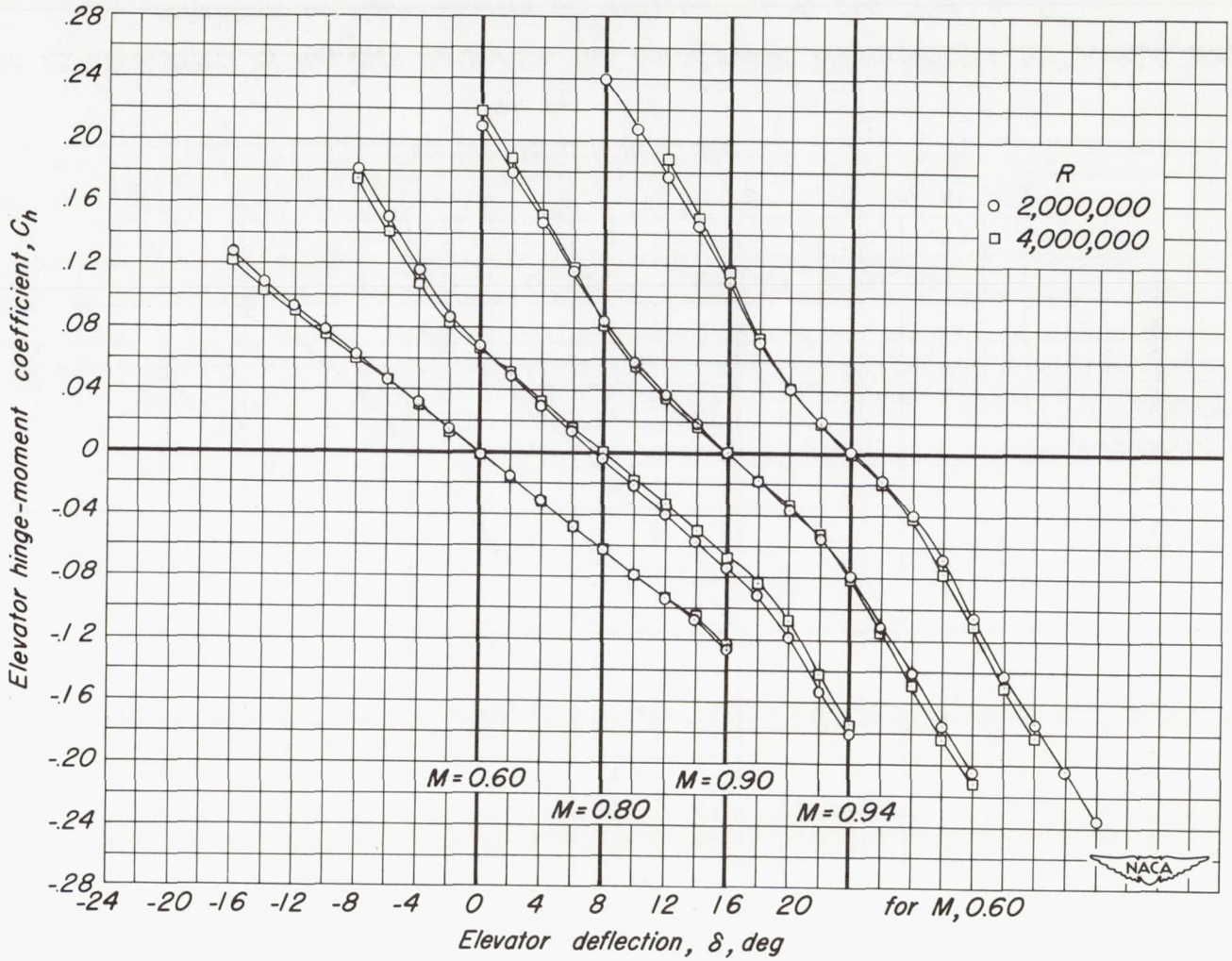

(b) C_h vs δ

Figure 12.— Continued.

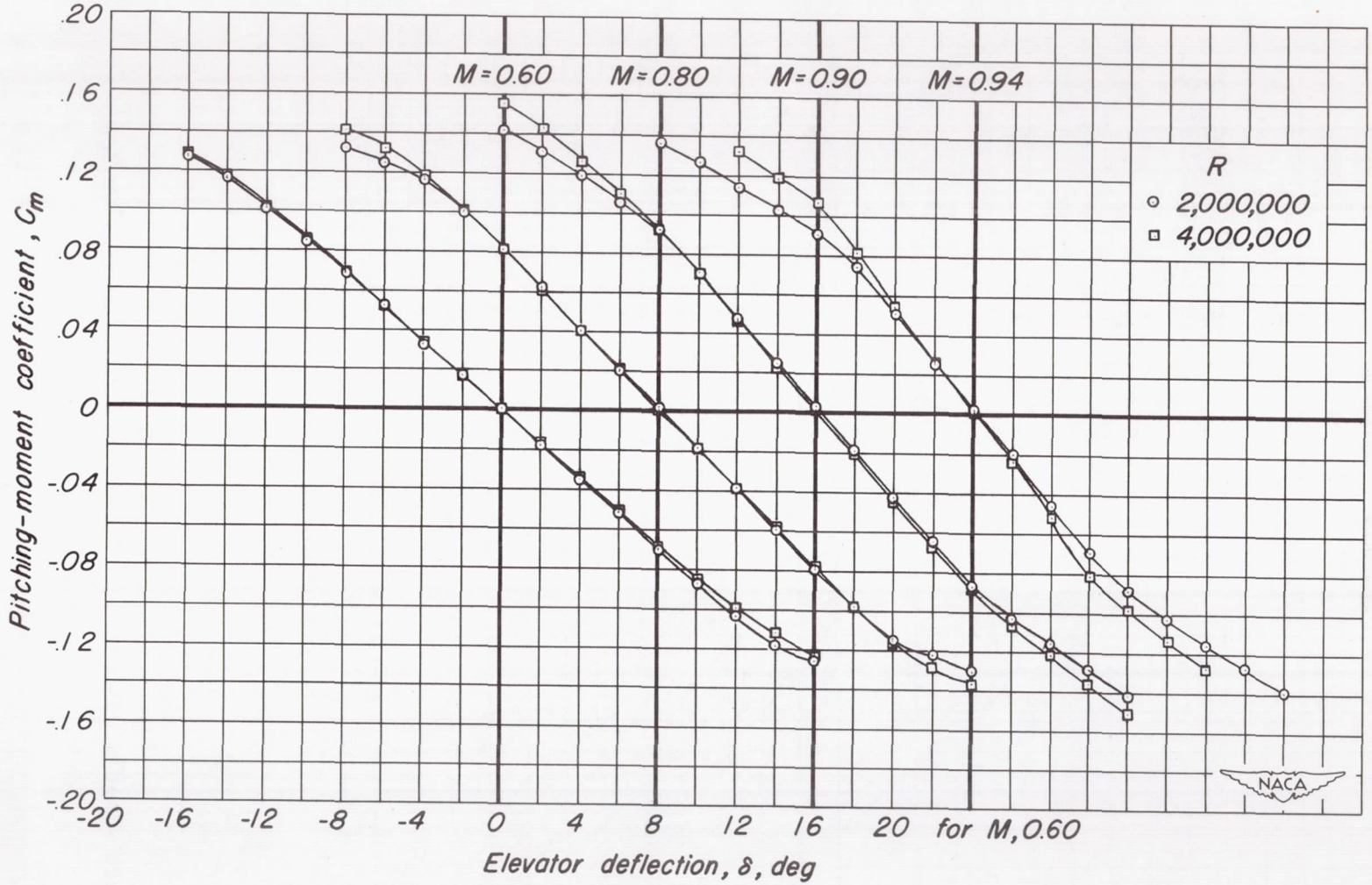

(c) C_M vs δ

Figure 12.— Concluded.

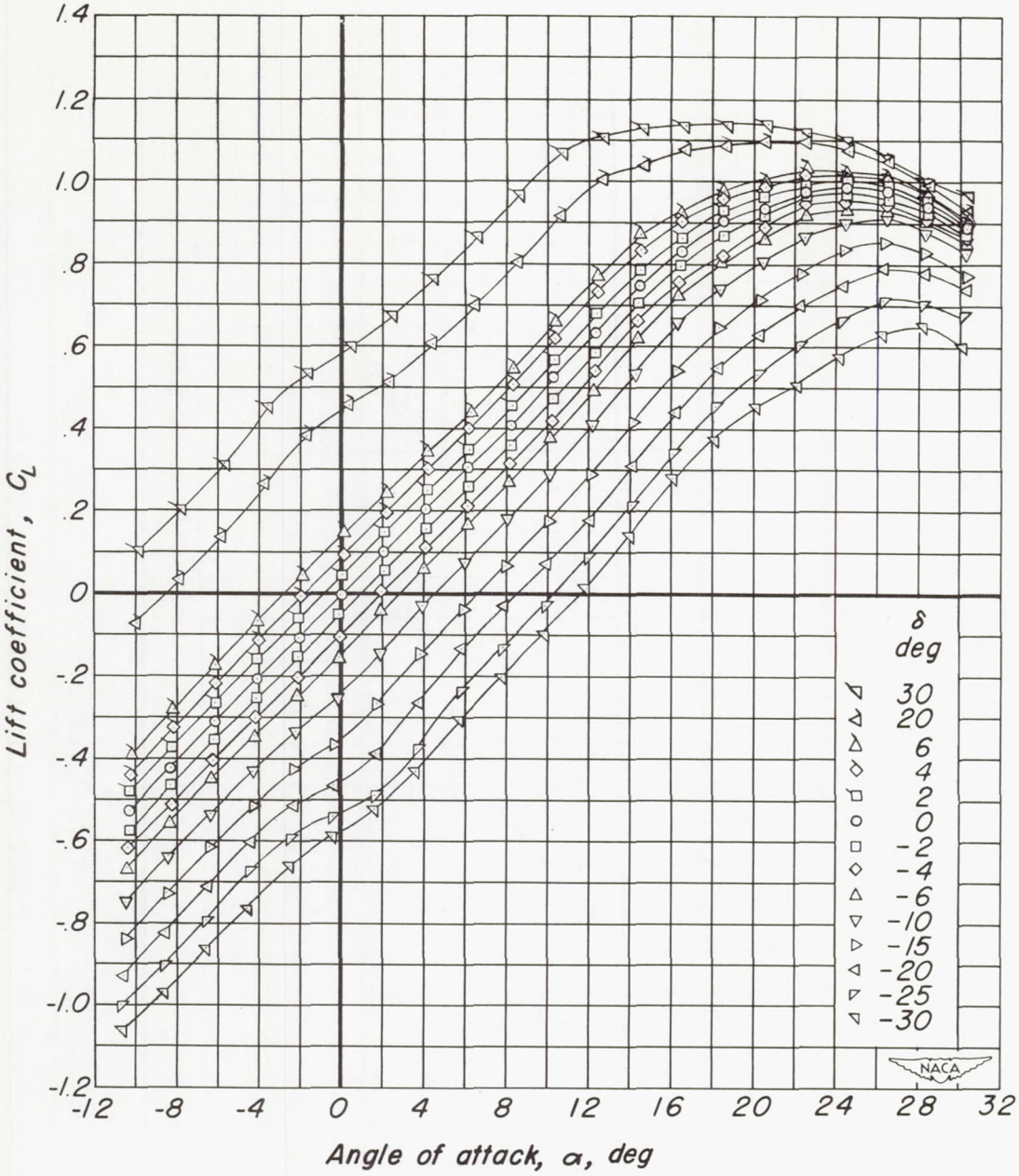

(a) M, 0.25

Figure 13.—The variation of lift coefficient with angle of attack. R, 4,000,000 .

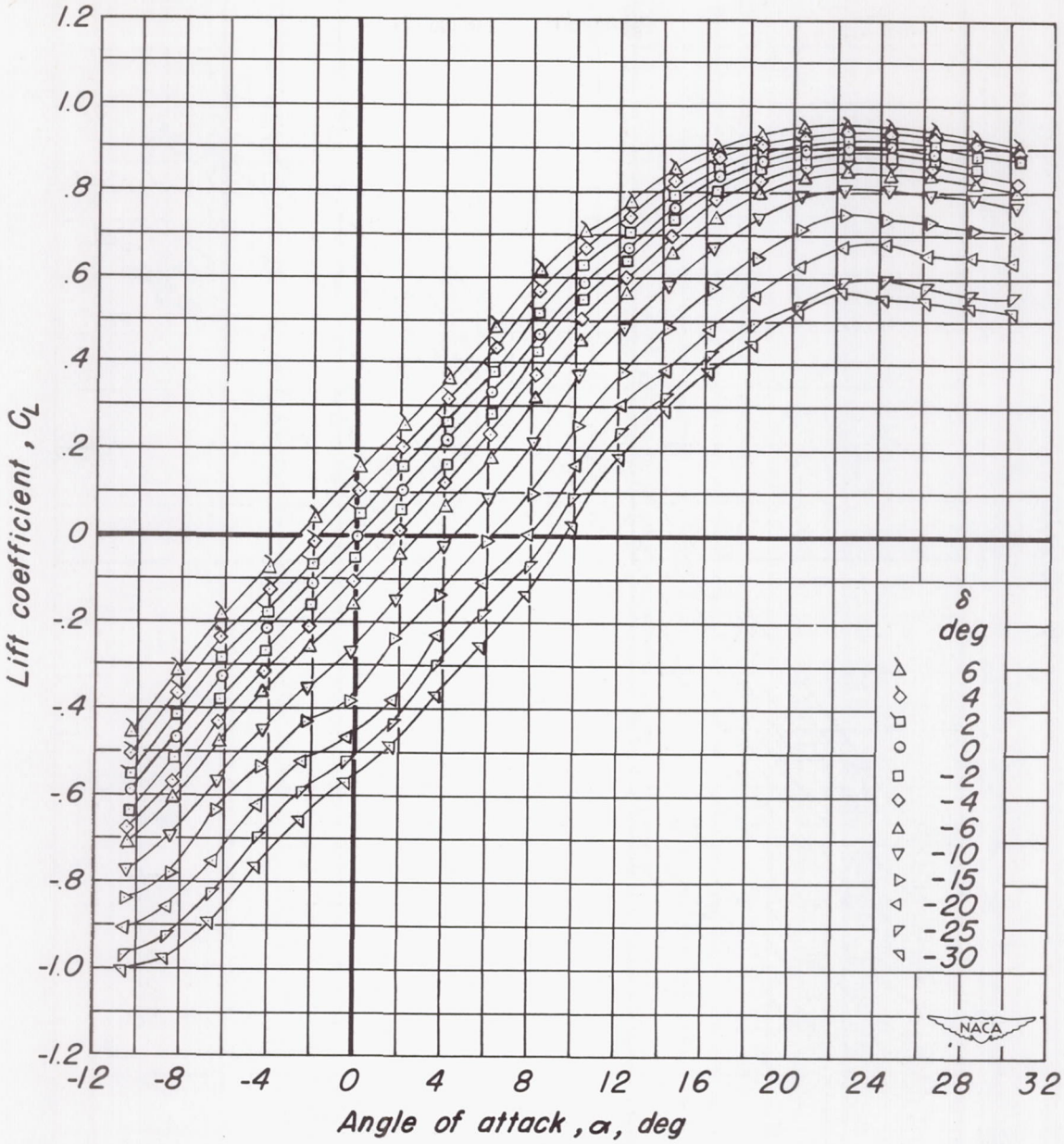

(b) M, 0.60

Figure 13.— Continued.

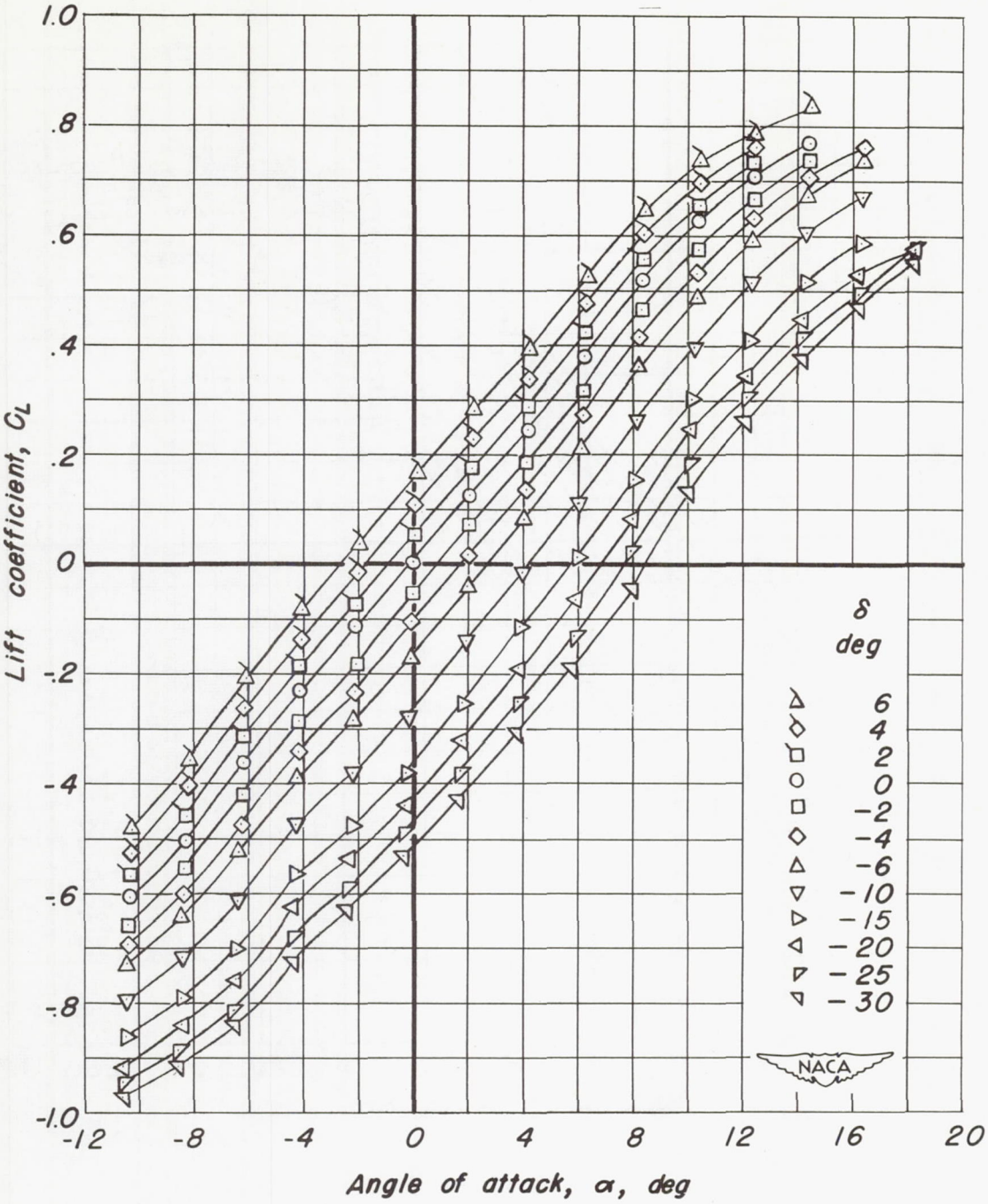

(c) M, 0.80

Figure 13.— Continued.

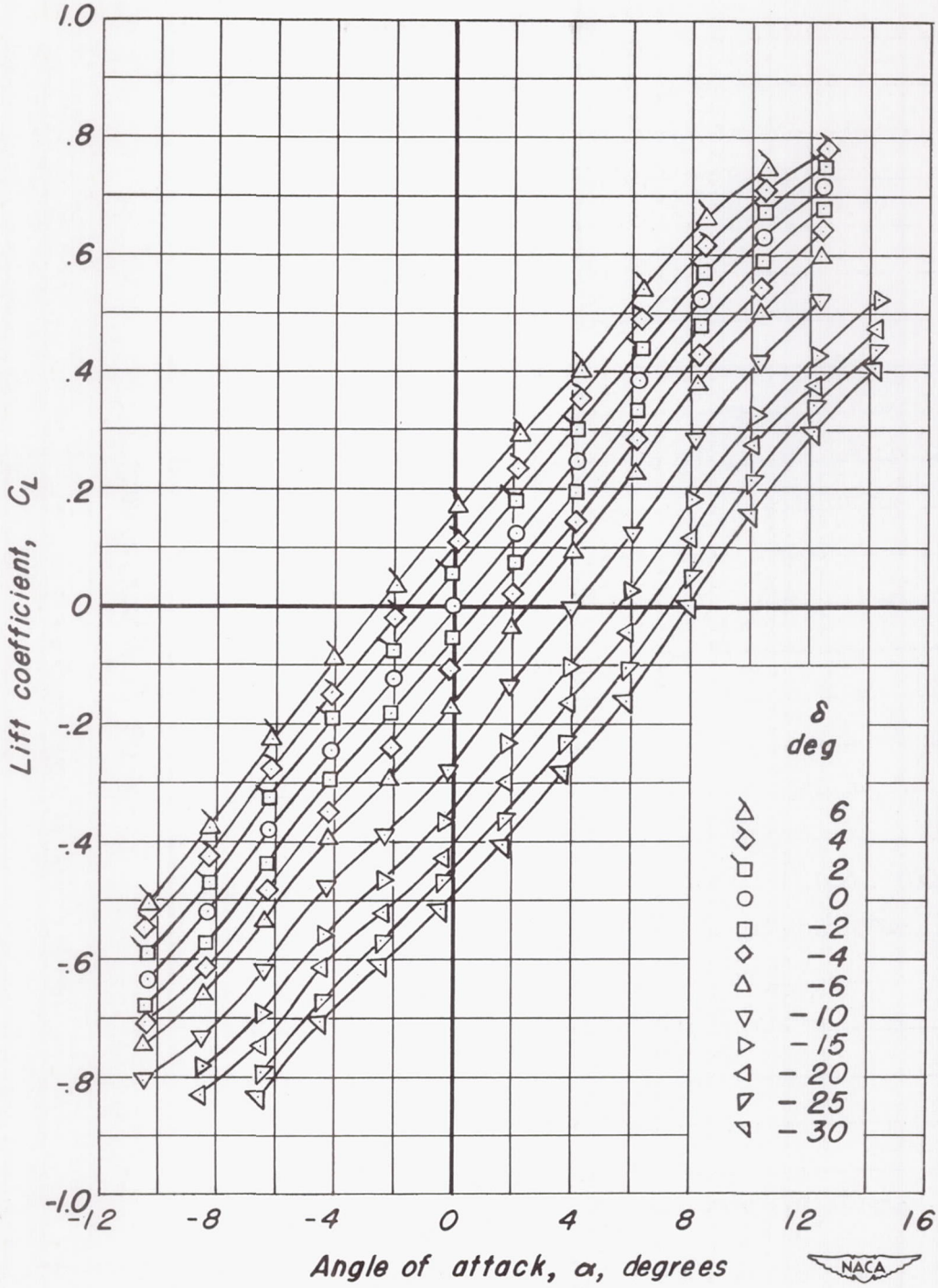

(d) M, 0.85

Figure 13.—Continued.

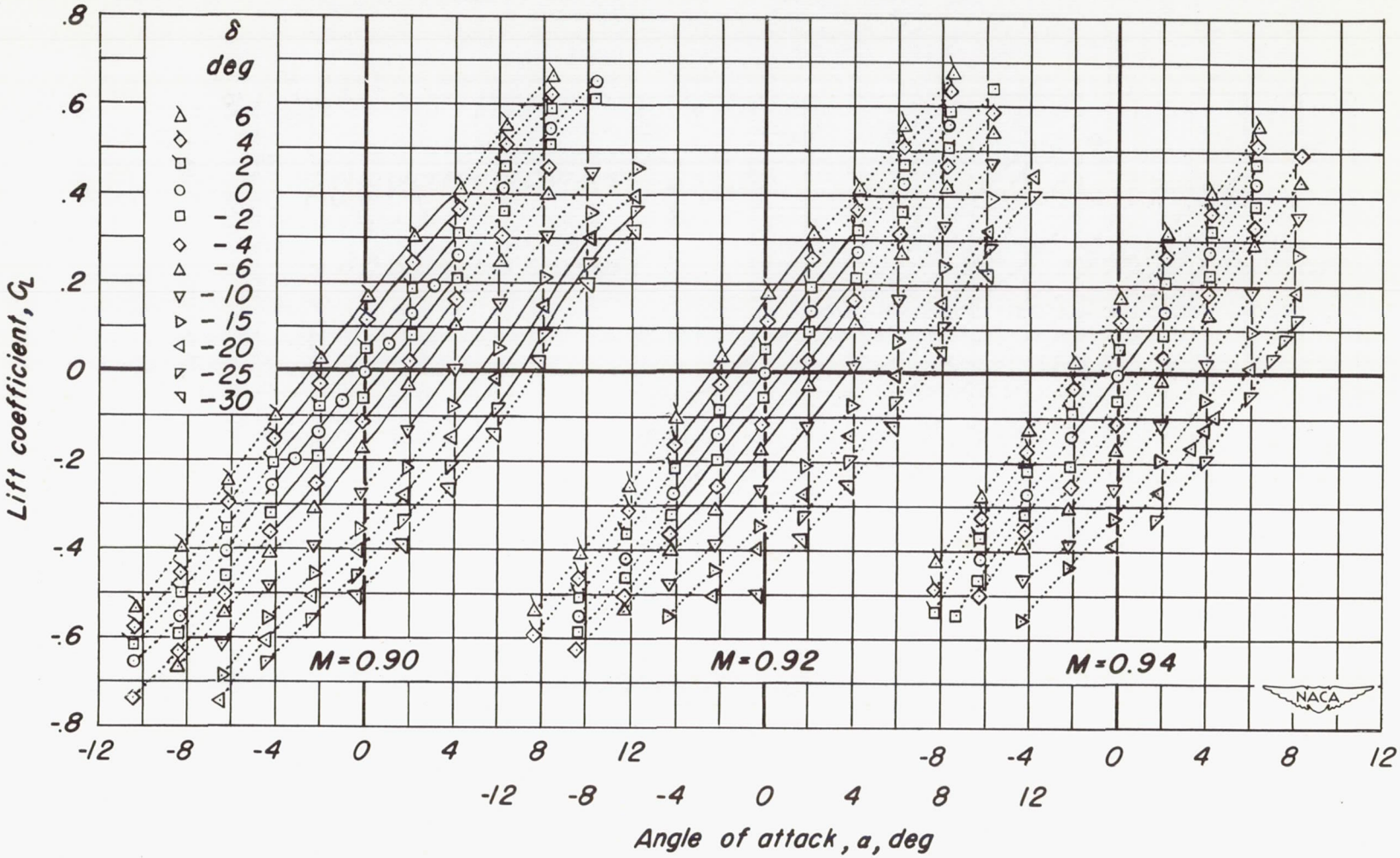

(e) M, 0.90; M, 0.92; M, 0.94

Figure 13.— Concluded.

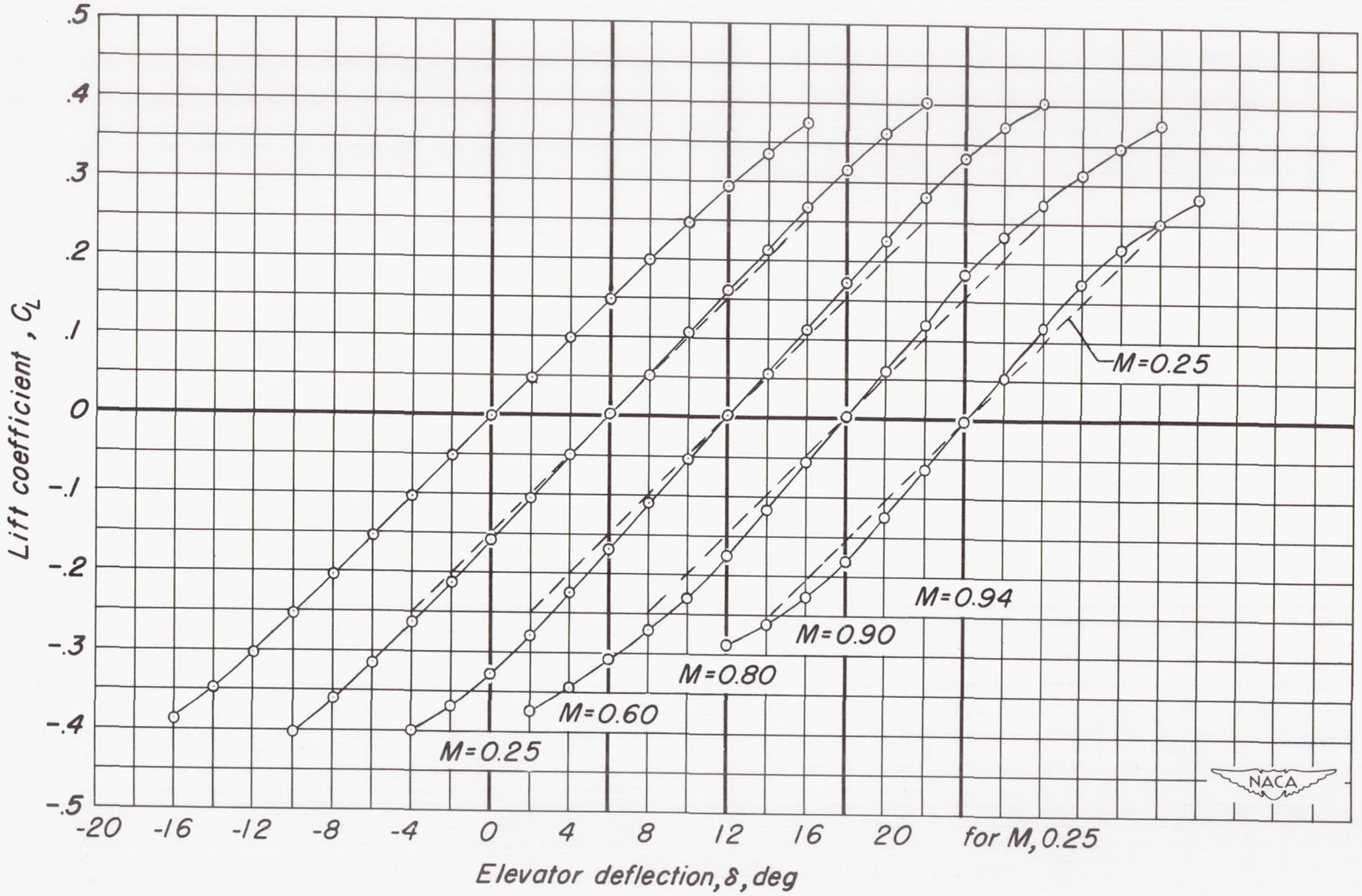

Figure 14.—The variation of lift coefficient with elevator deflection. α_u, 0°; R, 4,000,000.

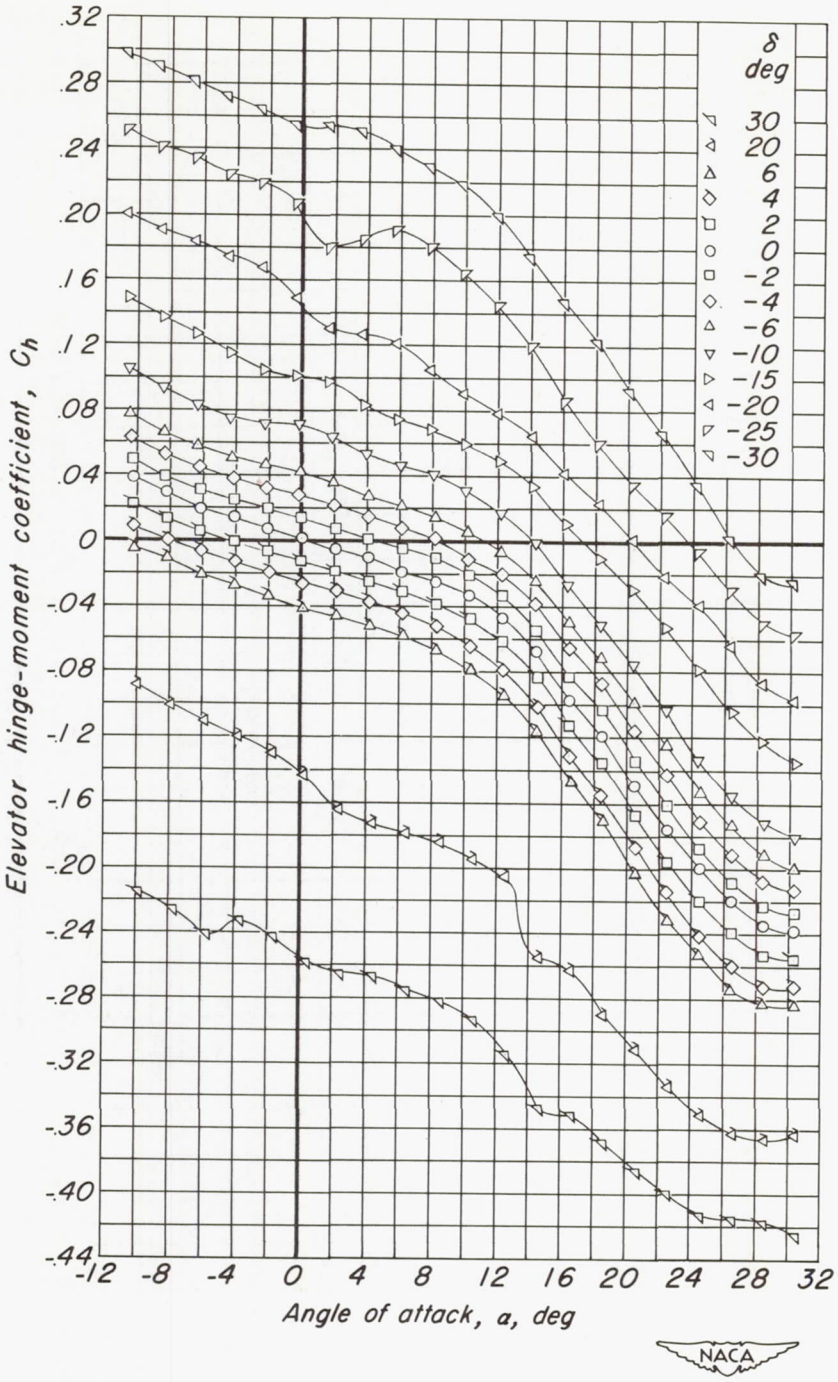

(a) M, 0.25

Figure 15.—The variation of elevator hinge-moment coefficient with angle of attack. R, 4,000,000.

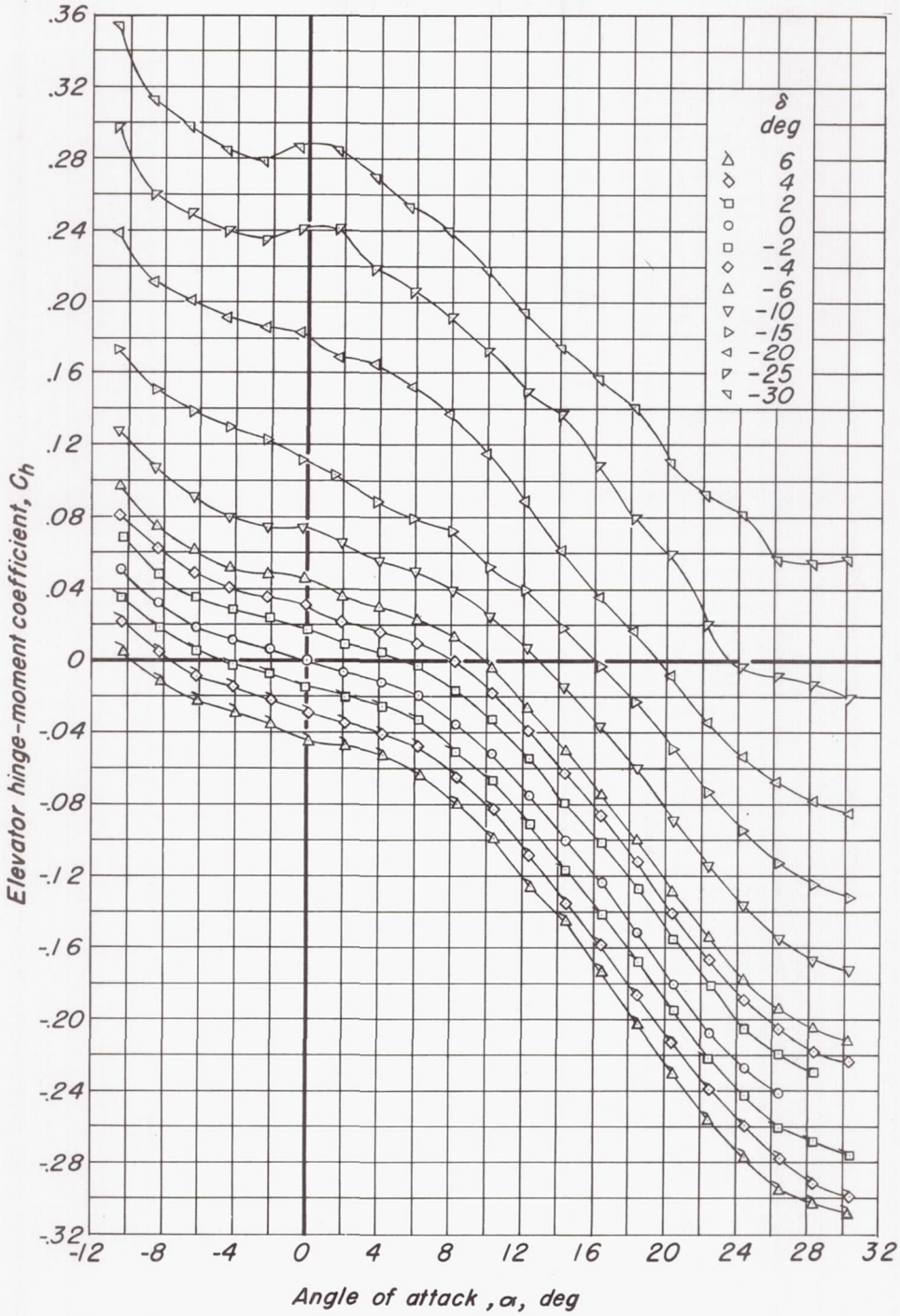

(b) M, 0.60

Figure 15.— Continued.

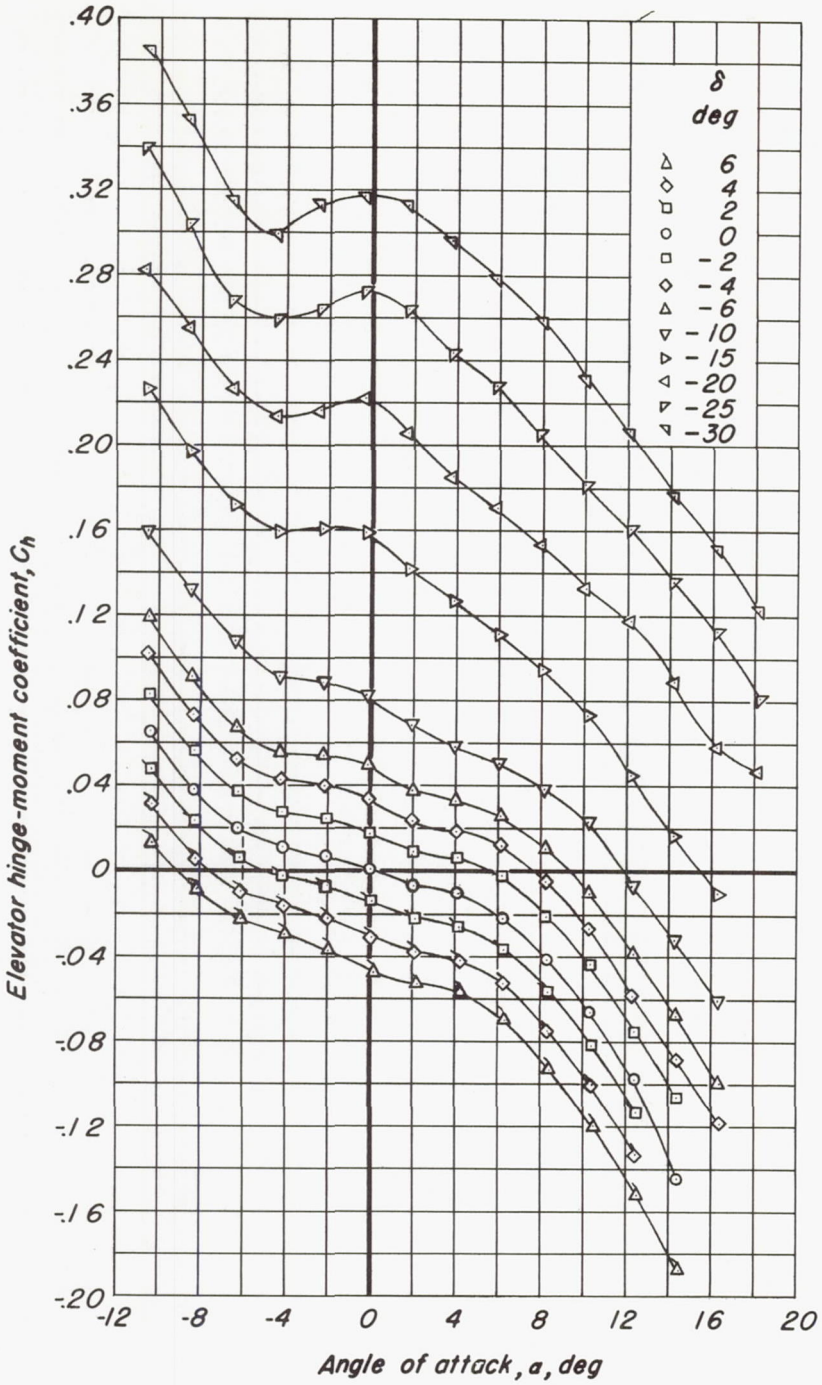

(c) M, 0.80

Figure 15. — Continued.

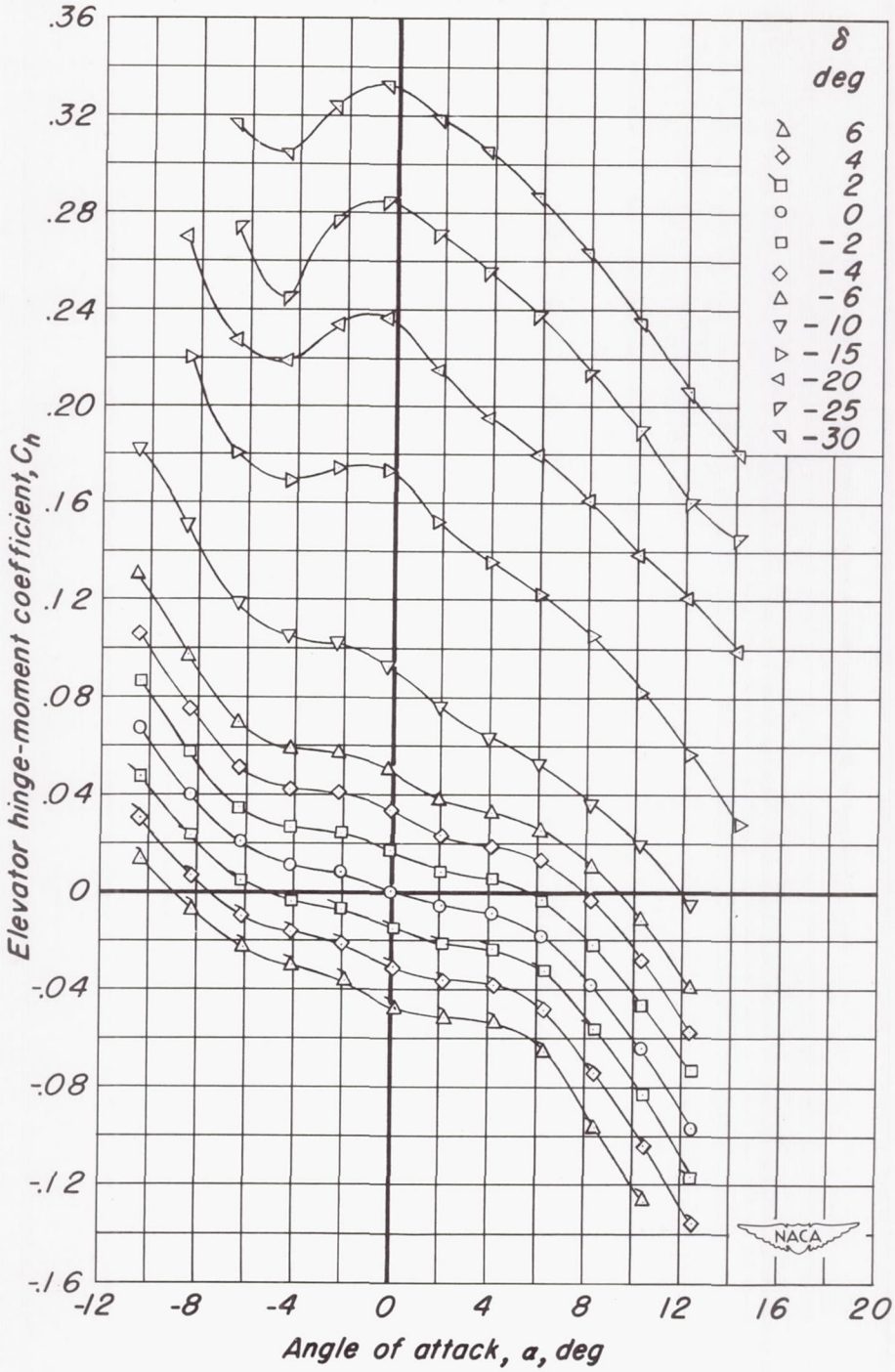

(d) M, 0.85

Figure 15.— Continued.

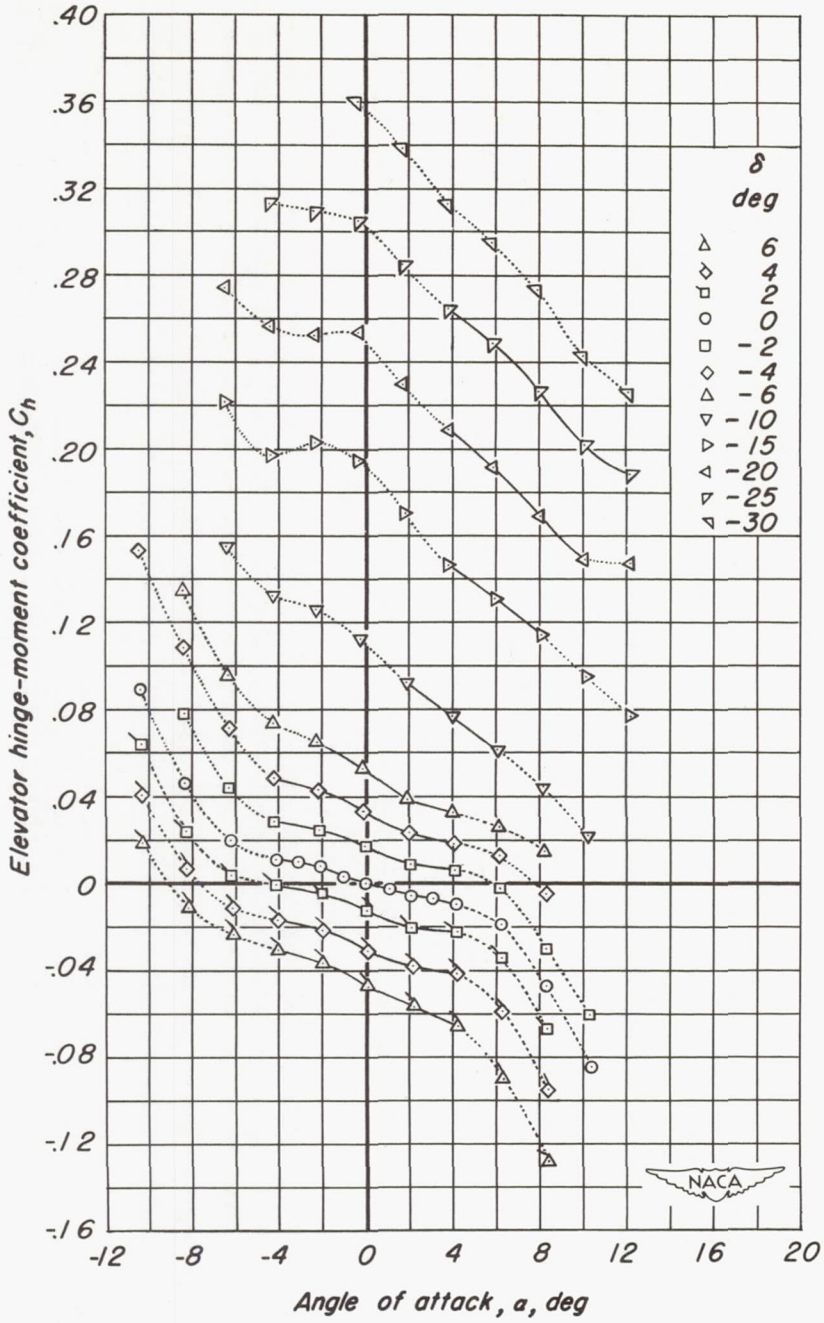

(e) M, 0.90.

Figure 15.— Continued.

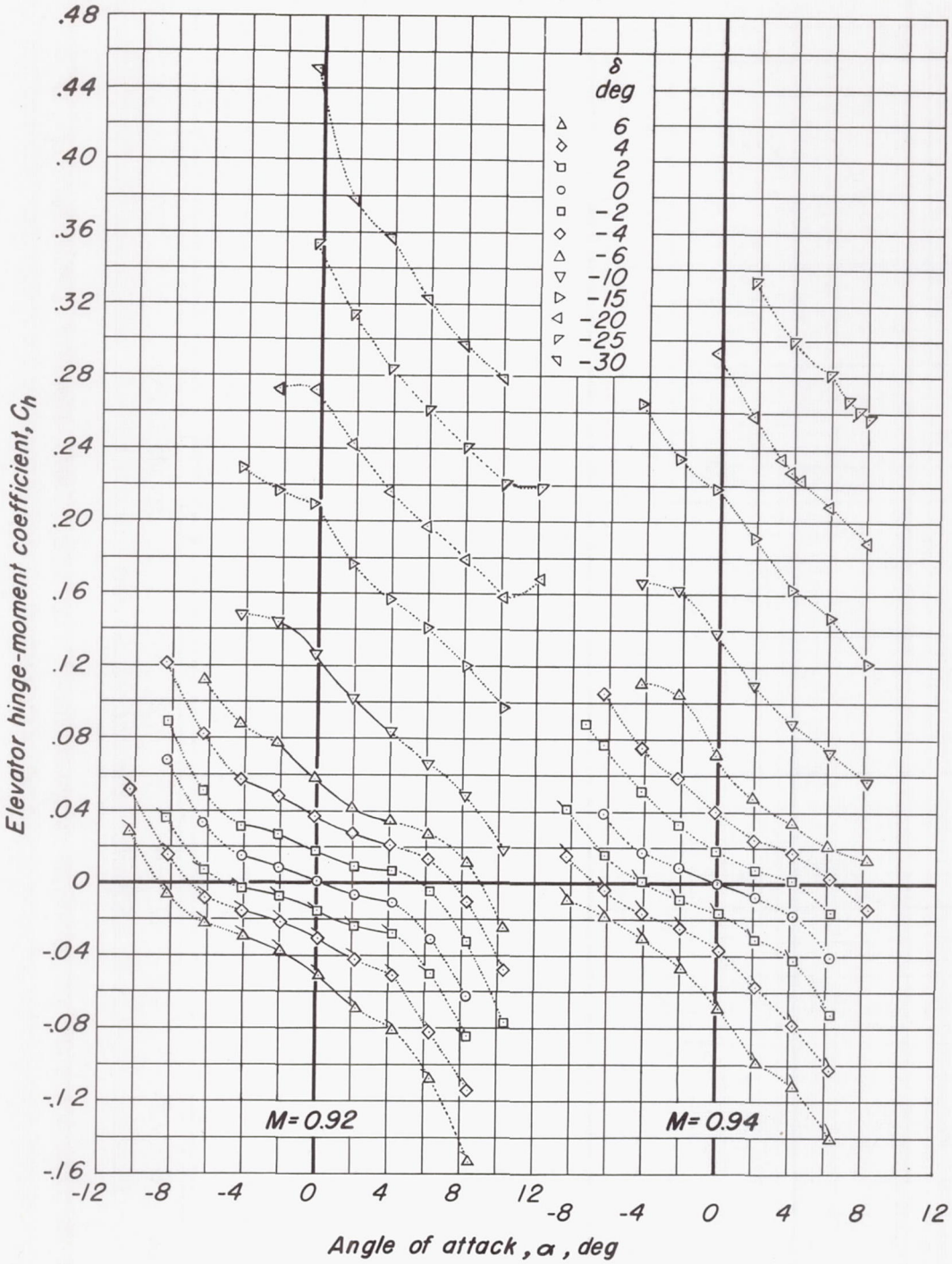

(f) M,0.92 ; M,0.94

Figure 15.— Concluded.

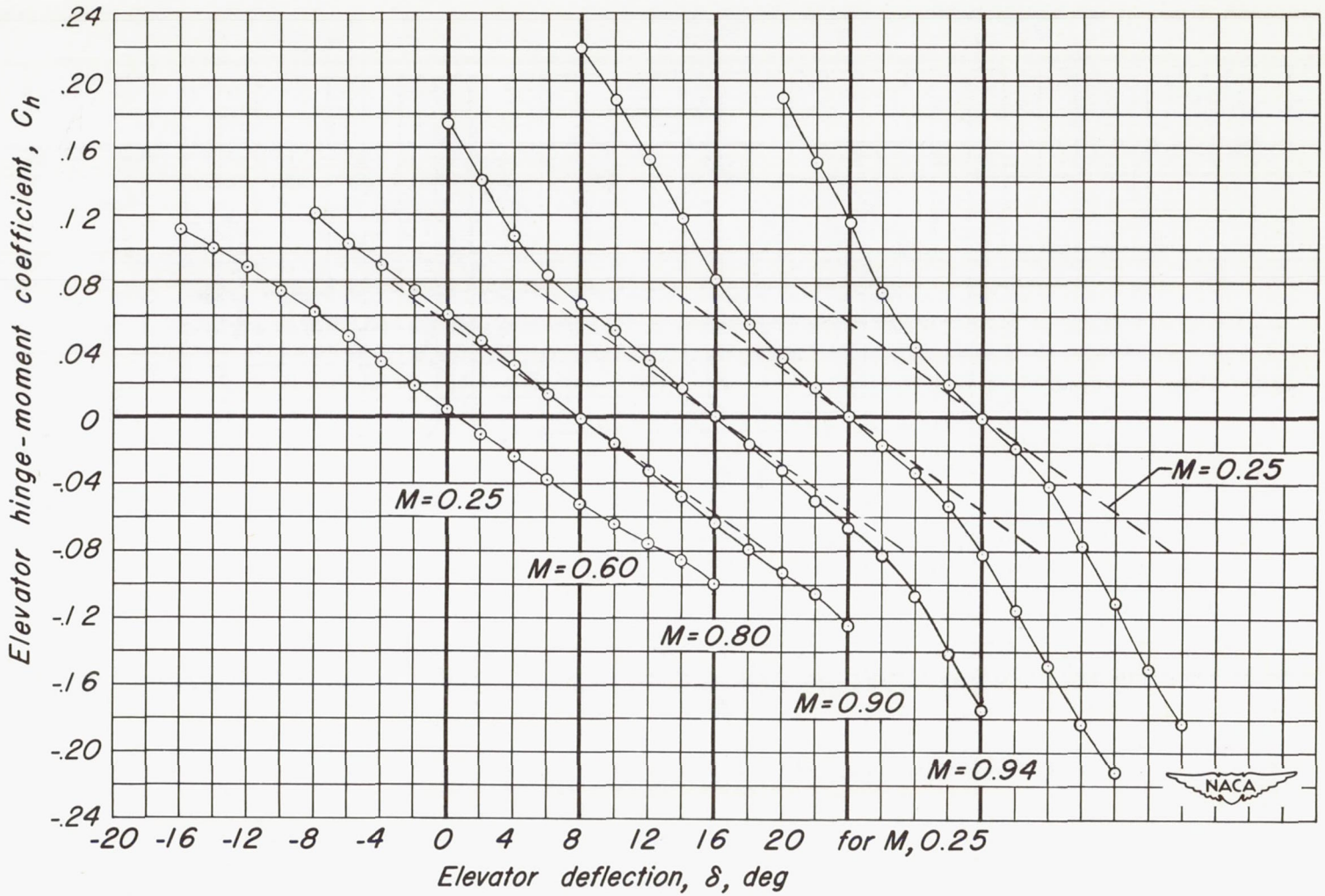

Figure 16.—The variation of elevator hinge-moment coefficient with elevator deflection. α_u, 0°; R, 4,000,000.

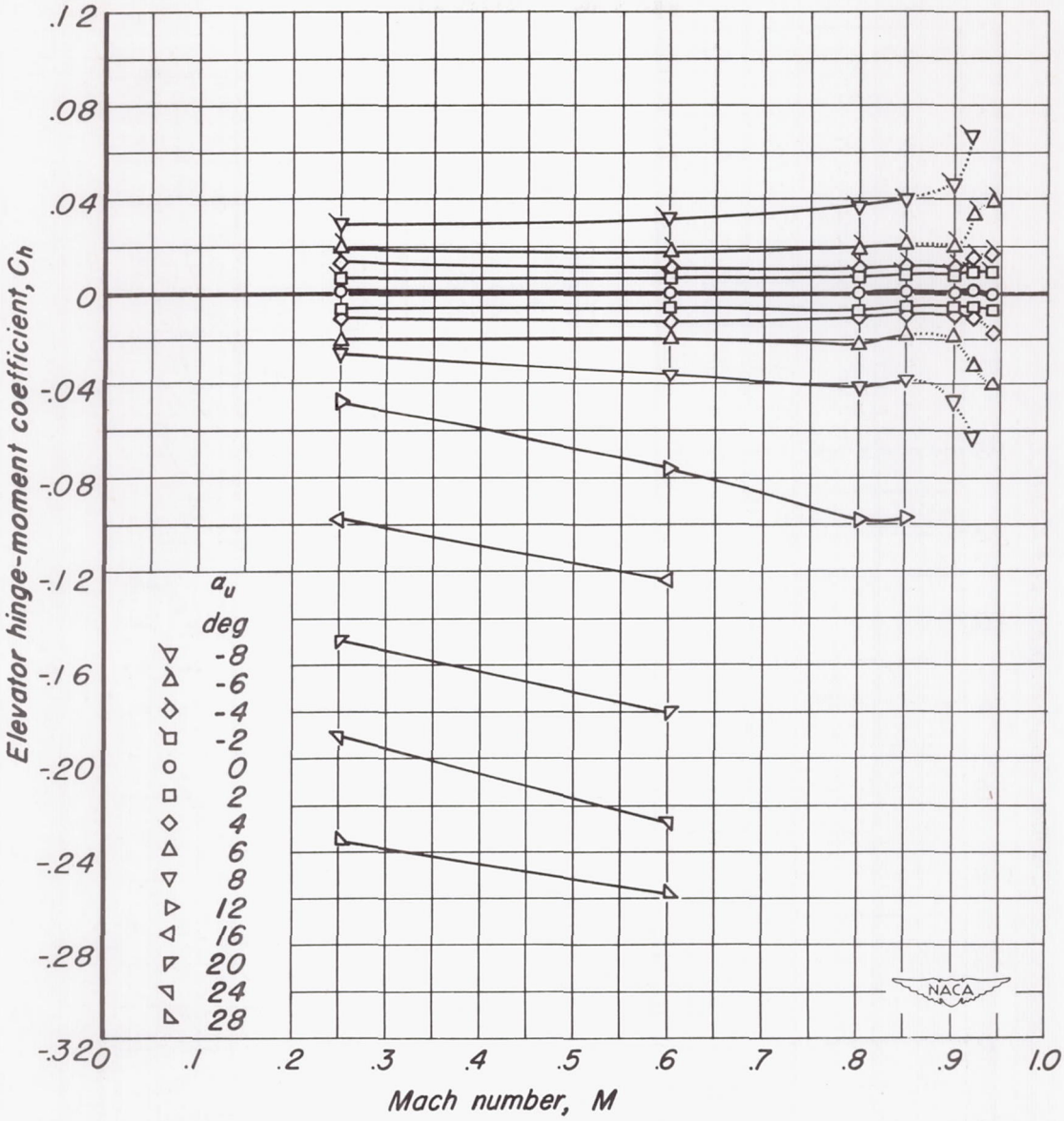

(a) $\delta, 0^\circ$

Figure 17.— The variation of elevator hinge-moment coefficient with Mach number. R, 4,000,000.

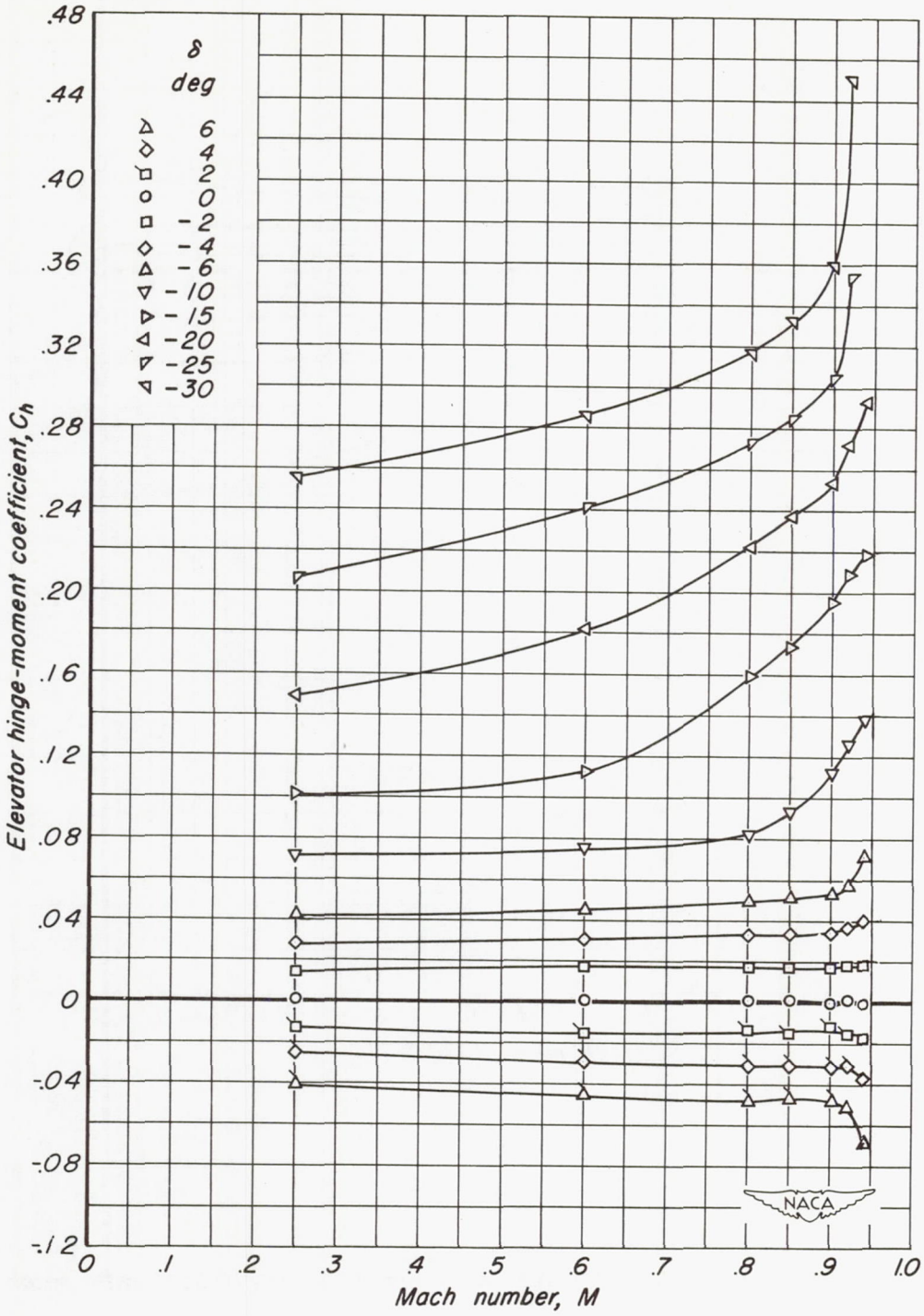

(b) a_u, 0°

Figure 17.— Concluded.

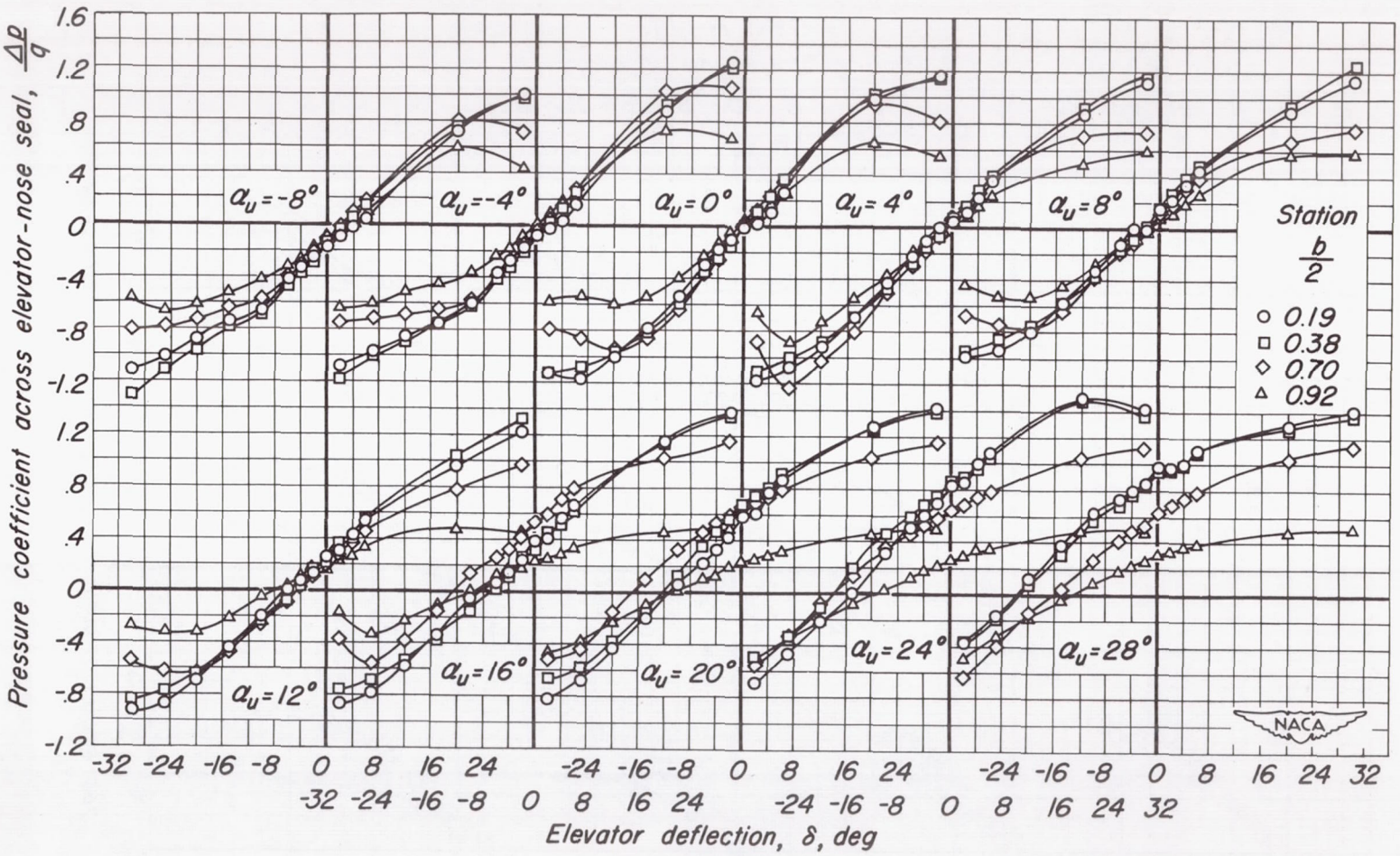

(a) M, 0.25

Figure 18.—The variation of pressure coefficient across the elevator-nose seal with elevator deflection. R, 4,000,000.

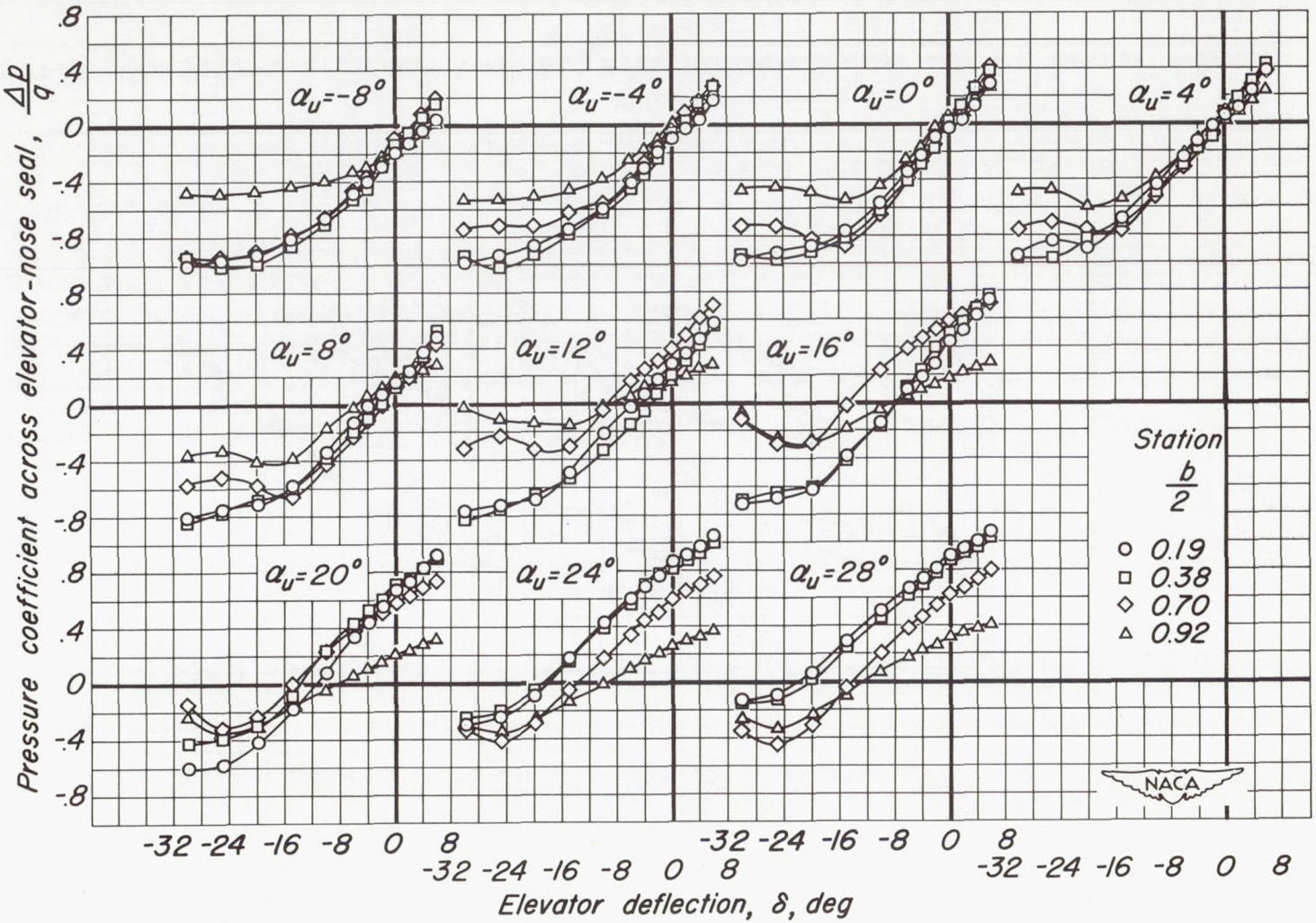

(b) M, 0.60

Figure 18.— Continued.

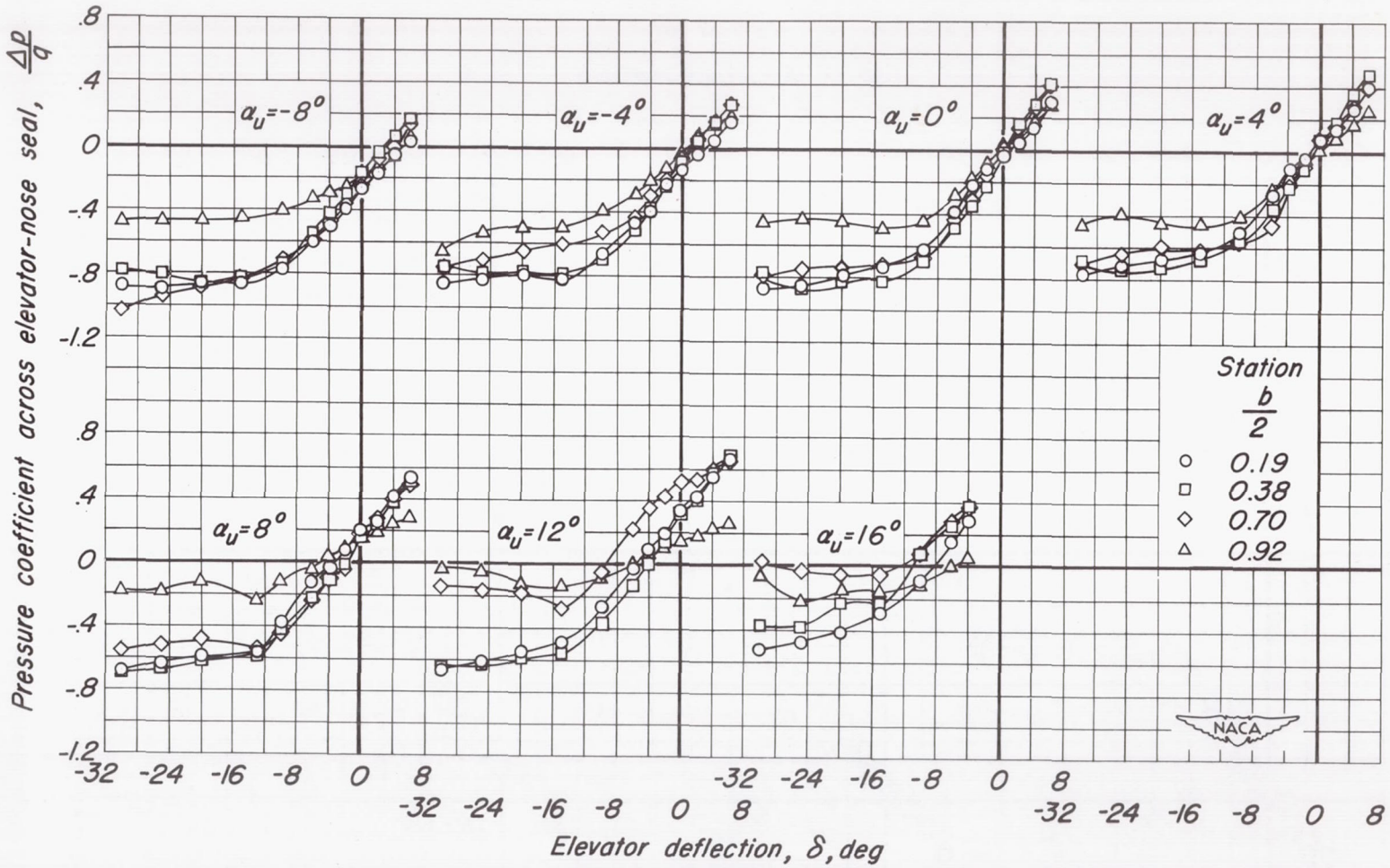

(c) M,0.80

Figure 18.— Continued.

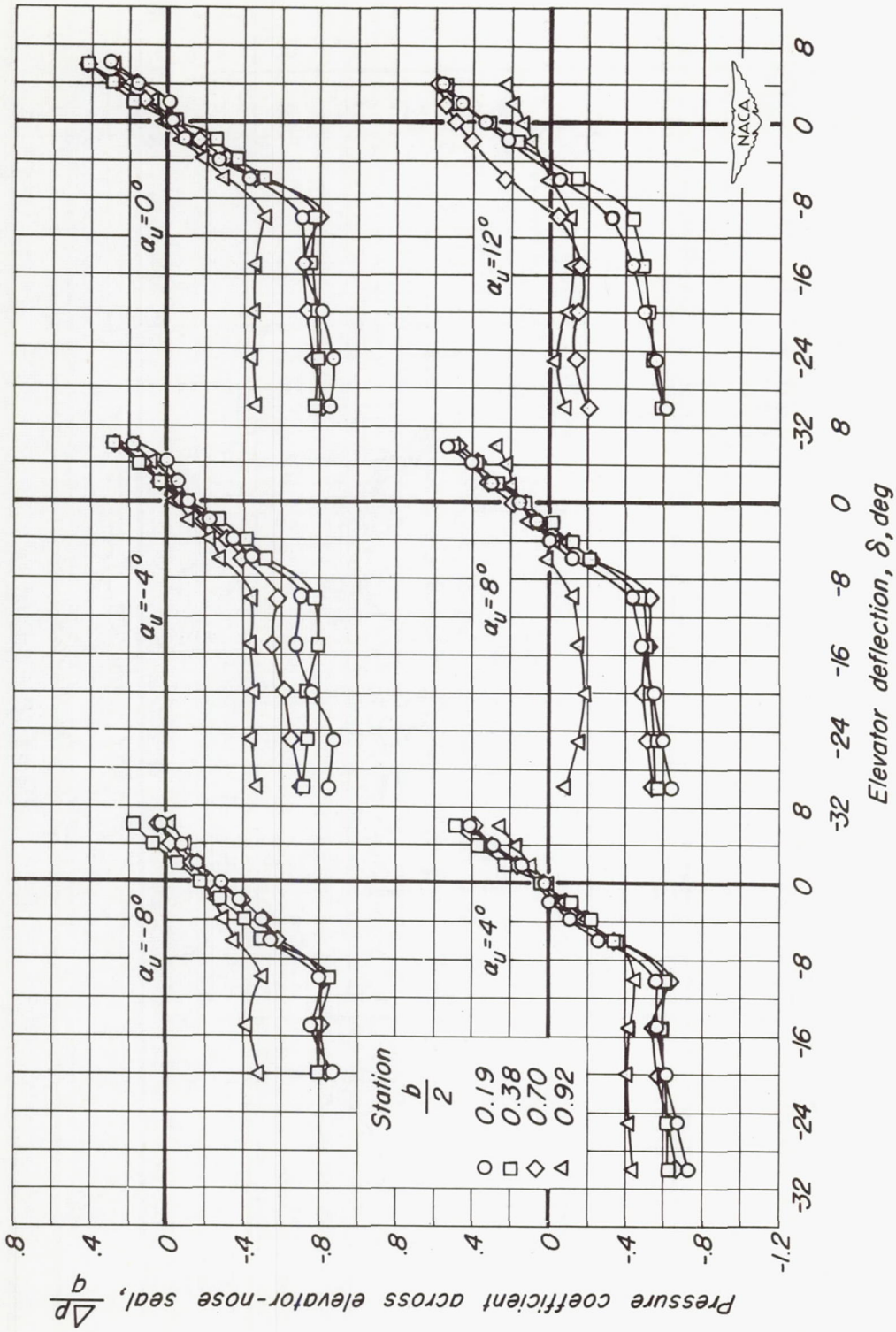

(d) M, 0.85

Figure 18.— Continued.

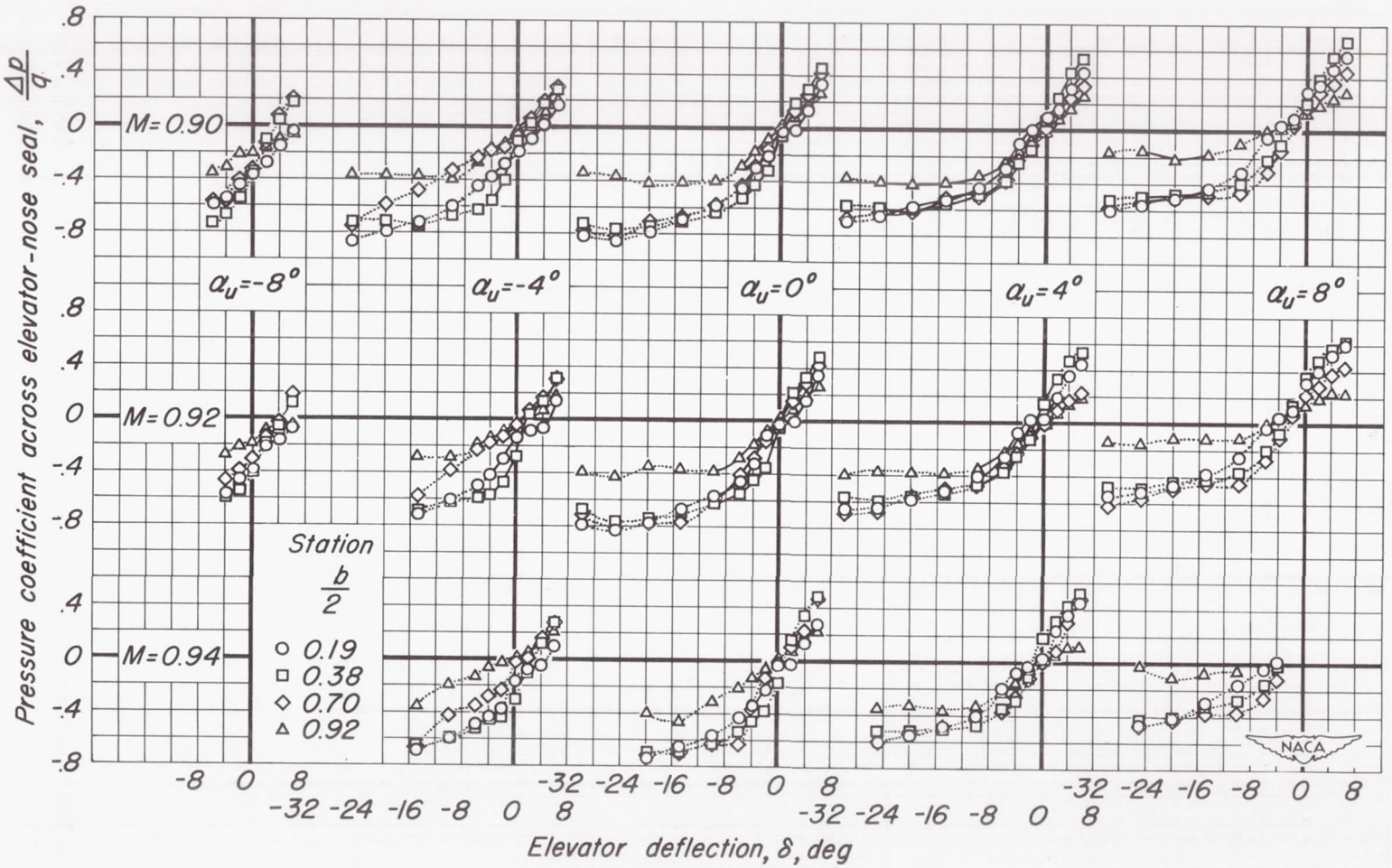

(e) M,0.90; M,0.92; M,0.94

Figure 18.—Concluded.

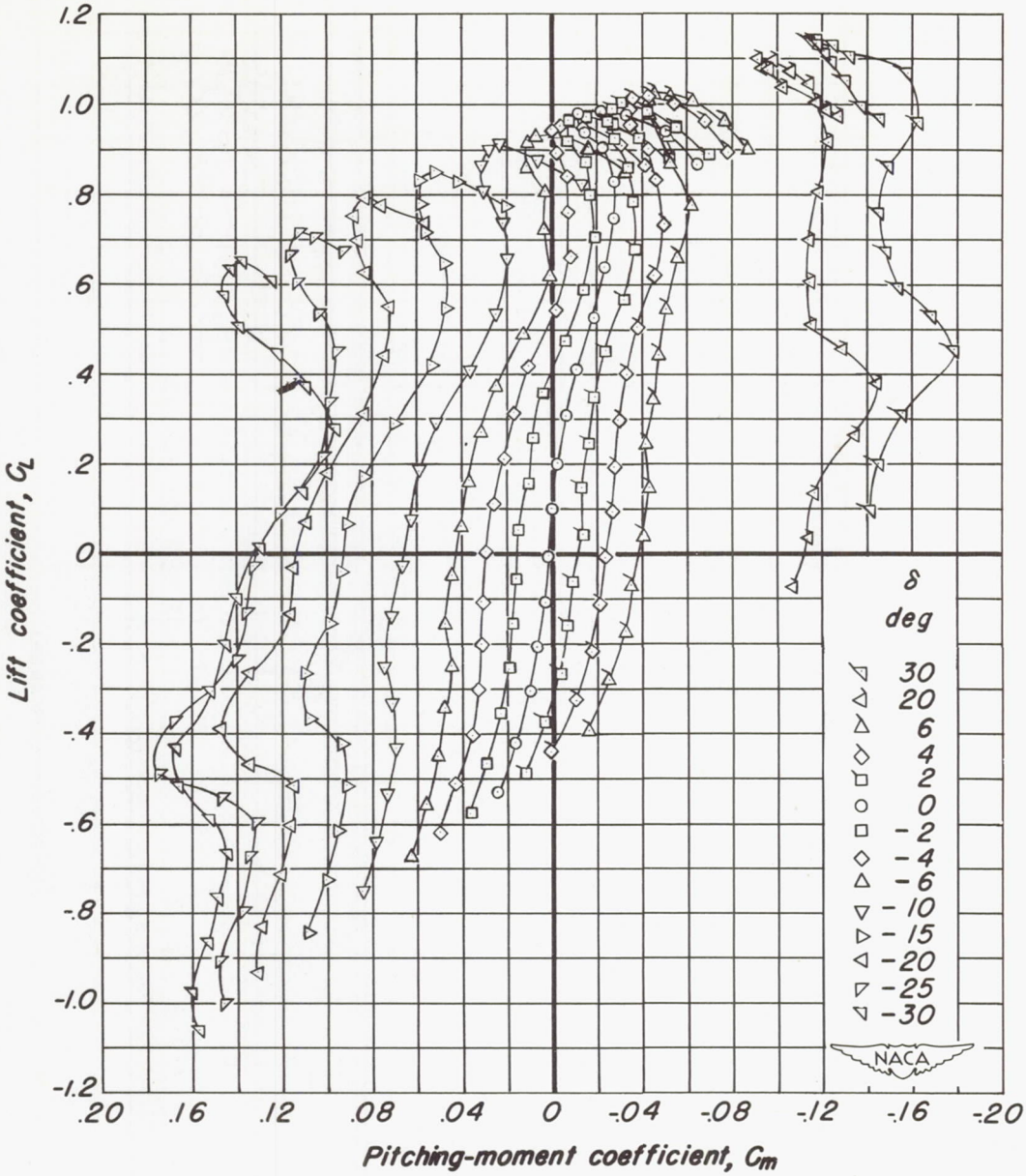

(a) M,0.25

Figure 19.— The variation of lift coefficient with pitching-moment coefficient. R,4,000,000.

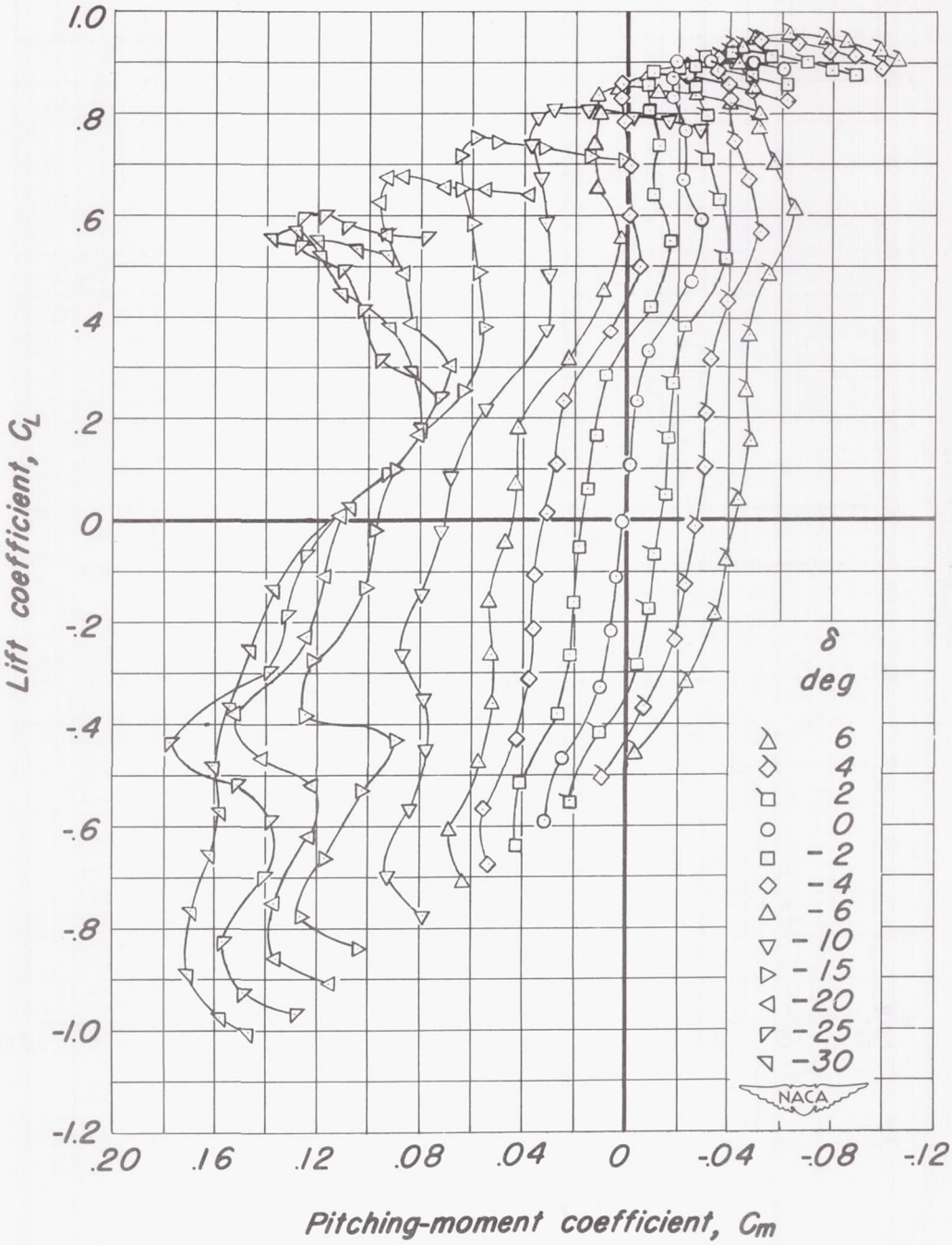

(b) M, 0.60

Figure 19.— Continued.

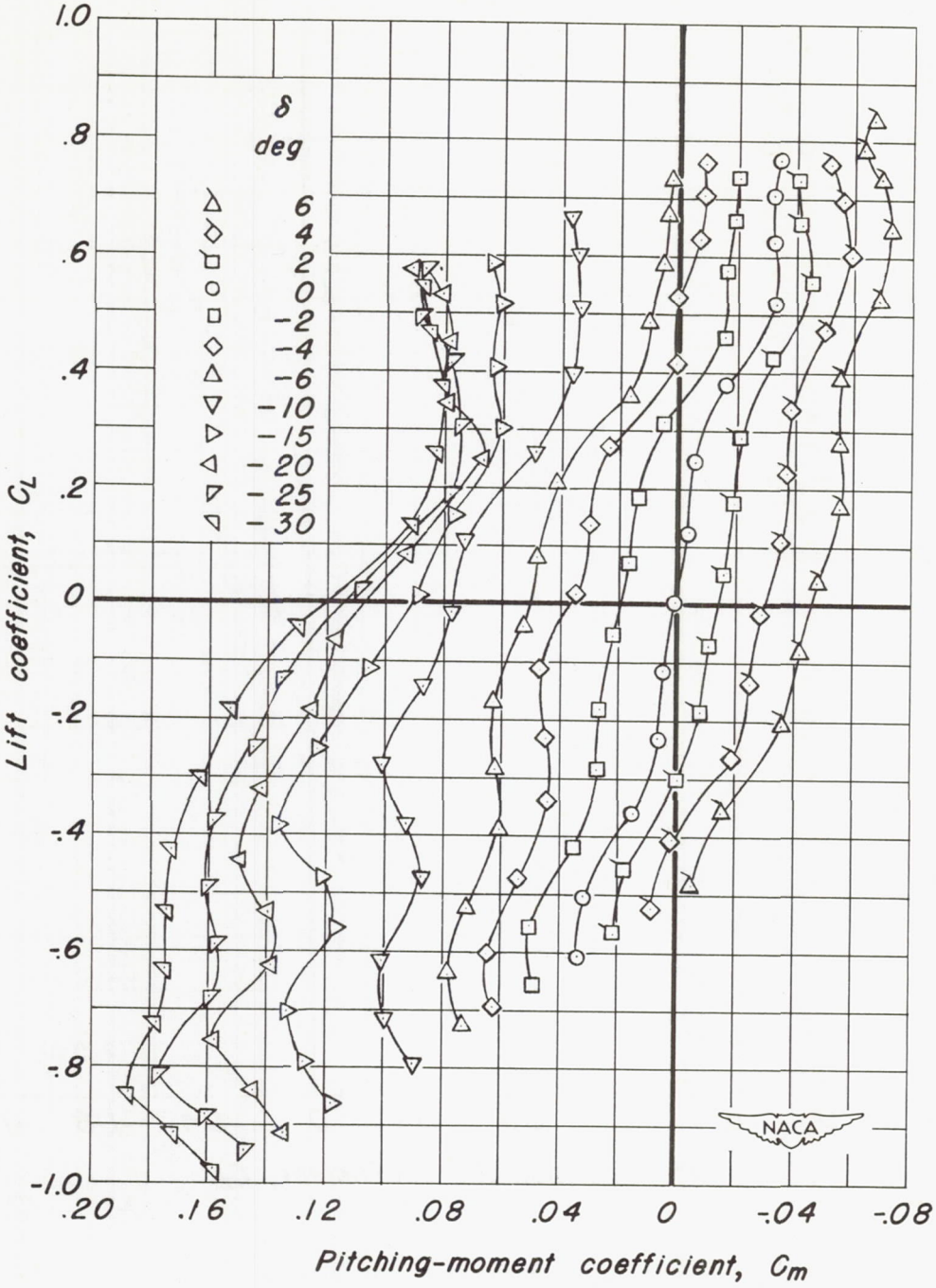

(c) M,0.80

Figure 19.— Continued.

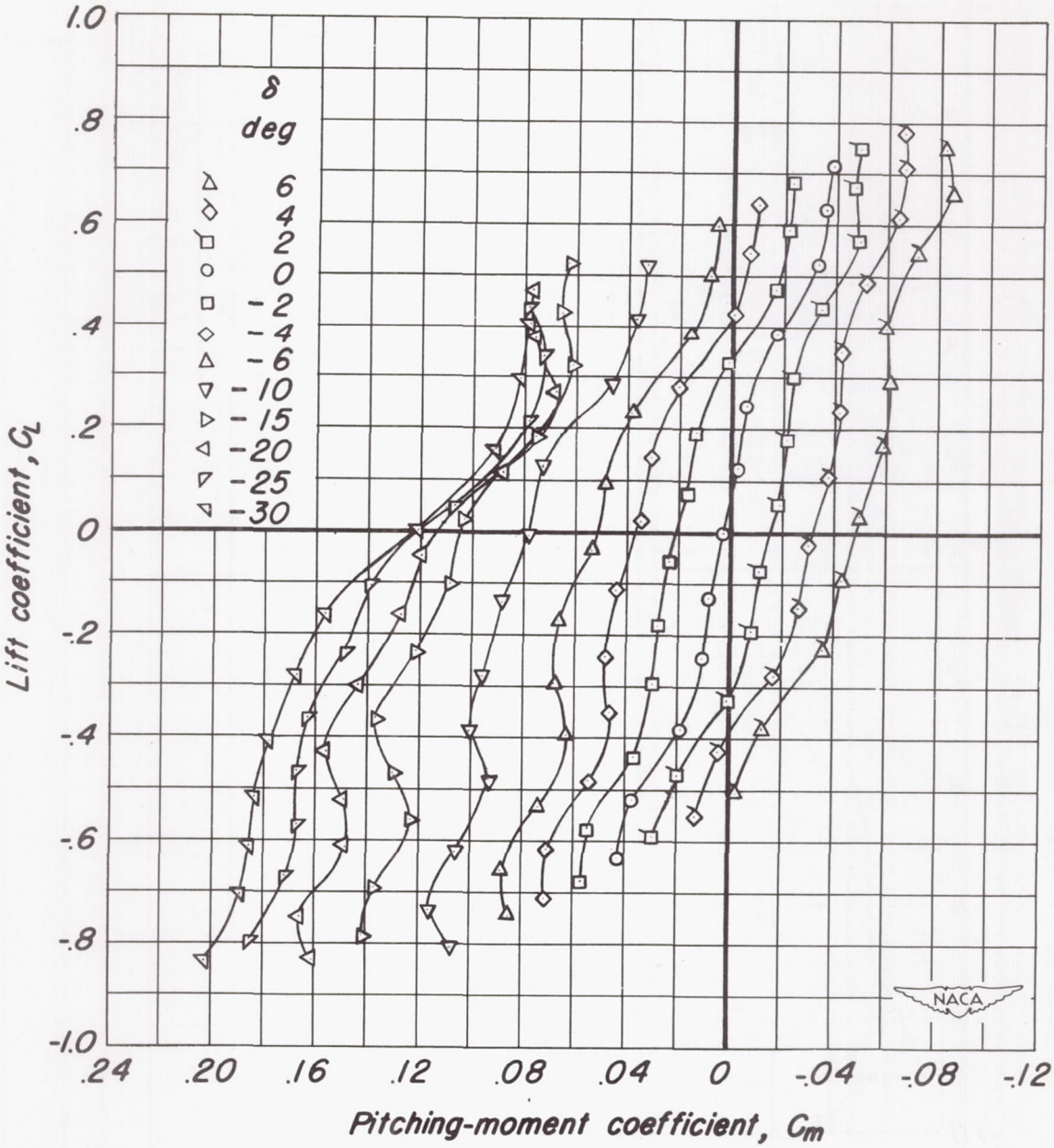

(d) M, 0.85

Figure 19.— Continued.

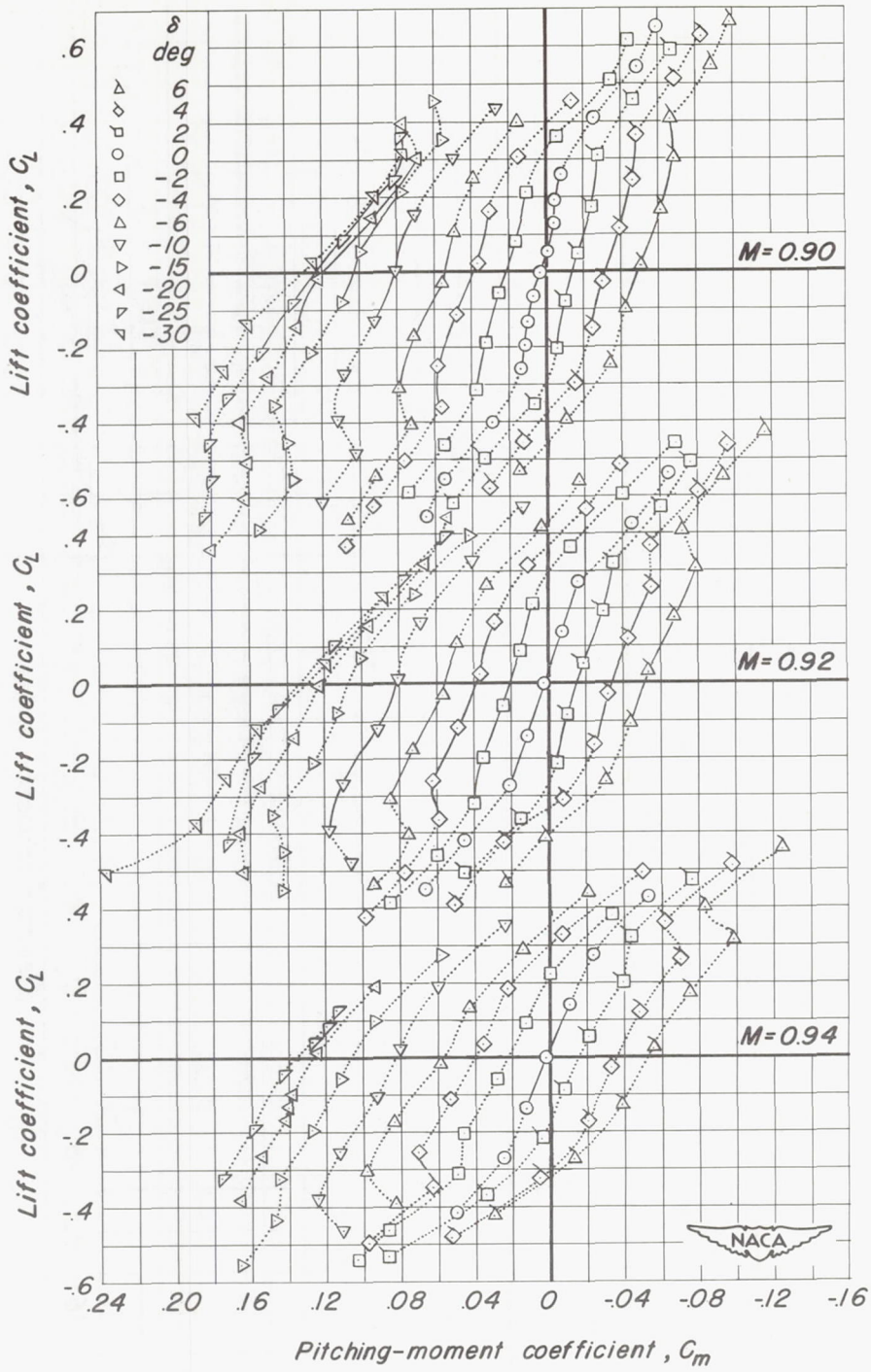

(e) M, 0.90; M, 0.92; M, 0.94

Figure 19.— Concluded.

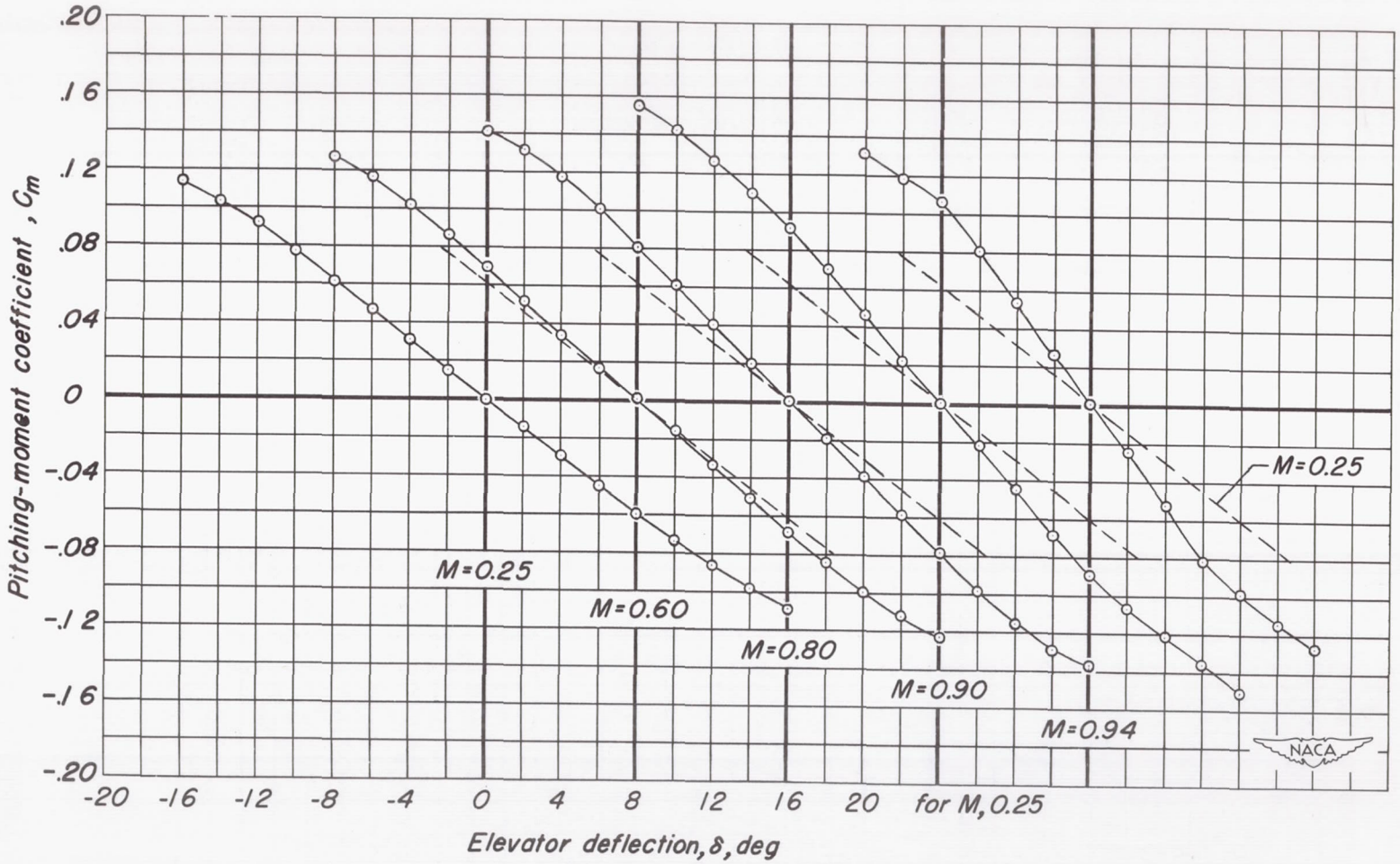

Figure 20.—The variation of pitching-moment coefficient with elevator deflection. α_u, 0°; R, 4,000,000.

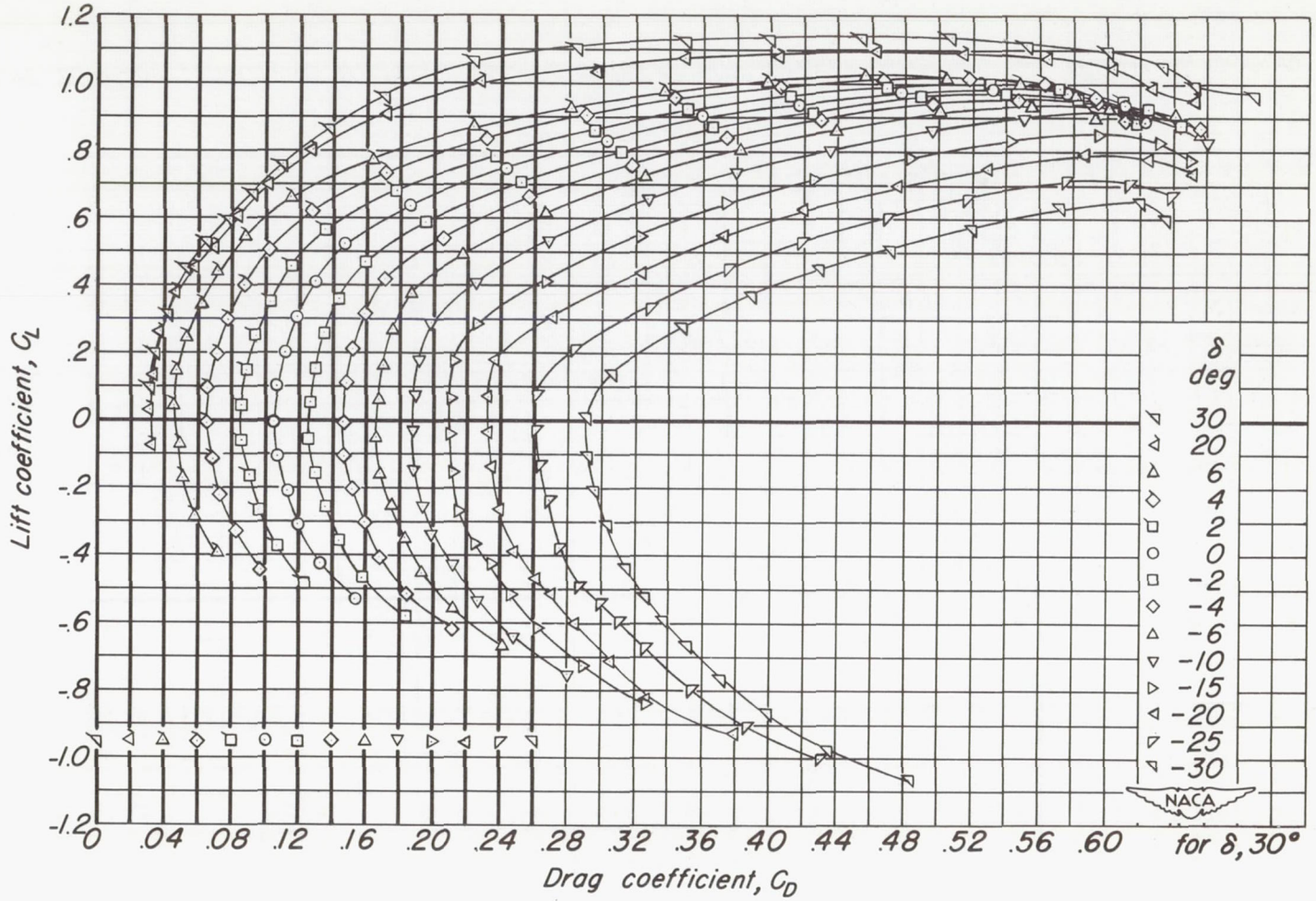

(a) M, 0.25

Figure 21.—The variation of lift coefficient with drag coefficient. R, 4,000,000.

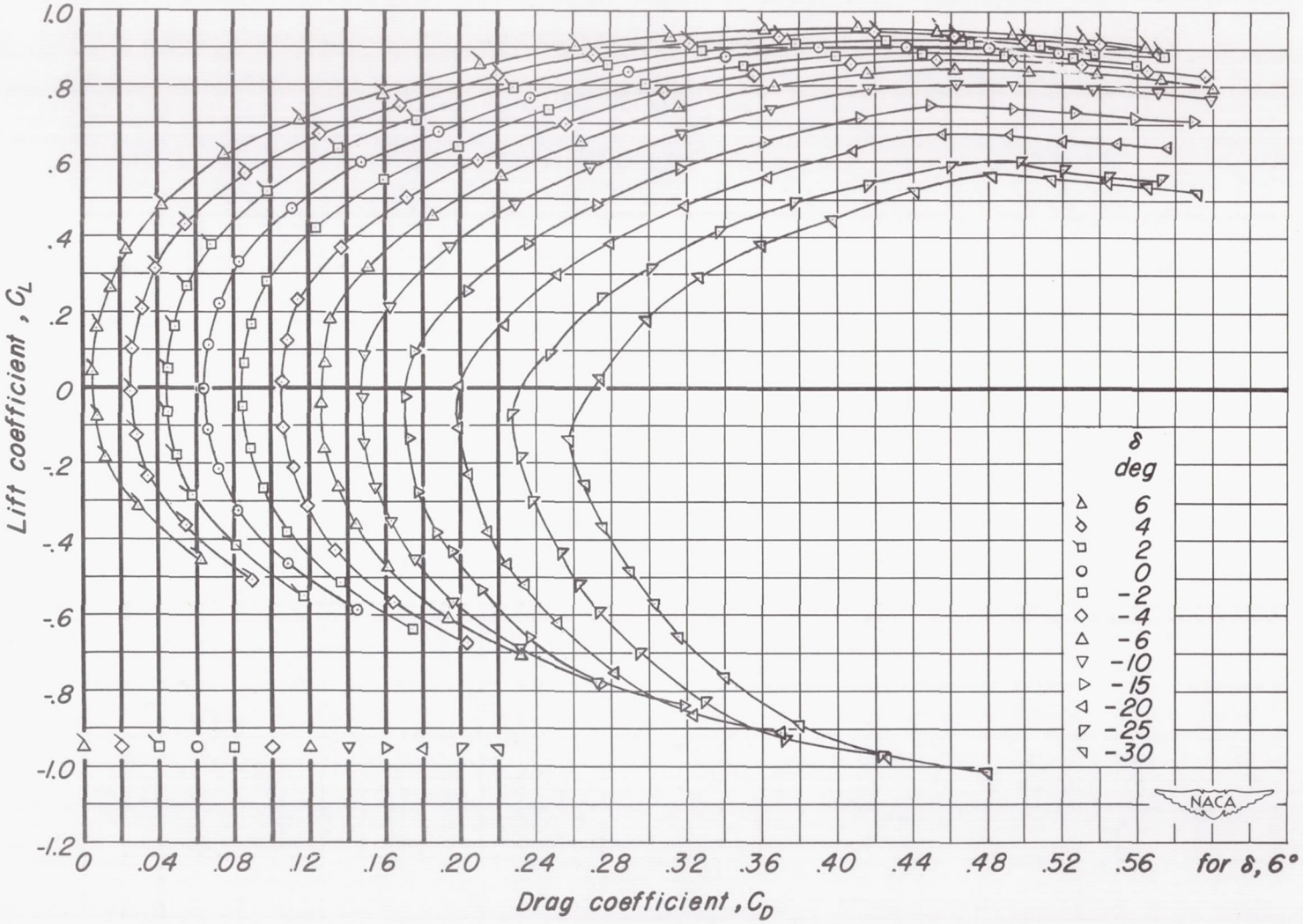

(b) M, 0.60

Figure 21.— Continued.

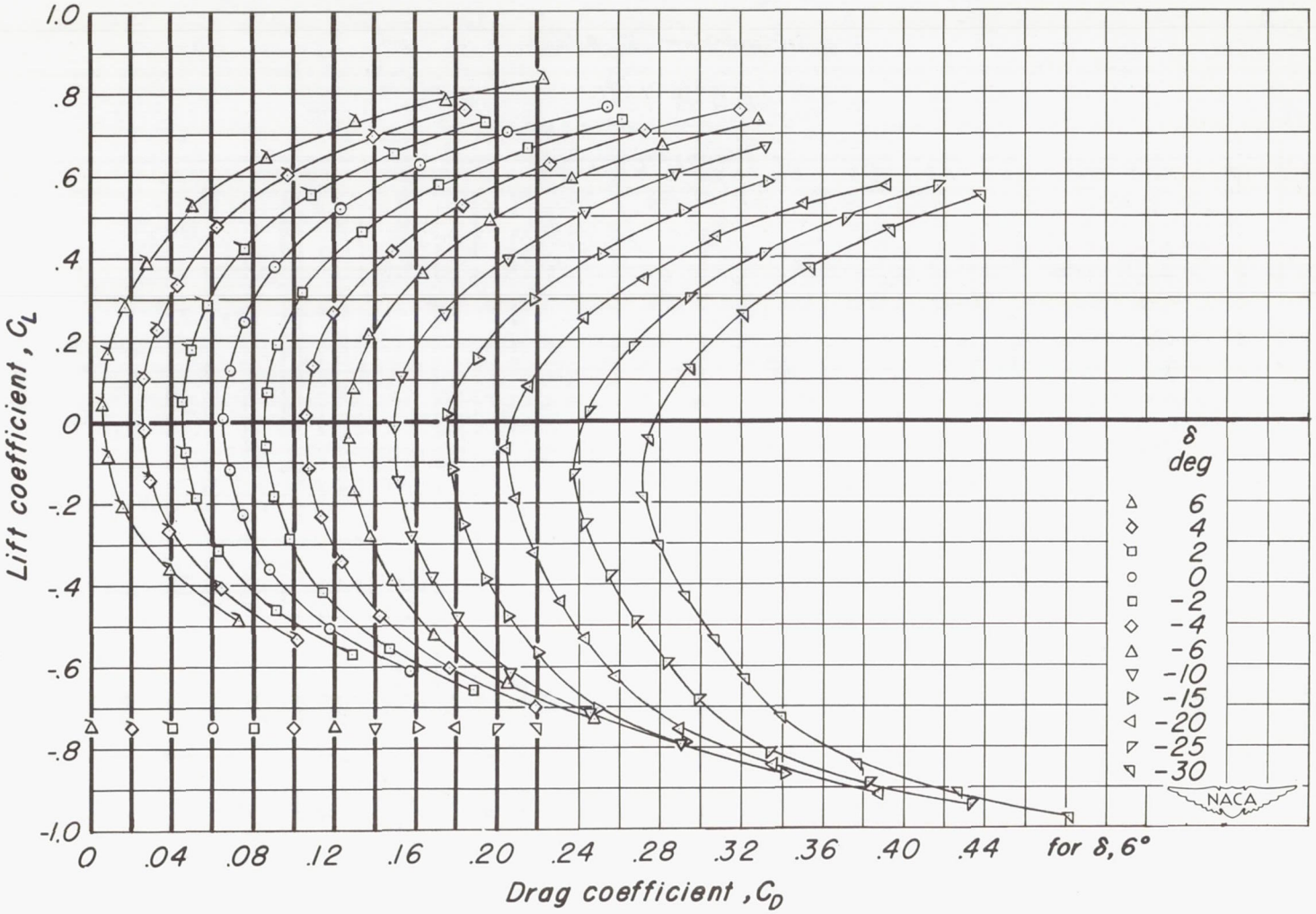

(c) M, 0.80

Figure 21.— Continued.

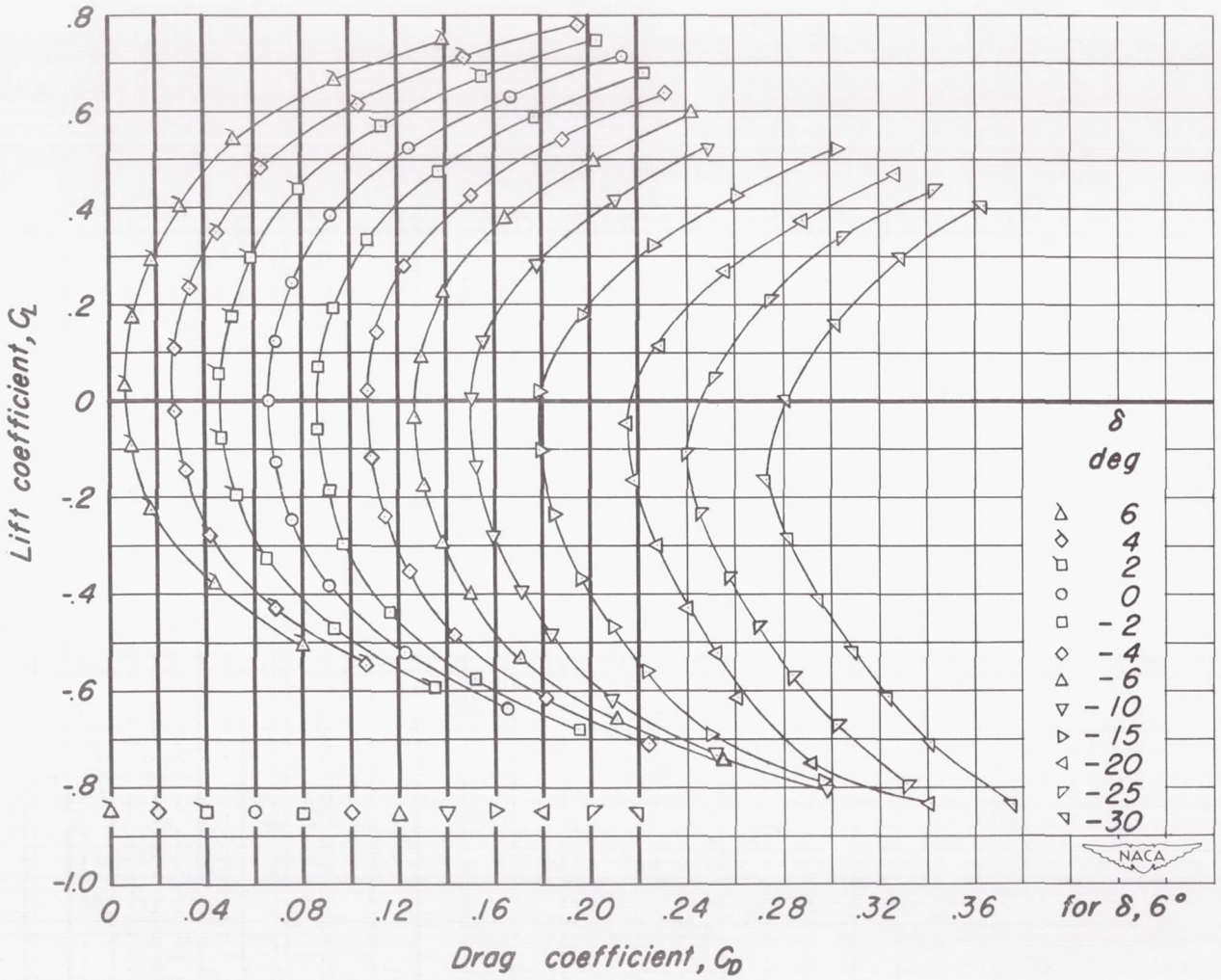

(d) M, 0.85

Figure 21. — Continued.

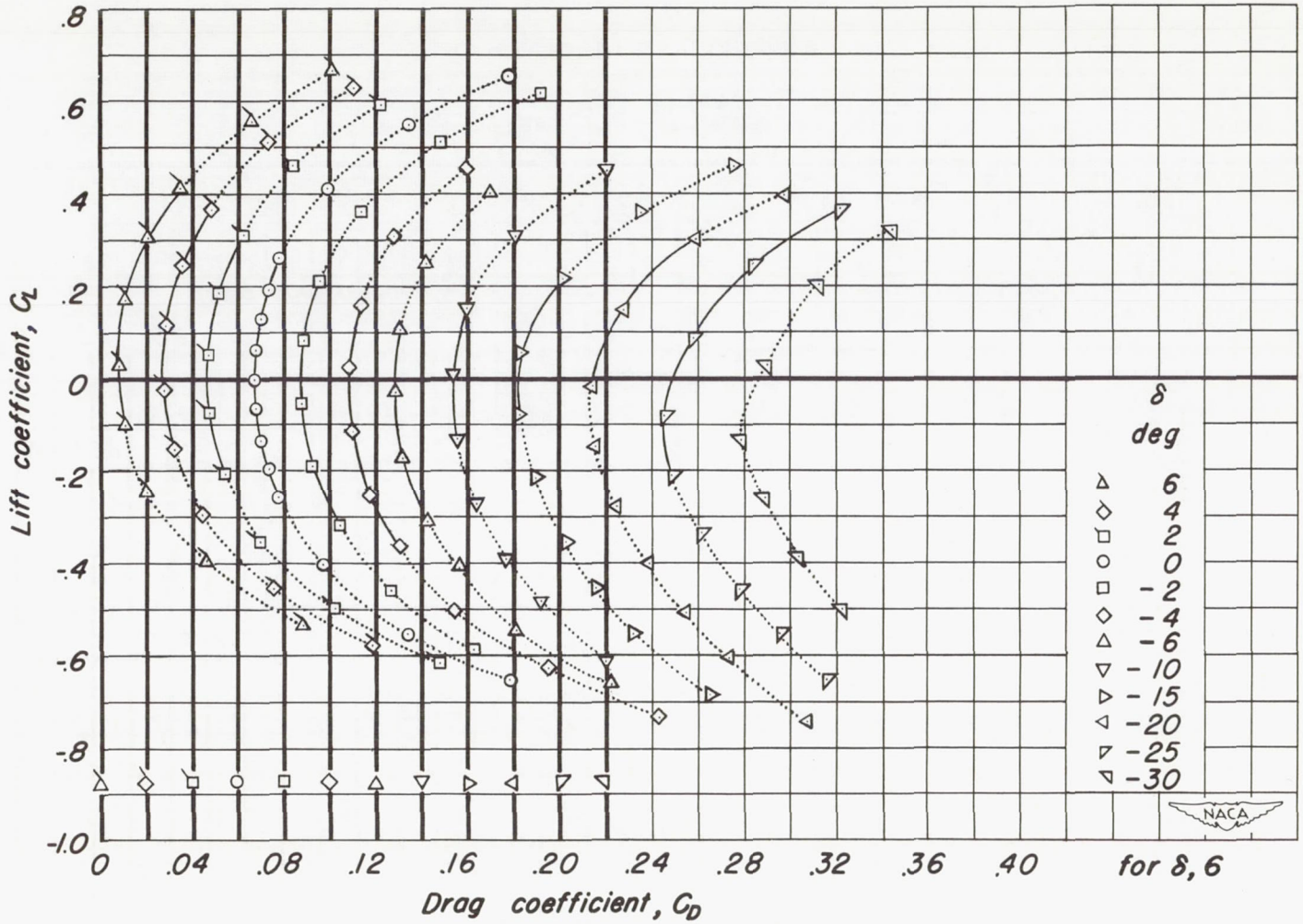

(e) M, 0.90.

Figure 21.— Continued.

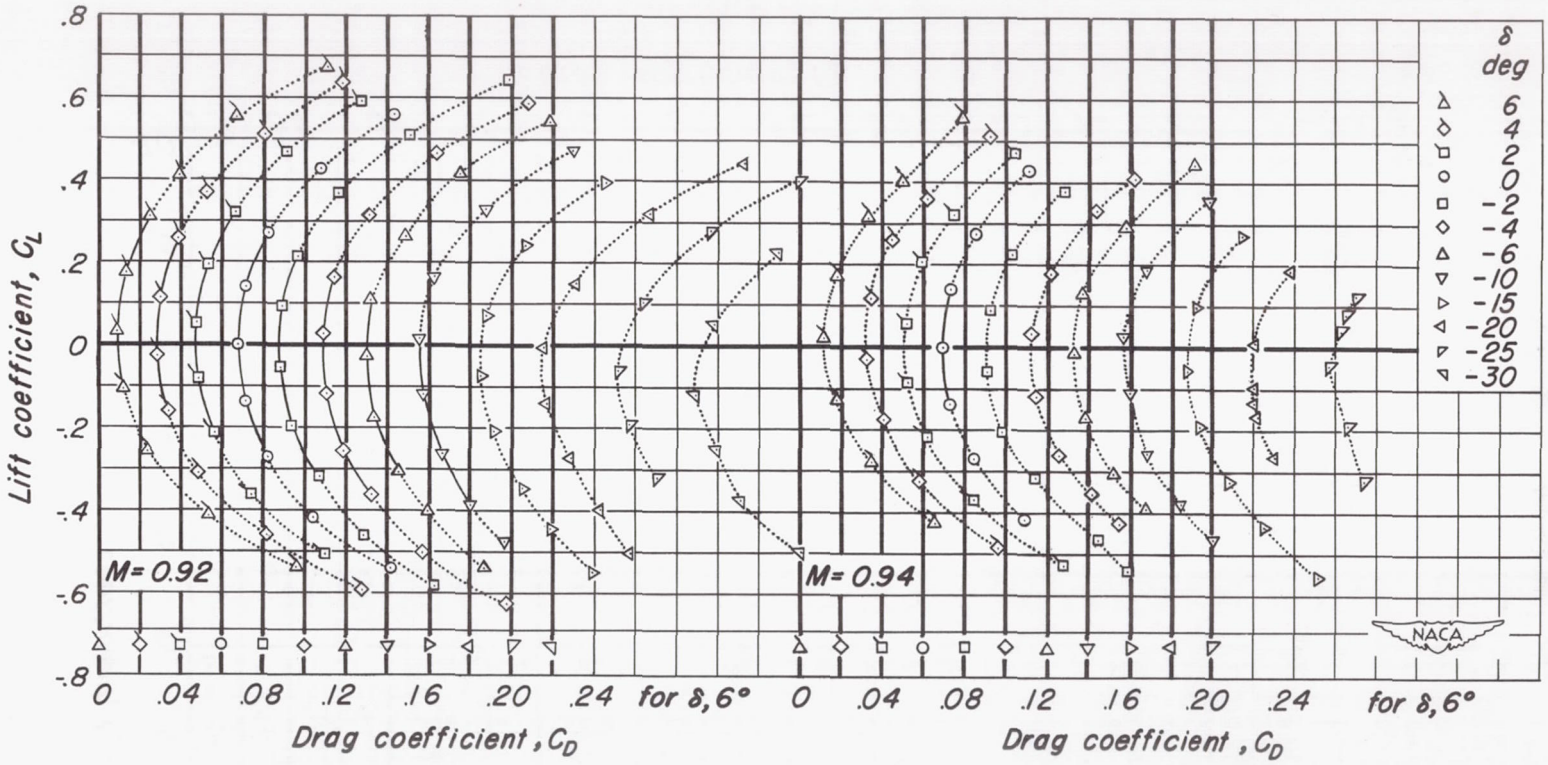

(f) M,0.92 ; M,0.94

Figure 21.— Concluded.

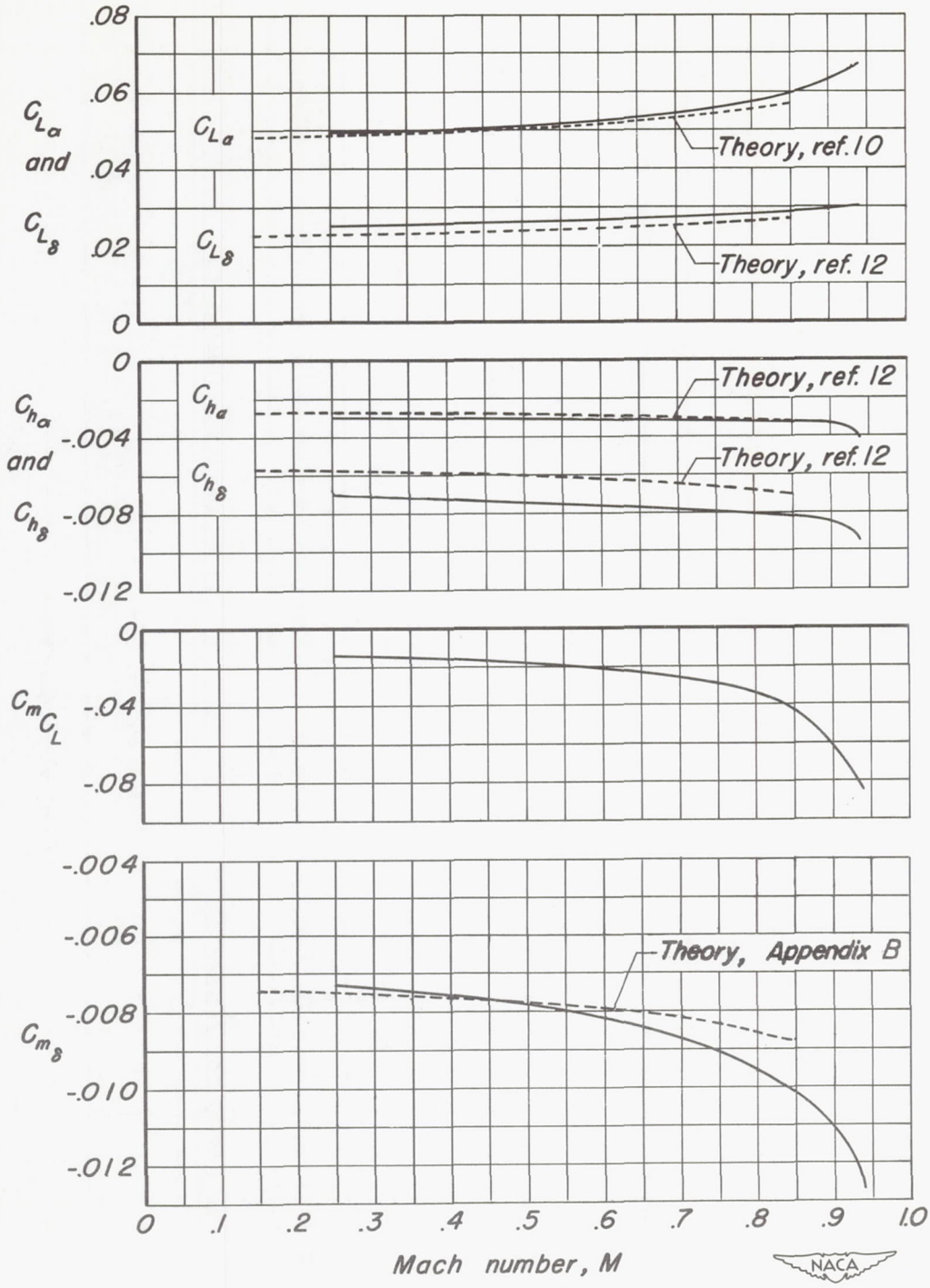

Figure 22.- The variations of C_{L_α}, C_{L_δ}, C_{h_α}, C_{h_δ}, $C_{m_{C_L}}$, and C_{m_δ} with Mach number. R, 4,000,000.

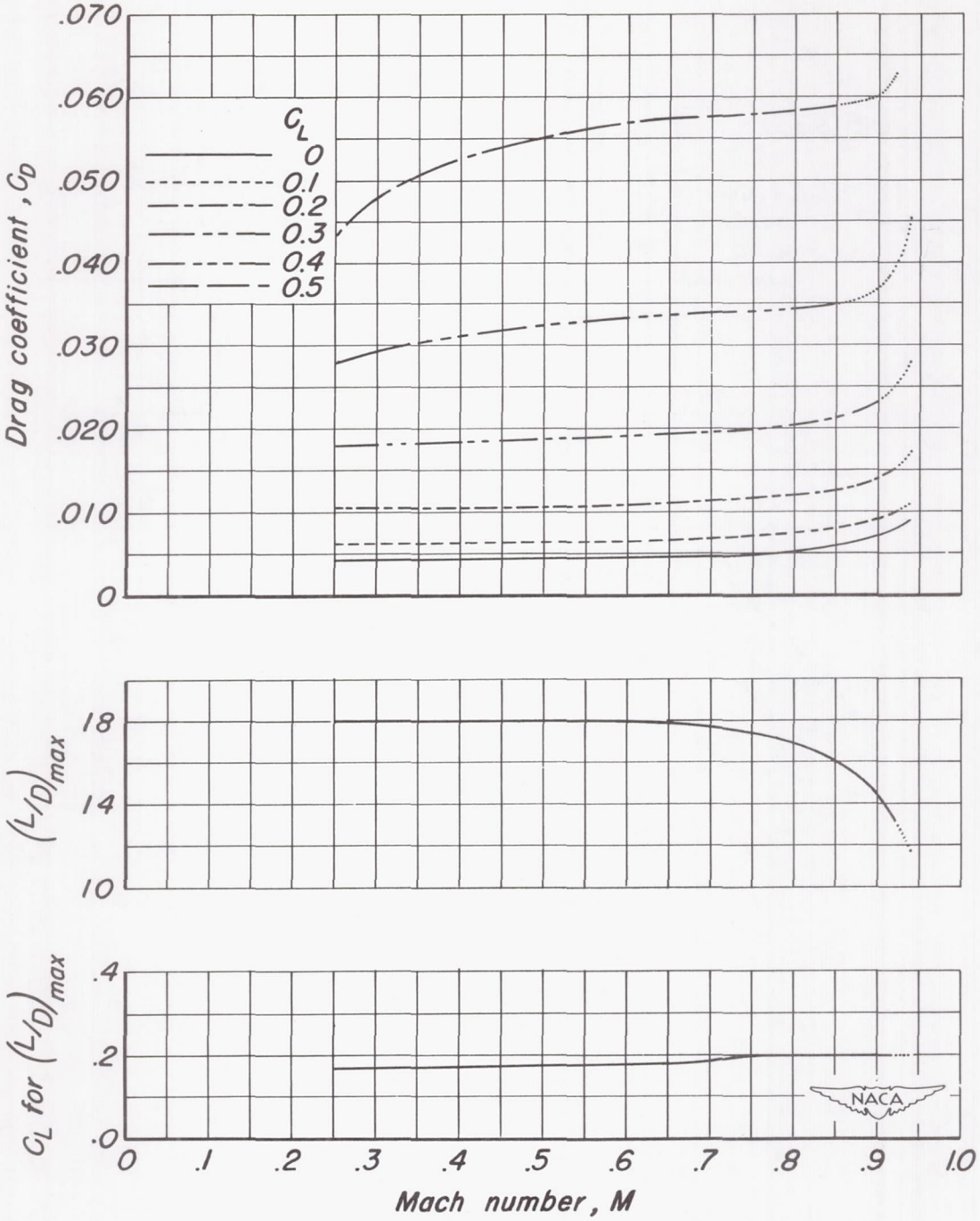

Figure 23.- The variations of drag, maximum lift-to-drag ratio, and lift coefficient for maximum lift-to-drag ratio with Mach number. R, 4,000,000; δ, 0°.

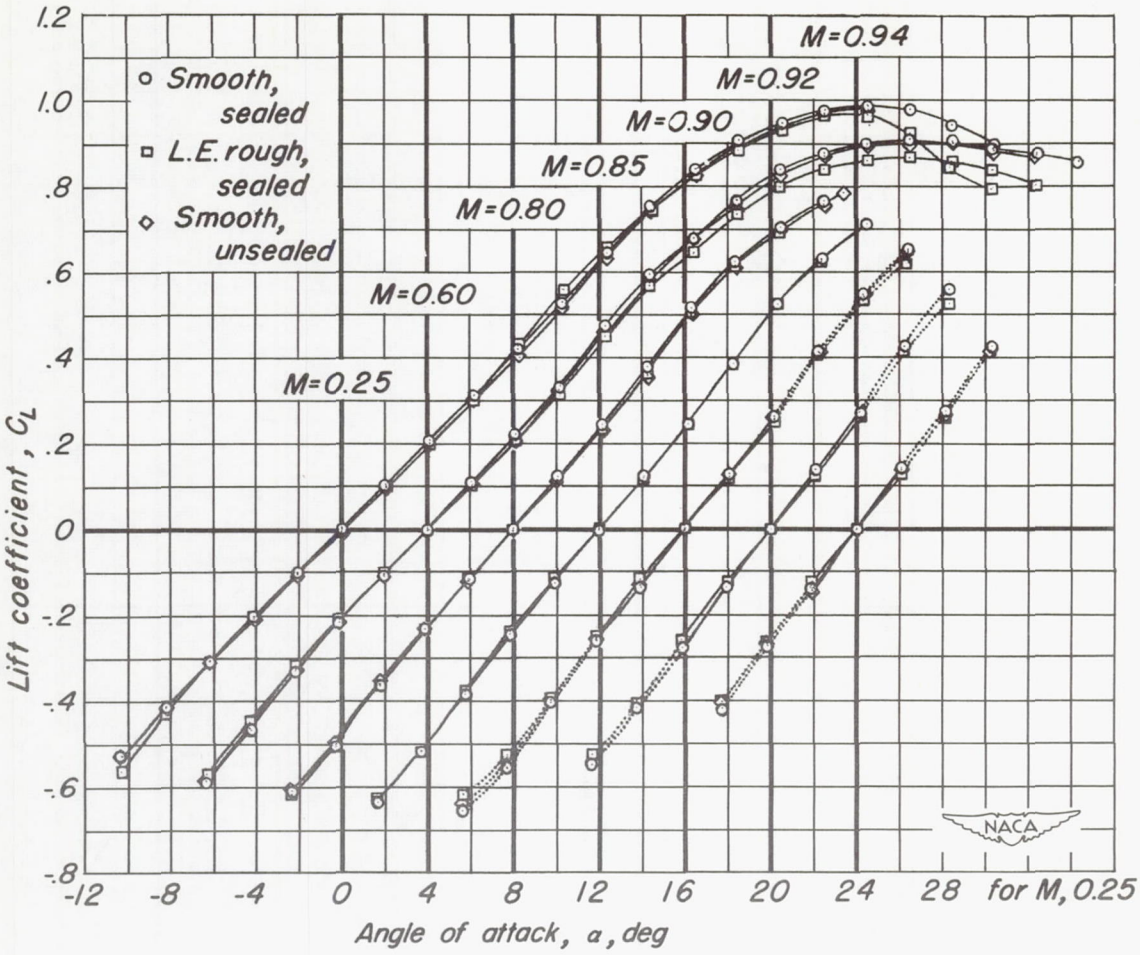

(a) C_L vs α

Figure 24.—The effects of leading-edge roughness and elevator-nose seal on the aerodynamic characteristics. δ, 0°; R, 4,000,000.

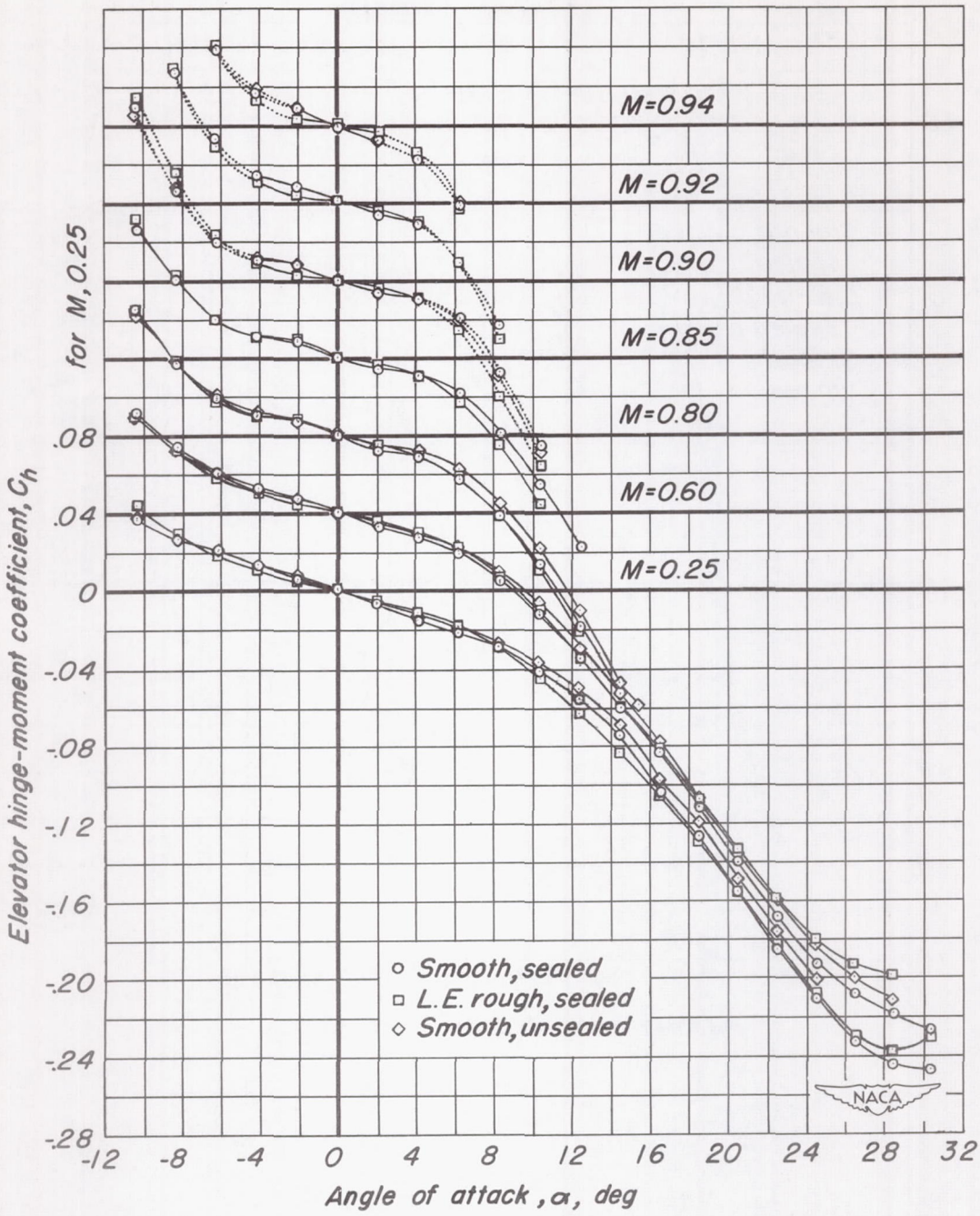

(b) C_h vs α

Figure 24.— Continued.

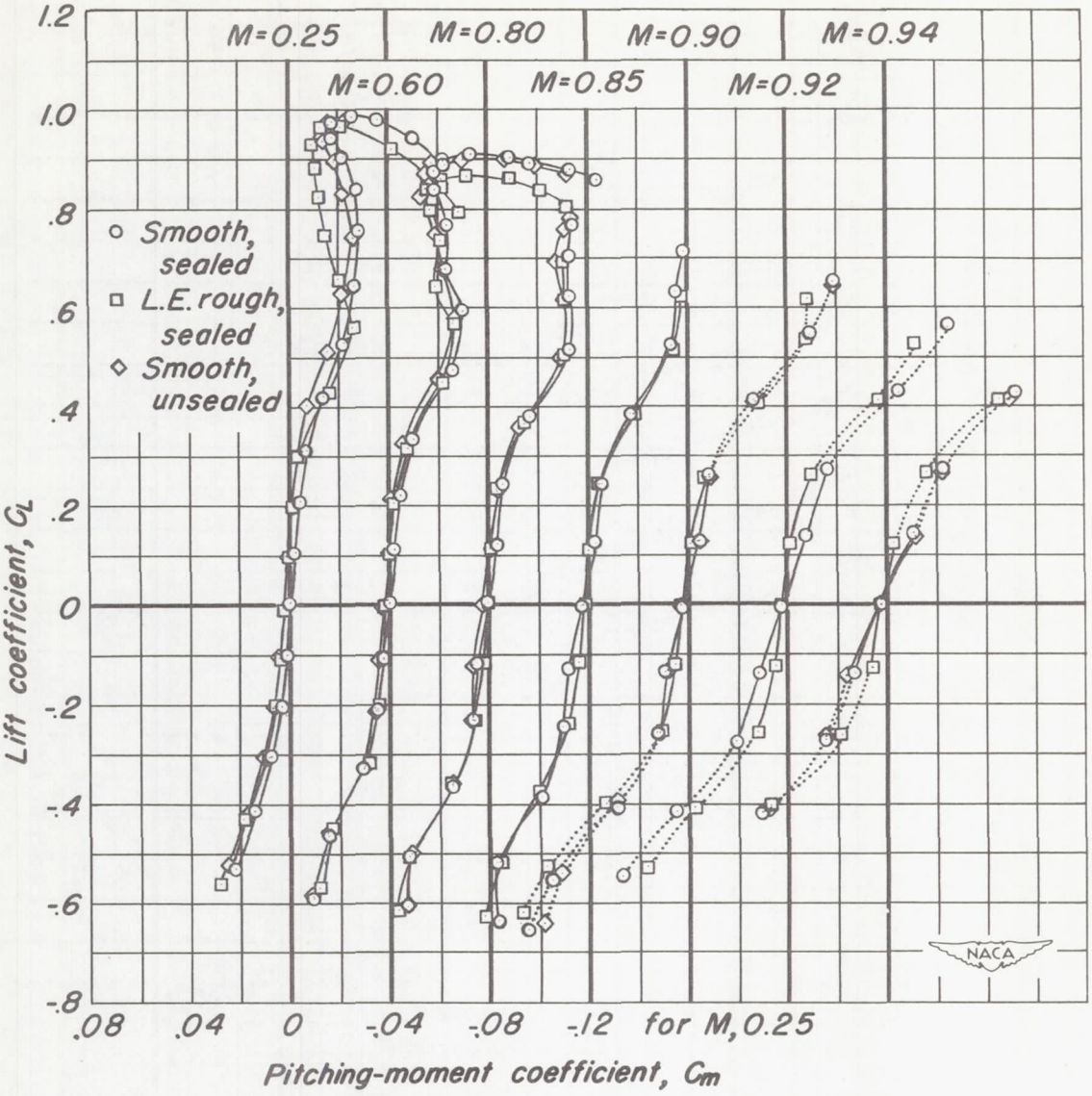

(c) C_L vs C_M

Figure 24.— Continued.

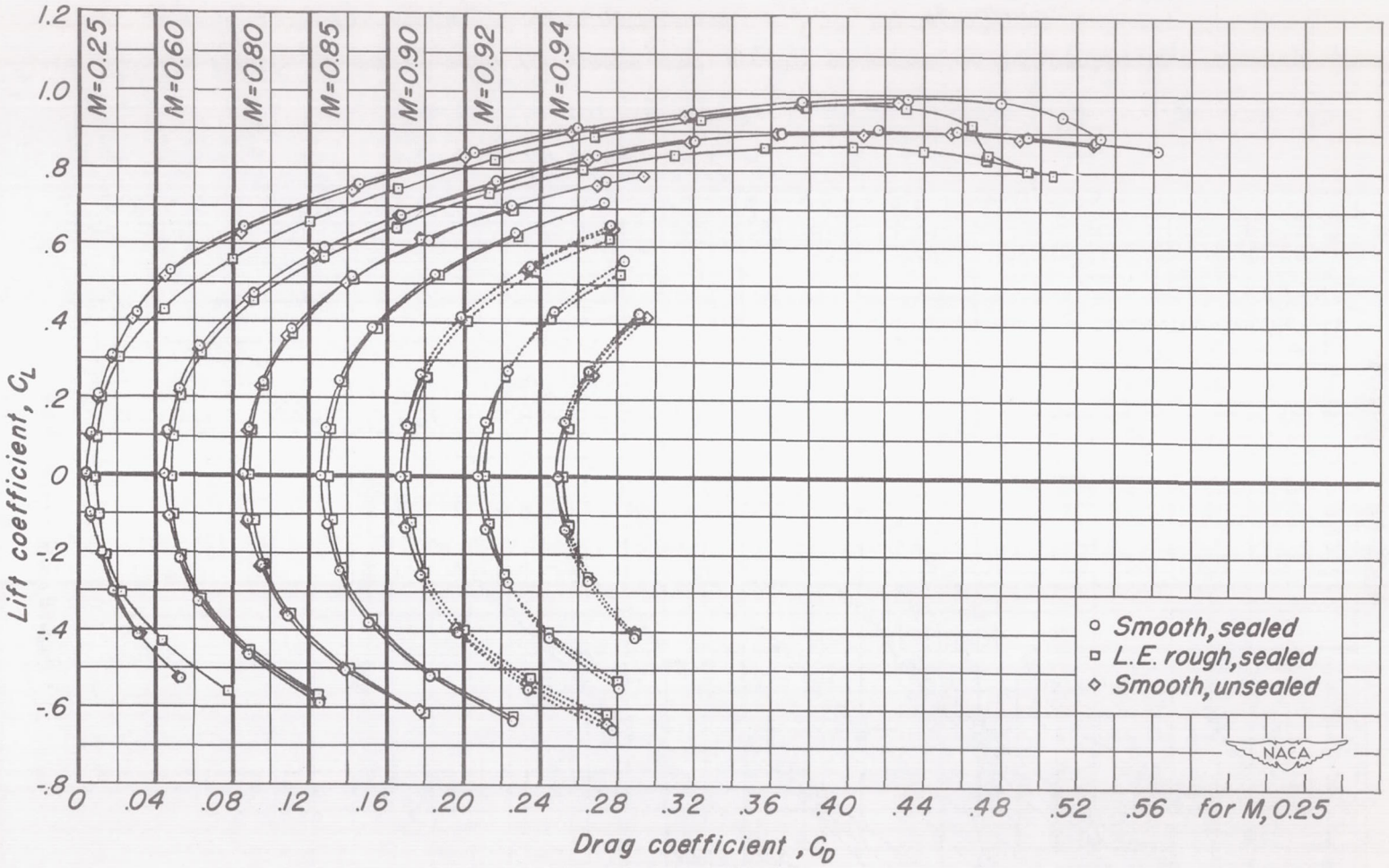

(d) C_L vs C_D

Figure 24.— Concluded.

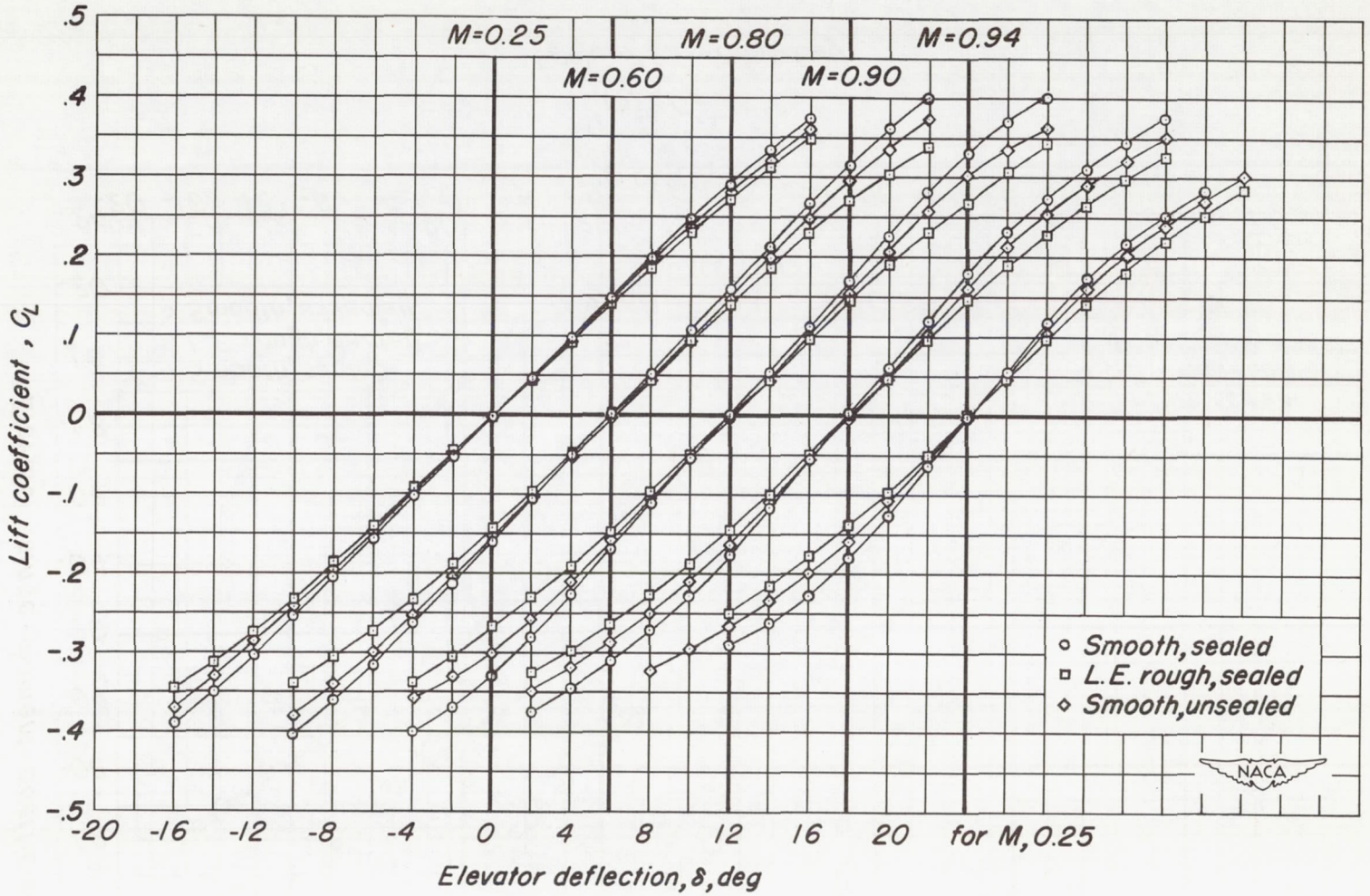

(a) C_L vs δ

Figure 25.—The effects of leading-edge roughness and elevator-nose seal on the aerodynamic characteristics for various elevator deflections. α_u, 0°; R, 4,000,000.

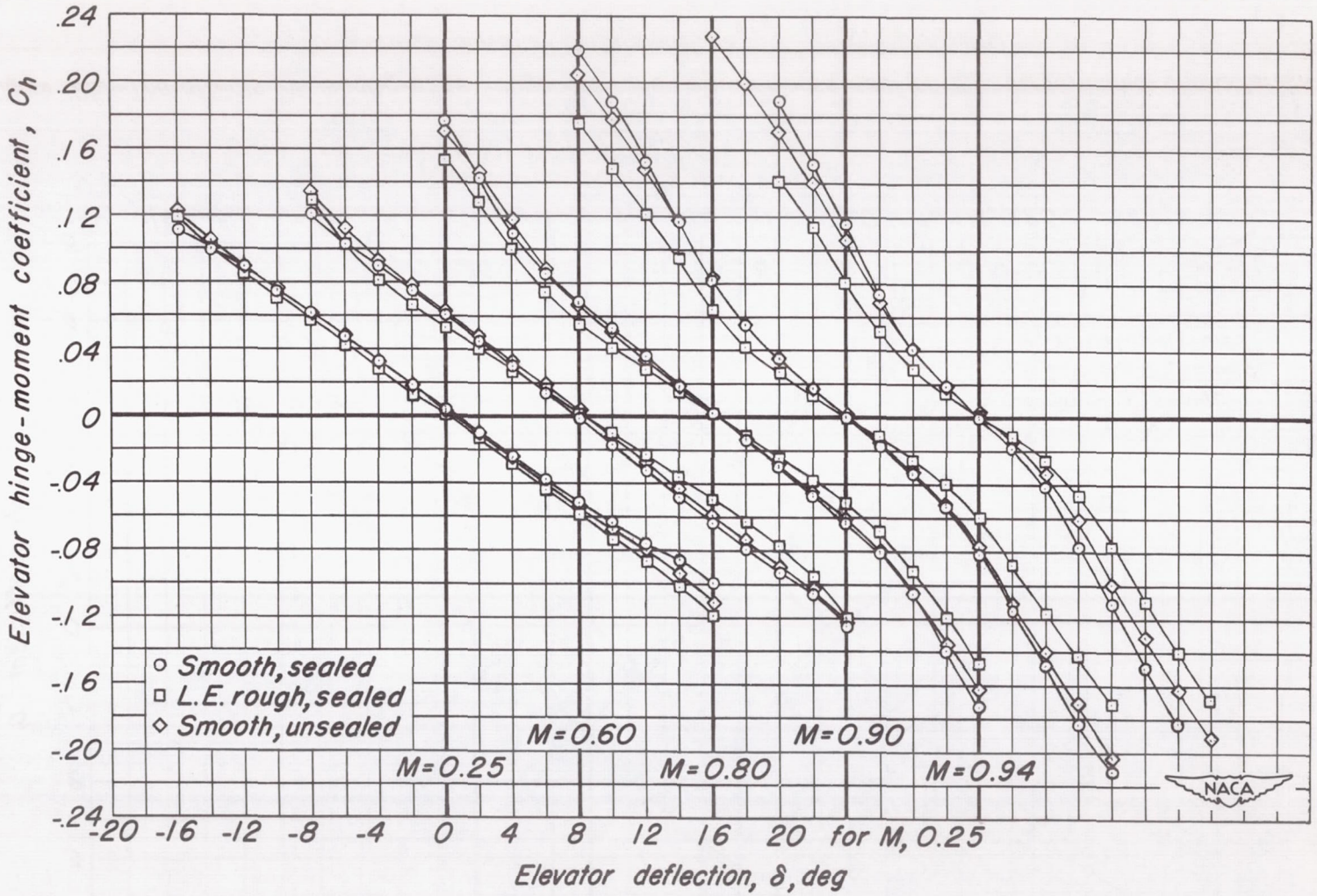

(b) C_h vs δ

Figure 25.—Continued.

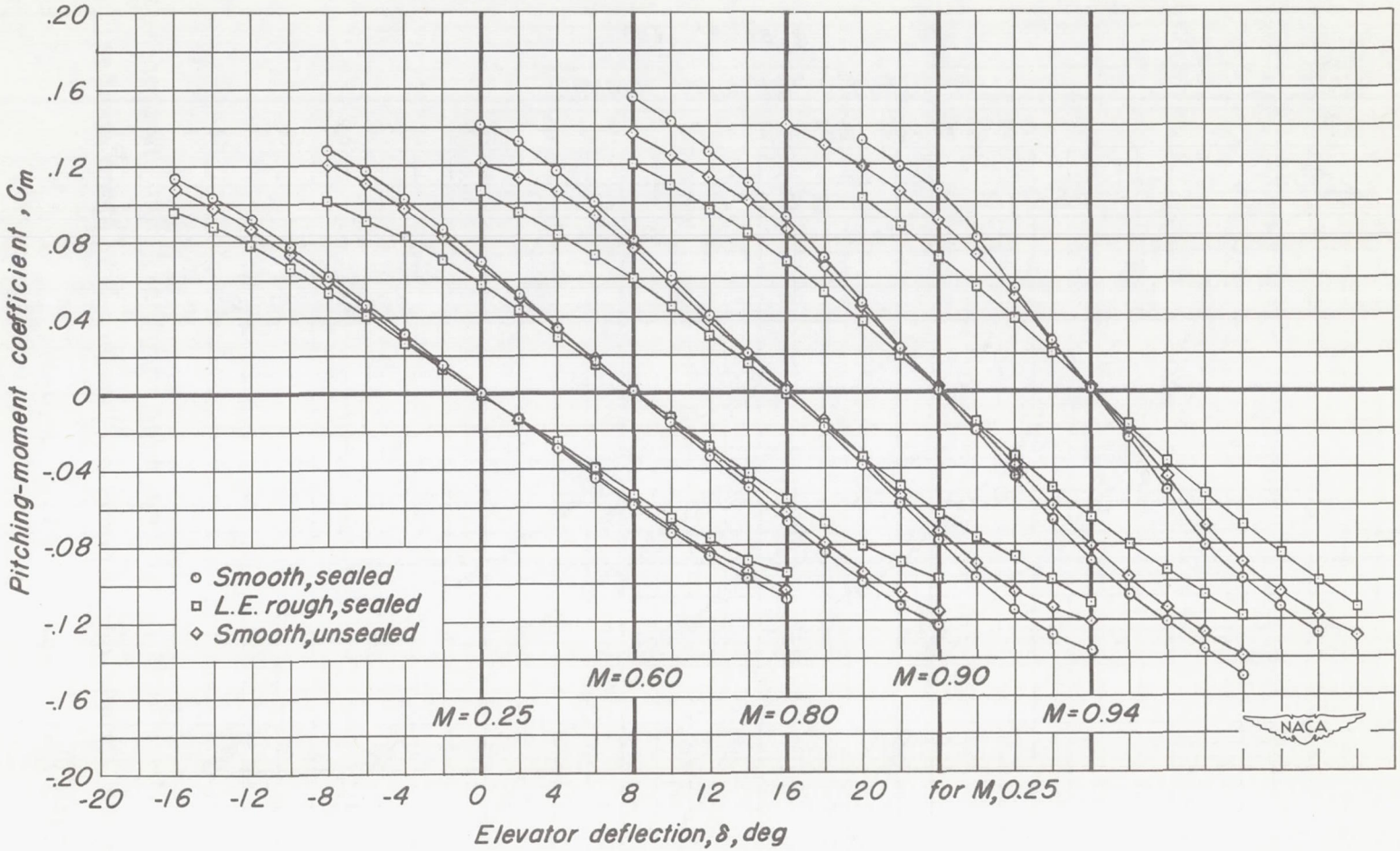

(c) C_M vs δ

Figure 25.— Concluded.

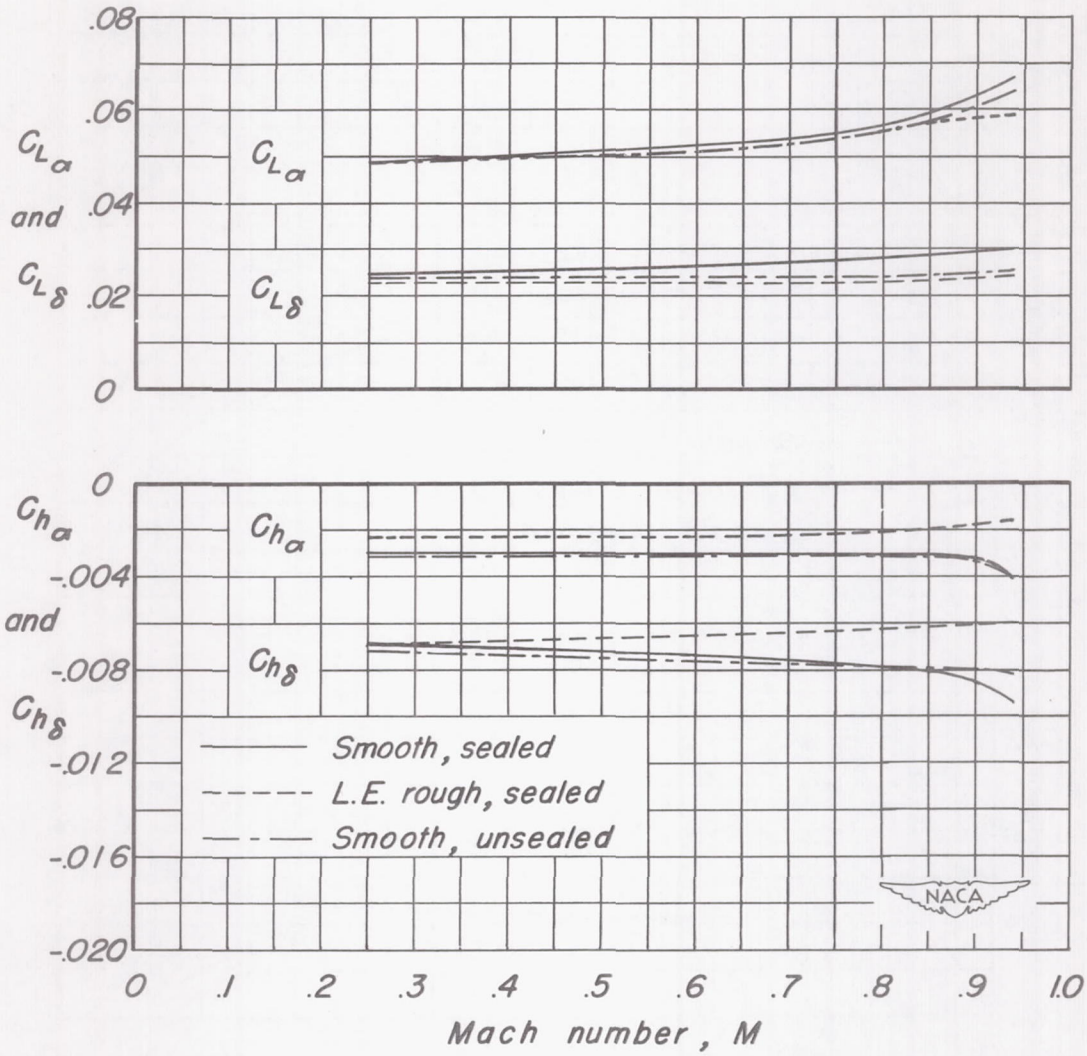

(a) $C_{L_\alpha}, C_{L_\delta}, C_{h_\alpha}$, and C_{h_δ} vs M

Figure 26.- The effects of leading-edge roughness and elevator-nose seal on the various aerodynamic parameters with Mach number. R, 4,000,000.

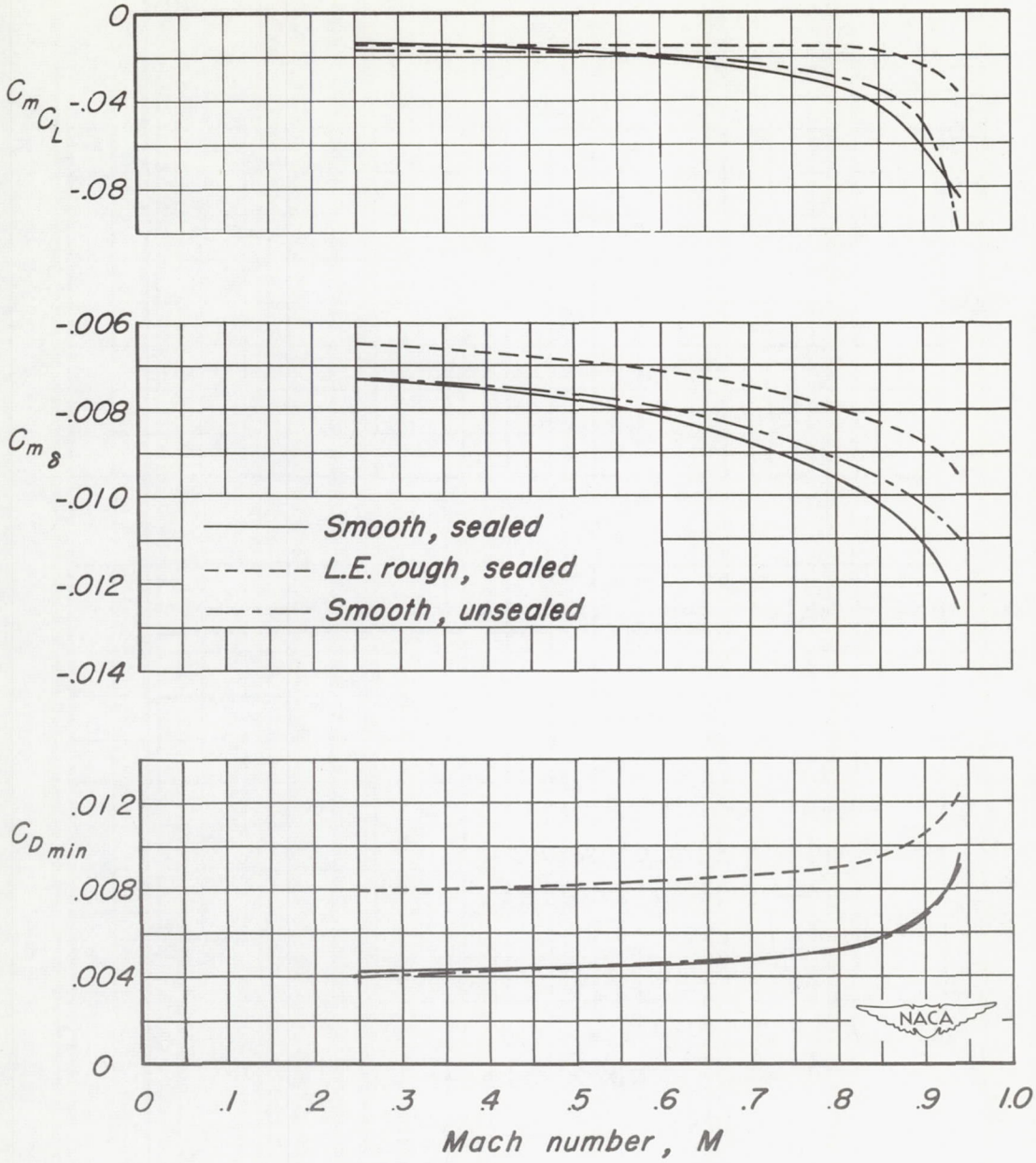

(b) $C_{m_{C_L}}$, C_{m_δ}, and $C_{D_{min}}$ vs M

Figure 26.- Concluded.

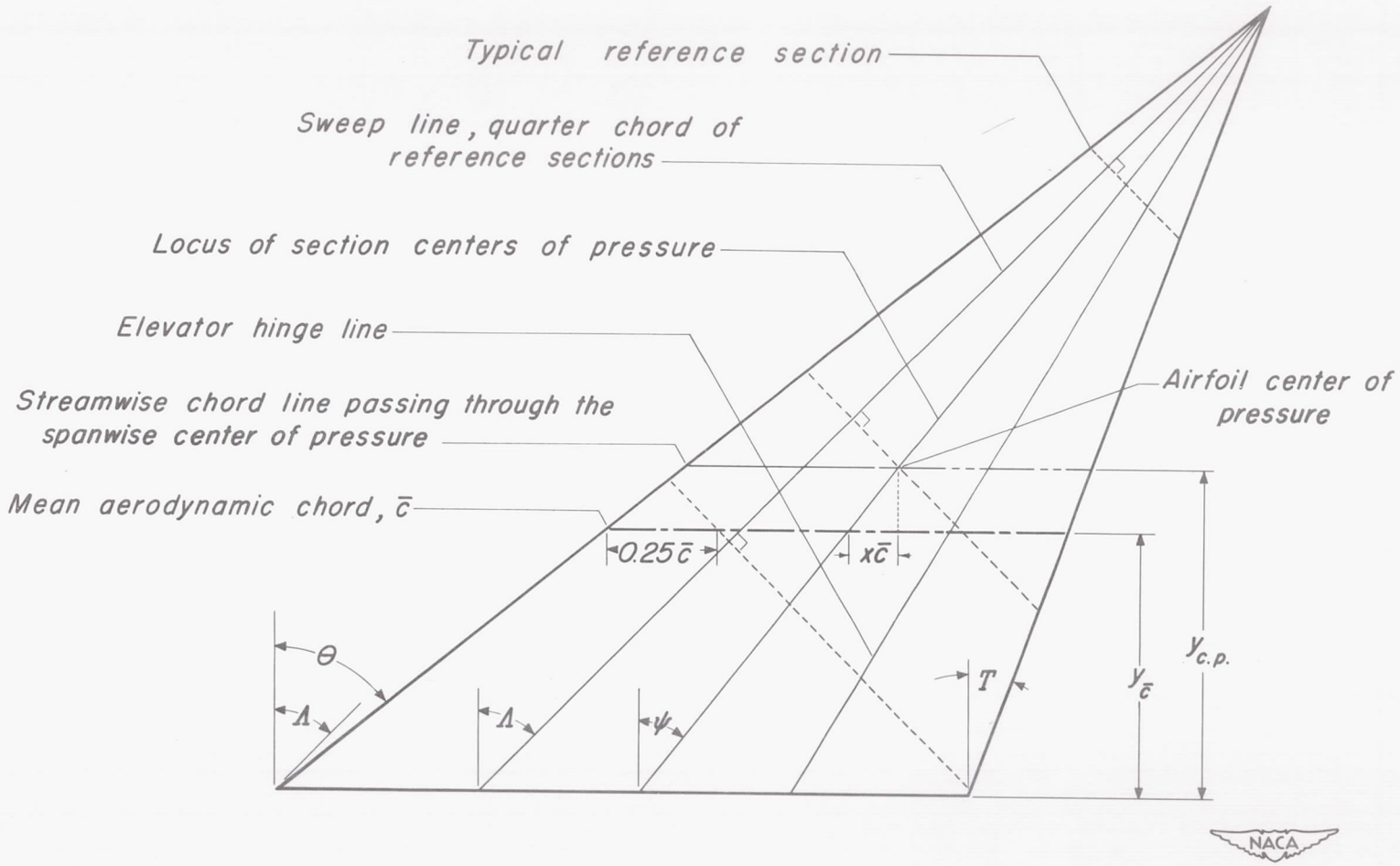

Figure 27 -. Sketch showing the geometric relations used in calculating the parameter, C_{m_δ}

NACA-Langley - 2-17-54 - 75